T · H · E
OHIO
STATE
UNIVERSITY

Study of a Novel Adaptive Printed Antenna Element for GPS Applications

R.G. Rojas and K.W. Lee

The Ohio State University

ElectroScience Laboratory

Department of Electrical Engineering
1320 Kinnear Road
Columbus, Ohio 43212

Final Report 735571-2
Grant No. F49620-98-1-0372
March 1999

AFOSR/NM
801 North Randolph Street, Room 732
Arlington, VA 22203-1977

AFRL-SR-BL-TR-99-

0512

50272-101

REPORT DOCUMENTATION PAGE	1. REPORT NO.	2.	
4. Title and Subtitle Study of a Novel Adaptive Printed Antenna Element for GPS Applications			5. Report Date March 1999 6.
7. Author(s) R.G. Rojas and K.W. Lee			8. Performing Org. Rept. No. 735571-2
9. Performing Organization Name and Address The Ohio State University ElectroScience Laboratory 1320 Kinnear Road Columbus, OH 43212			10. Project/Task/Work Unit No. 11. Contract(C) or Grant(G) No. (C) (G) F49620-98-1-0372
12. Sponsoring Organization Name and Address AFOSR/NM 801 North Randolph Street, Room 732 Arlington, VA 22203-1977			13. Report Type/Period Covered Final Report 14.
15. Supplementary Notes			

16. Abstract (Limit: 200 words)

This report discusses the development of a novel adaptive printed antenna element for GPS applications. This antenna element consists of a microstrip patch antenna and several diode-loaded parasitic metallic strips on top of the dielectric substrate. It is shown through computer simulations that the beamwith of the antenna can be modified by turning the diodes on or off. This implies that the radiated pattern level can be modified along the horizon ($\pm 10°$) This concept is based on controlling the surface wave behavior by adding metallic strips. The metallic strips convert, if properly designed, surface waves into leaky waves which radiated away from the surface of the substrate. It is shown through computer simulations and measurements that microstrip antennas can be built with thick substrates without the usual surface wave problem. An optimization algorithm is developed (Genetic algorithm) to design the metallic strips. The proper choice of the dimensions of the strips is important because their behavior is frequency sensitive.

17. Document Analysis a. Descriptors

b. Identifiers/Open-Ended Terms

c. COSATI Field/Group

18. Availability Statement	19. Security Class (This Report) Unclassified	21. No. of Pages 95
	20. Security Class (This Page) Unclassified	22. Price

(See ANSI-Z39.18) *See Instructions on Reverse* OPTIONAL FORM 272 (4-77)
Department of Commerce

Contents

List of Figures

Chapter 1

Introduction

1.1 Overview

This final report discusses the work that has been done on the study of a novel "adaptive" printed antenna element for GPS applications. The idea consists of using an array of diode-loaded metal strips mounted on the same substrate as the patch antenna to modify its radiation pattern. It is shown here (through computer simulations) that the beamwidth of the antenna can be modified by turning the diodes on or off. Note that by changing the beamwidth we are actually changing the radiated power level along the horizon ($\pm 10°$).

1.2 Technology Transition

Customer: Juan Vasquez, Capt, USAF, Ph.D.
AFRL/SNAR Bldg 620
2241 Avionics Circle
WPAFB, OH 45433-7321
Phone: (937) 255-5668 x4014, FAX: (937) 656-4301

Results: Novel scheme to control surface waves in planar printed antennas.

Applications "Adaptive" printed element for GPS antennas mounted on military aircraft.

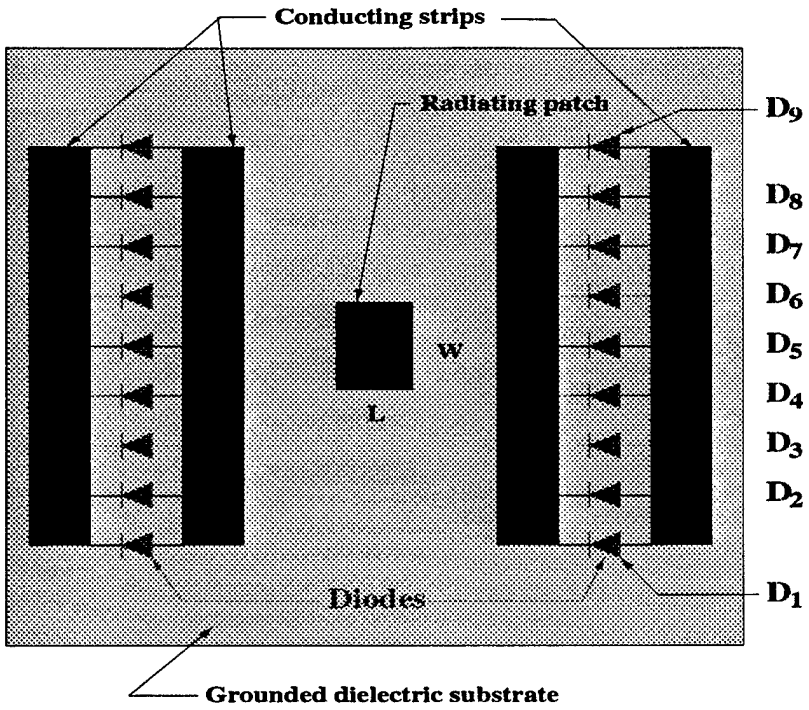

Figure 1.1: "Adaptive" Microstrip antenna element

1.3 Summary

A novel concept to design an "adaptive" printed antenna element is introduced. This antenna element, shown in Figure 1.1, is a microstrip patch with parasitic diode-loaded metal strips. The concept is based on the control of surface waves excited in the dielectric substrate.

This report addresses two main topics. The first topic is a novel scheme developed in this study to control surface waves by using parasitic metallic strips. Chapters 3 through 4 discuss this topic where calculated as well as measured results are shown. Control of surface waves is critical because they can adversely affect the performance of most printed antennas. The strength of these waves depend on the substrate thickness and substrate dielectric constant because they control the amount of energy coupled into surface wave modes guided by the substrate [1, 2]. Surface wave excitation occurs on most substrate-based printed antennas because the lowest order surface wave mode (TM_o) has a zero cutoff frequency. These guided waves become stronger as the substrate thickness increases. The surface waves propagate along the

surface of the substrate and radiate to free-space at the truncations of the dielectric substrate. The radiated surface-wave will often distort the radiation pattern of the antenna in the main-beam direction and increase the side-lobe and back-lobe levels.

Chapters 2 through 4 present a scheme for controlling these surface waves. The approach is to add metal strips on the top and (if necessary) in the bottom of the substrate. With the proper choice of strip lengths and widths, energy leaks away from the surface as the wave propagates. As a result, the edge diffraction is small because only a small amount of energy is left at the termination. In other words, the surface waves are converted into leaky waves and radiate out to free space before they reach the edge of the substrate. For a fixed substrate thickness, the width of the strips controls the propagation direction and the beamwidth of these radiated leaky waves. The separation between the strips has only a small effect on the leaky waves and the number of strips determines the pattern bandwidth. In addition, the width and length of the strips determine the transition (between surface wave and leaky wave) region in the frequency domain. Therefore, the antenna pattern can be changed by the leaky wave beams which in turn are controlled by the strip parameters (widths, lengths and separations).

To access the validity of the above scheme, a rectangular microstrip antenna is designed on an electrically thick ($\sim 0.1\lambda_d$) dielectric substrate. However, the scheme can be adapted to other types of printed antennas as well. The microstrip patch is designed to operate in its first dominant mode (TM_{10}), and hence, has a maximum in the radiation pattern at broadside. The main goal is to obtain a "flat-top" antenna main-beam pattern, and low side and back lobe levels.

In Chapter 2, some background information and a design procedure for electrically thick microstrip antennas are presented. Many design formulas available in the literature are limited to electrically thin (in the range of $0.003\lambda_o$ to $0.05\lambda_o$) microstrip antennas [3, 4]. In order to obtain a more accurate result, the patch is first designed using design equations given by Bahl and Bhartia [5]. Then a finite difference time domain (FDTD) method, developed at the ElectroScience Laboratory, is applied to fine tune the design to the desired resonant frequency [6] - [7].

The analysis of the effect of the strips is presented in Chapter 3. It is found that the most critical parameter of the design is the width of the strip closest to the radiating patch. By varying the width of the strip, the radiation pattern of the microstrip antennas changes dramatically. When the strip width is electrically small, the structure acts like a surface wave guiding structure, which makes these guided surface waves stronger and distort the radiation pattern. However, when the strip width becomes electrically large, this guiding structure no longer supports surface waves, it supports leaky waves. Energy leaks out and contributes to the main-beam before the wave reaches the truncation of the substrate. Thus, the antenna has a higher gain and lower level of side and back lobes. Note that additional strips can be added to optimize the design. In this study, a Genetic Algorithm has been implemented to obtain an optimum design. In Appendix A, a brief review of different genetic operators and a simple overview of genetic algorithms is presented. In addition, an adaptive genetic algorithm (AGA) is also introduced. In the AGA, the improvement of the average performance of the population is not as important as in the case of other genetic algorithms. AGA is concerned more on finding the optimum as quickly as possible.

After obtaining the optimal design, the antenna is then fabricated and tested. The results are shown in Chapter 4 along with the implementation of the objective function used in the optimization. The antenna radiation pattern measurement was performed in the Compact Range of the ElectroScience Laboratory. It is important to note that the antenna was designed and built for operation around 5 GHz. The reason for choosing this frequency was the availability of substrate material.

The second key topic, presented in Chapter 5, discusses preliminary results regarding the design of an adaptive antenna element. The scheme for controlling surface waves, developed in the previous chapters, is extended to demonstrate that diode-loaded strips can be used to develop an adaptive printed antenna element. By means of computer simulations, it is shown that it is possible to modify the beamwidth of a patch antenna by turning the diodes on and off. As mentioned before, the calculations were done with a 3-D FDTD code developed at the ElectroScience Laboratory.

The diodes are modeled by thin metallic wires when they are "on". They are ignored when they are off. The calculations were conducted at 1.227 GHz, which is one of the frequencies assigned to the GPS system. No attempt was made to optimize the antenna element. The goal of this last chapter was to simply introduce the concept of an adaptive printed antenna element.

Chapter 2

Design of Microstrip Antennas on Electrically Thick Substrate

2.1 Introduction

The microstrip antenna concept was first introduced by Deschamps more than 40 years ago. Since then, microstrip antennas have become popular for a wide variety of application areas. This is because of their many advantages over conventional antennas, such as being comparably lightweight, low profile, low cost, their conformity to surface, and direct integrability with microwave circuitry [5, 8]. On the other hand, there are some limitations compared to conventional antennas. These drawbacks are mainly due to its low gain and narrow bandwidth performance. Most microstrip antennas have a typical bandwidth of 1-4 percent around the center frequency and efficiency of 40-70 percent [8]. Different approaches have been attempted to increase the bandwidth, such as using multi-layers of dielectric substrates with different permittivities [9, 10], loaded elements [11], and matching structures [12]. Nonetheless, these methods tend to increase the complexity and decrease the efficiency of the antenna.

It is well known that the bandwidth of the microstrip antenna can be improved simply by increasing the electrical thickness of the antenna. In addition, the fabrication tolerances are less critical with thicker substrates [13]. Furthermore, when the operating frequencies are high, even antennas with physically thin substrates become thick when compared to the wavelength. Unfortunately, higher order surface wave

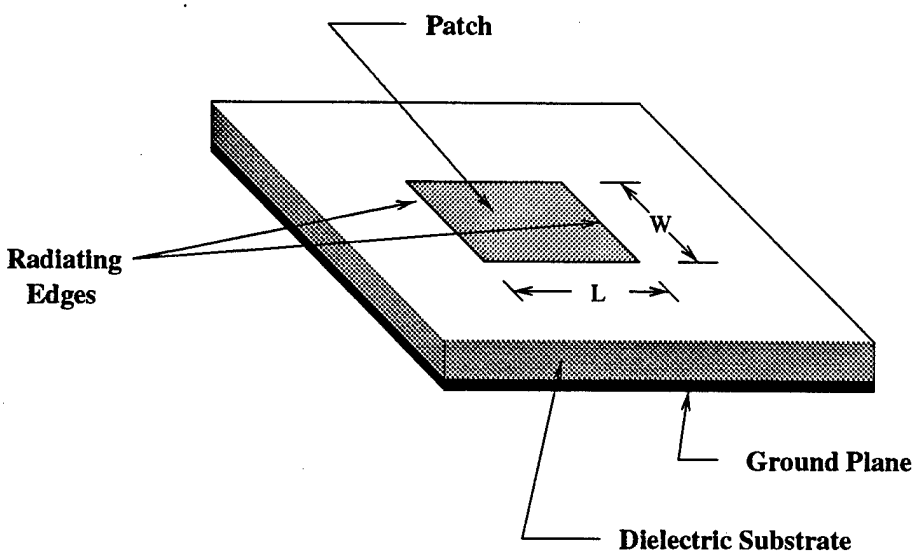

Figure 2.1: Rectangular microstrip antenna

modes are generated due to the increase in substrate thickness [5, 8]. This will in turn degrade the antenna performance. In this chapter, some issues and design procedures on electrically thick microstrip antennas are discussed.

2.2 Design Procedure

One of the most basic configurations for microstrip antennas is a resonant rectangular patch of metal mounted on the surface of a grounded dielectric substrate. The patch, which has resonant length L and width W as shown in Figure 2.1, is printed on a thin dielectric slab with thickness h and relative permittivity ϵ_r. Typical substrate thickness in the design of microstrip antenna is a small fraction of a wavelength ($0.003\lambda_o$ to $0.05\lambda_o$) so that the energy being couple into surface wave is negligible [14].

The design procedure provided by Bahl and Bhartia [5] is applied to design the antenna. The design equations are based on two empirical models (transmission line model and cavity model). These models have shown good accuracy in predicting the antenna performance for electrically thin microstrip antennas. As the substrate thickness increases, the accuracy of these models deteriorates. The failure is probably due to the fringing field effects and the presence of surface waves which are not properly accounted [3, 4]. However, these models give a good first-order solution to

the design problem. After obtaining an initial design from the design equations, a finite different time domain (FDTD) based full-wave analysis is applied to fine tune the design to obtain the desired antenna characteristics.

For an antenna with operating frequency, f_r, dielectric constant, ϵ_r, and thickness, h, the patch width (W) is given by the following equation,

$$W = \frac{c}{2f_r}\left(\frac{\epsilon_r + 1}{2}\right)^{-1/2} \tag{2.1}$$

where c is the velocity of light.

Other width lengths can also be chosen; however, antennas with widths smaller than W have lower efficiency. Antennas with widths larger than W may have higher efficiency, but higher order modes would result and distort the radiation pattern.

After obtaining the patch width, the patch length (L) is determined from the following expression,

$$L = \frac{c}{2f_r\sqrt{\epsilon_e}} - 2\Delta l \tag{2.2}$$

where ϵ_e is the effective dielectric constant and Δl is the line extension. The parameters ϵ_e and Δl are given by

$$\epsilon_e = \frac{\epsilon_r + 1}{2} + \frac{\epsilon_r - 1}{2}\left(1 + \frac{12h}{W}\right)^{-1/2} \tag{2.3}$$

$$\frac{\Delta l}{h} = 0.412\frac{(\epsilon_e + 0.3)(W/h + 0.264)}{(\epsilon_e - 0.258)(W/h + 0.8)} \tag{2.4}$$

Unlike the patch width, which can be chosen to be smaller or larger than the value obtained from (2.1), the patch length is an important parameter for obtaining the resonant frequency and input impedance matching. The effective dielectric constant takes into account the fact that the upper part of the microstrip antenna is usually air, so that the fringing field lines are in both the air and dielectric. Hence, the value of ϵ_e is usually larger than the dielectric constant of the air and smaller than the dielectric constant of the substrate. The extra term (Δl) in (2.2) also accounts for the fringing field effect. Since the fringing fields result in a larger effective length, the physical length L should be shorter to compensate such an extension (see (2.2)).

After obtaining the width and length of the rectangular microstrip antenna, the next step is to determine the feed location for optimum matching. The transmission line model is used to find such a location. The model is based on the radiation mechanism of the rectangular microstrip antenna. The radiation from microstrip antennas are contributed mainly from the fringing fields between the edge of the patch and the ground plane. The field distribution usually is uniform along the width and varies along the patch length. Therefore, the rectangular patch behaves as two slots separated by a transmission line with length L.

The input admittance, $Y_1(y)$, obtained from the above model is given as

$$Y_1(y) = 2G\left[\cos^2(\beta y) + \frac{G^2+B^2}{Y_o^2}\sin^2(\beta y) - \frac{B}{Y_o}\sin(2\beta y)\right] \tag{2.5}$$

where the parameter y is the position along the length of the patch and the various terms in the equation are defined in the following expressions. The conductance G is given by $G = G_{11} \pm G_{12}$, where G_{11} is the self conductance and G_{12} is the mutual conductance. The plus sign corresponds to the odd modes and the minus sign to the even modes. The self conductance is given by

$$G_{11} = \frac{I_1}{120\pi^2} \tag{2.6}$$

with I_1 as

$$I_1 = \int_0^{\pi} \sin^2\left(\frac{k_o W\cos\theta}{2}\right)\tan^2\theta\sin\theta d\theta \tag{2.7}$$

where k_o is the free space propagation constant. The mutual conductance G_{12} between the two radiating ends is given by the following expression.

$$G_{12} = \frac{1}{120\pi^2}\int_0^{\pi} \sin^2\left(\frac{\pi W\cos\theta}{\lambda_o}\right)\tan^2\theta J_o\left(\frac{2\pi L}{\lambda_o}\sin\theta\right)d\theta \tag{2.8}$$

where $J_o(x)$ is the Bessel function of order zero and argument x. The expression for the susceptance B is

$$B = Y_o k_o \Delta l\sqrt{\epsilon_e}\ . \tag{2.9}$$

The characteristic admittance (Y_o), for the case when $W/h \geq 1$ and assuming an infinitesimally thin conductor ($t \sim 0$), is

$$Y_o = \frac{\sqrt{\epsilon_e}}{120\pi}\left[\frac{W}{h} + 1.393 + 0.667\ln\left(\frac{W}{h} + 1.444\right)\right]\ . \tag{2.10}$$

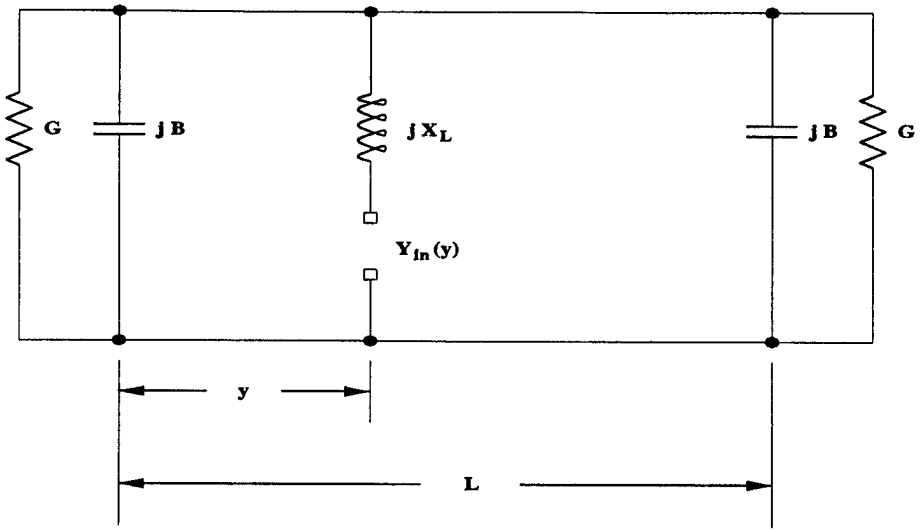

Figure 2.2: The equivalent circuit for a patch element including probe effect

And the propagation constant β is given by

$$\beta = \frac{2\pi\sqrt{\epsilon_e}}{\lambda_o} . \tag{2.11}$$

A coaxial-probe feed and a microstrip-line feed are two common ways of feeding a microstrip antenna. Here, the microstrip antenna is fed by a coaxial line. The center conductor of the cable is attached to the patch, while the outer conductor line is attached to the back side of the printed circuit board. It is shown that this feed mechanism introduces an inductive reactance X_L in series to the radiating elements [9]. When the thickness of the substrate is electrically thin, this feed reactance is small compared to the resonant resistance. However, for thicker substrates, the feed reactance become larger and needs to be taken into account. The feed reactance is given by

$$X_L = \frac{377}{\sqrt{\epsilon_r}} \tan(\frac{2\pi h}{\lambda_o}) \tag{2.12}$$

The final expression for the input admittance $Y_{in}(y)$ at any location along the length taking X_L into account is given as follows:

$$Y_{in}(y) = Y_1(y) + jX_L . \tag{2.13}$$

The equivalent circuit for this model is shown in Figure 2.2.

Finally, a FDTD algorithm is applied to fine tune the antenna to the desired resonant frequency. In general, the patch length calculated from the design equations is a little longer than the patch length calculated from the FDTD program. The feed location obtained from FDTD method is also more accurate. However, it is computationally more expensive to use the FDTD algorithm than the above simple design equations. The measurement results of the S_{11} parameter and the input impedance are shown in Figure 2.3 and 2.4, respectively.

2.3 2-D Magnetic Line Source Model

Two magnetic dipoles are often used to model the two radiating edges of a linearly polarized patch antenna [5, 14, 15]. This three dimensional model predicts the antenna patterns very well in both E- and H- planes. However, three dimensional models are often computationally expensive. In addition, the diffracted surface waves are stronger in the E-plane than in the H-plane. Hence, it is more important to control the surface wave diffractions in the E-plane.

A two-dimensional model can be very useful and effective for studying the more complex rectangular microstrip antenna if one considers the radiation patterns in the E-plane for a linearly polarized antenna [16]. Equivalent electric and magnetic current sources, $\vec{J}$ and $\vec{M}$, can be used to replace the radiating patch to determine the far field antenna pattern.

In the E-plane, which is the plane of interest, the radiating patch can be replaced by two in-phase magnetic current sources to obtain the far field pattern as shown in Figure 2.5. The pattern is calculated with the General 2D Moment Method Code (G2DMM), a 2-D method of moment code developed at the Ohio State University. Note that the G2DMM is an extension of the General Cylinder Code (GCYL) also developed at the Ohio State University [17]. A comparison between a calculated result from the 2-D model and a measured result is shown in Figure 2.6. The calculated result shows good agreement with the measurement. The result in Figure 2.6 demonstrates that two magnetic line sources are a good model for the E-plane radiation pattern when the patch is operating in the TM_{10} mode.

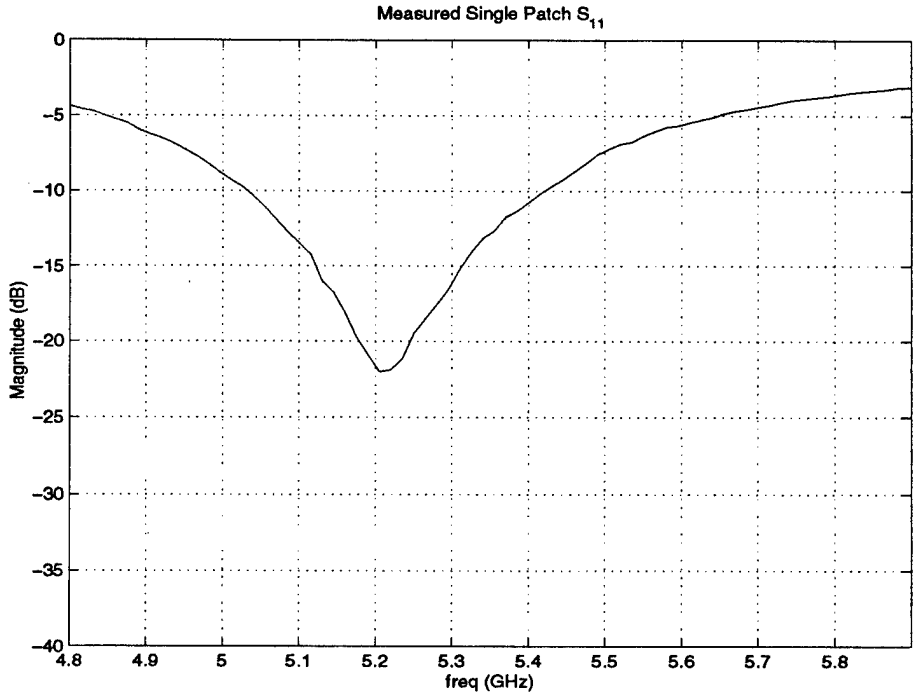

Figure 2.3: S_{11} of the patch antenna - Measured Result

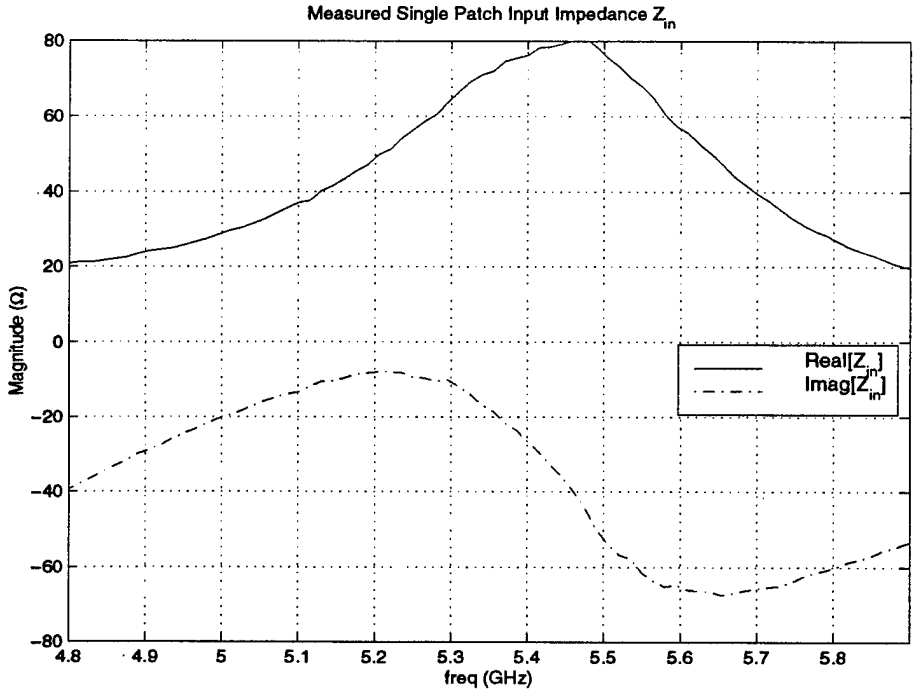

Figure 2.4: Input impedance Z_{in} of the patch antenna - Measured Result

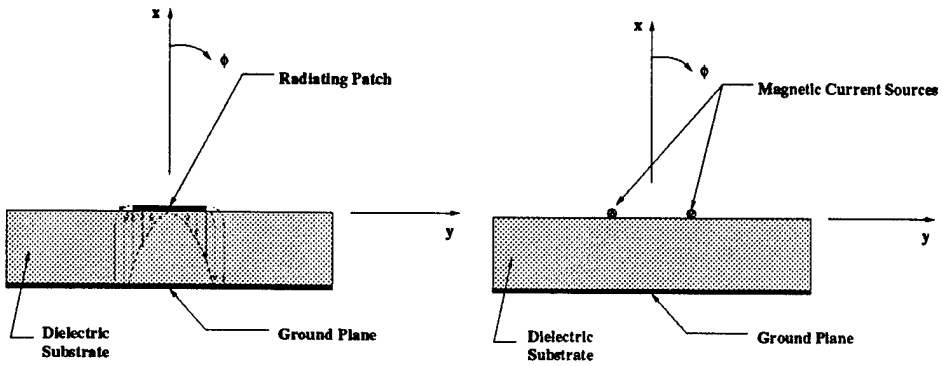

(a) Field (b) Model

Figure 2.5: 2-D model (E-Plane) of a patch antenna

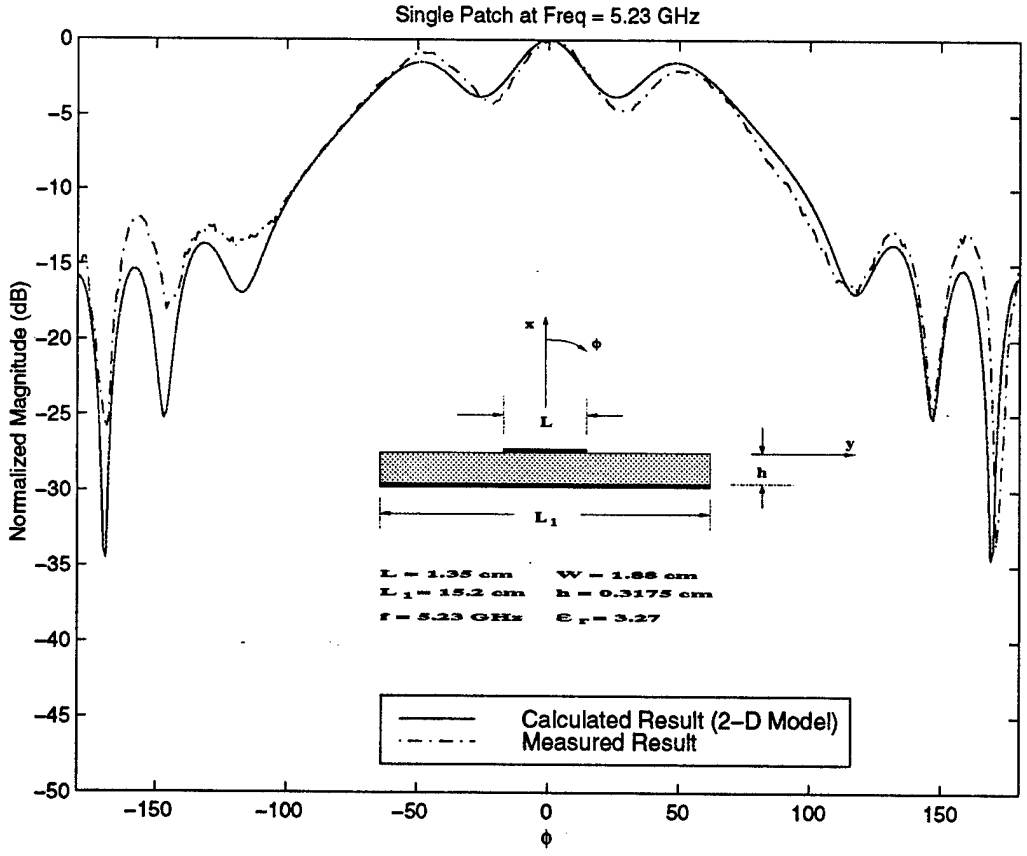

Figure 2.6: E-Plane pattern of the patch antenna at f = 5.23 GHz

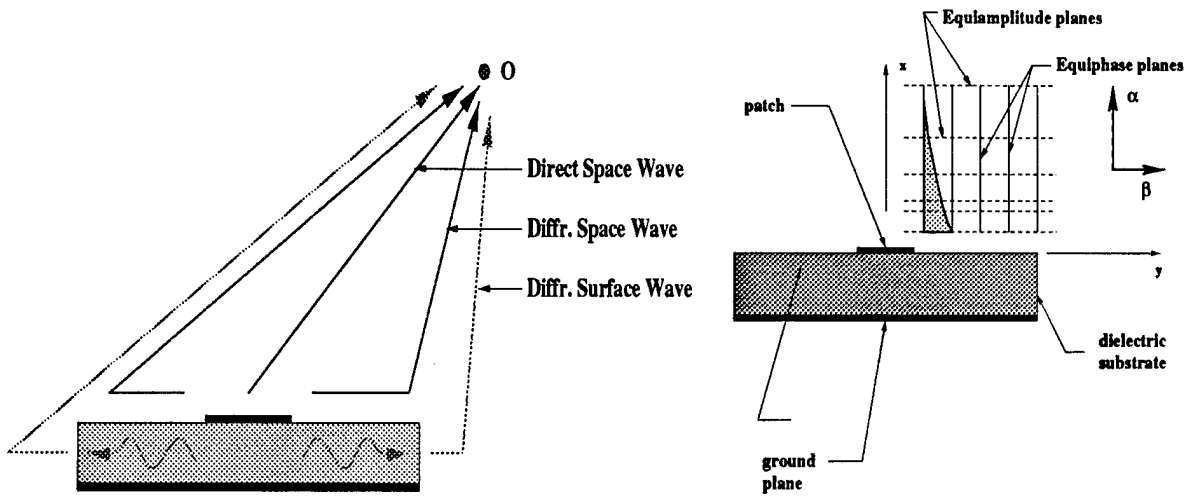

(a) Radiation mechanism

(b) Surface wave

Figure 2.7: Various field components for a microstrip antenna

2.4 Surface Waves

The far field of a typical microstrip antenna contains three field components as shown in Figure 2.7(a) [16]. The direct space wave is the radiated field that travels directly from the patch to the observation point O without interacting with the edge of the dielectric substrate. The diffracted space wave is the diffracted field of the space wave due to the presence of the edge. Surface waves are excited on the air-dielectric interface due to the grounded dielectric substrate as shown in Figure 2.7(b). The diffracted surface wave is the diffracted field of the surface wave due to the truncation of the dielectric substrate.

When the substrate is electrically thin, the main contribution to the antenna pattern is coming from the direct space wave and the diffracted space wave. The surface wave is weak and hence, the diffracted surface wave is almost negligible. However, this diffracted space wave becomes weaker as the total antenna length increases, because this field diverges spatially and gets weaker as the distance between the patch and the edge increases.

When the substrate is electrically thick, the diffracted surface wave becomes stronger and has a dominant contribution on the total field. In addition, the surface

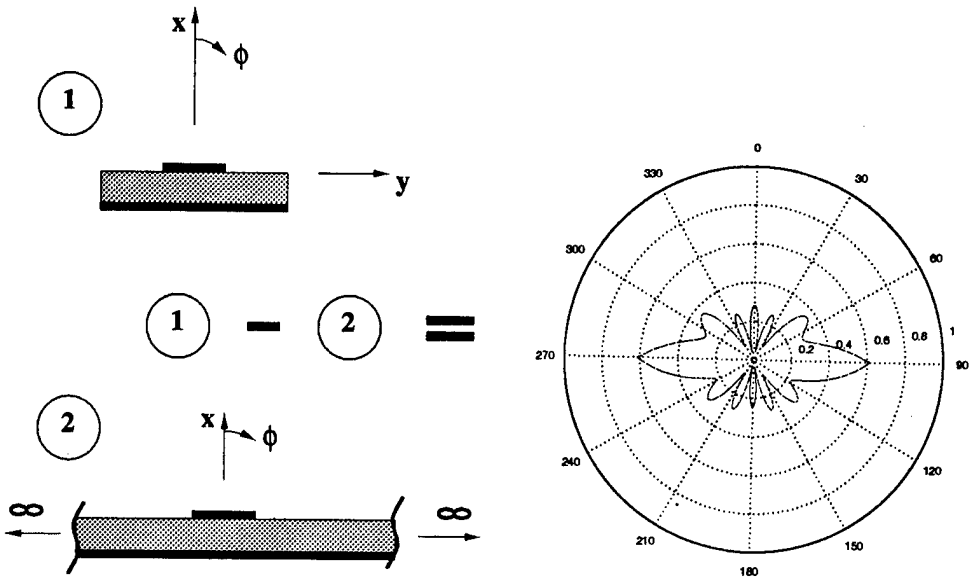

Figure 2.8: Diffracted surface wave field of the patch antenna

wave does not attenuate (if the substrate is lossless), so that the diffracted surface wave is always present. Hence, the diffracted surface wave cannot be decreased by simply increasing the length of the substrate.

A good way to study the surface wave diffraction is to separate the diffracted surface wave from the total field as shown in Figure 2.8. This is done by subtracting the pattern of the infinite grounded dielectric substrate pattern from the pattern of the microstrip antenna. The far field ($k_o\rho \rightarrow$ large) expression for the two magnetic line sources separated by $\lambda_d/2$ radiating in the presence of the infinite grounded dielectric substrate is given by

$$E_\phi(\rho,\phi) \simeq -\frac{1}{\eta_o}\sqrt{\frac{j2k_o}{\pi}}\left[\frac{cos(\frac{k_o\lambda_d}{4}\sin\phi)}{1+j\frac{k_x\tan(k_xh)}{\epsilon_r k_o\cos\phi}}\right]\frac{e^{-jk_o\rho}}{\sqrt{\rho}} \qquad \text{for } -\pi \le \phi \le \pi \tag{2.14}$$
$$= \quad 0 \qquad\qquad \text{otherwise}$$

with

$$k_x = k_o\sqrt{\epsilon_r - \sin^2\phi} \tag{2.15}$$

where η_o is the intrinsic impedance of free space, k_o is the phase constant, and λ_d is the wavelength in dielectric. A typical resultant diffracted surface wave field is shown in the right hand side of Figure 2.8. It is clear that the surface wave diffracts most

strongly in the end-fire directions and does not contribute to the main-beam pattern. As the electrical thickness of the antenna increases, more energy is being coupled into surface wave and hence results in a stronger diffracted surface wave field. This not only decreases the efficiency of the antenna, but often distorts the main-beam pattern (i.e. the ripples in the main-beam of the antenna pattern in Figure 2.6).

In general, both TM and TE surface wave modes can be excited for a grounded dielectric substrate. The cutoff frequency of these surface wave modes is given as follow [5],

$$f_c = \frac{nc}{4h\sqrt{\epsilon_r - 1}} \tag{2.16}$$

where c is the speed of light, and $n = 0, 1, 2, 3, \ldots$ for the TM_0, TE_1, TM_2, TE_3 ... surface mode. Since the lowest order surface wave (TM_0) has a zero cutoff frequency, this mode is always present in the substrate regardless of the values of the substrate thickness and relative dielectric constant. On the other hand, by choosing thin and low dielectric constant substrate, the higher order surface wave modes can be made non-propagating. Unfortunately, thin substrate microstrip antennas have a narrow bandwidth, and low dielectric constant microstrip antennas require large patch size to obtain desired resonant frequency. These limit the design of microstrip antennas.

2.5 Bandwidth and Efficiency

Most microstrip antennas have narrow bandwidth (typically a few percent). It is shown that as the substrate thickness increases, the bandwidth of patch elements increases [14].

$$\mathrm{BW} = \frac{\mathrm{VSWR} - 1}{Q\sqrt{\mathrm{VSWR}}} \tag{2.17}$$

Power loss is mainly due to metal loss and some dielectric loss in thin microstrip antennas. However, both the metal loss and dielectric loss decrease rapidly as the substrate thickness increases [18]. Since the fields are more concentrated for thin substrate than that for thick substrate, so that dielectric loss is higher in thin substrate antennas than it is in thick substrate antennas. Hence, the dielectric loss is ignored in

calculating the radiation efficiency. At the same time, a slowly increasing amount of power is loss due to surface waves, which reduces the radiation efficiency. In general, surface wave power is launched in the end-fire direction and would not contribute to the main-beam radiation, so that it can be viewed as a loss mechanism. A radiation efficiency is then defined as [18]

$$\eta = \frac{P_{rad}}{P_{rad} + P_{sw}} \tag{2.18}$$

where P_{rad} is the power radiated in the main-beam direction, and P_{sw} is the power coupled into surface waves. Thus, $P_{rad} + P_{sw}$ is the total power input into the patch. Note that η is independent of the feed location of the patch and the patch width W. Hence, the antenna efficiency can be increased by decreasing the surface wave power loss.

Chapter 3

Microstrip Antenna with Parasitic Strips

3.1 Introduction

The excitation of the surface wave modes is often considered to be a disadvantage in many microstrip antenna applications. The surface wave power is treated as a loss mechanism when calculating the radiation efficiency, because most surface are waves generally difficult to control and are not radiated in the main-beam direction, but in the direction parallel to the air-dielectric interface. For electrically thin microstrip antennas, this surface wave power is small and can be neglected. However, when the antenna becomes electrically thick, more power is lost because the strength of surface waves increases and more surface wave modes are excited. In general, these waves have a detrimental effect on the performance of printed antennas.

In this chapter, a scheme shown in Figure 3.1 for controlling these surface waves is presented. Metal strips are being added along the surface of the substrate. Due to the presence of the metal strips, surface waves are converted to leaky waves, so that energy leaks out along the surface and the waves become very weak by the time they reach the edge of the substrate. Thus, the edge diffraction is decreased. In addition, the radiated leaky wave fields can have a positive contribution to the main-beam (if designed properly), and hence, improve the antenna efficiency.

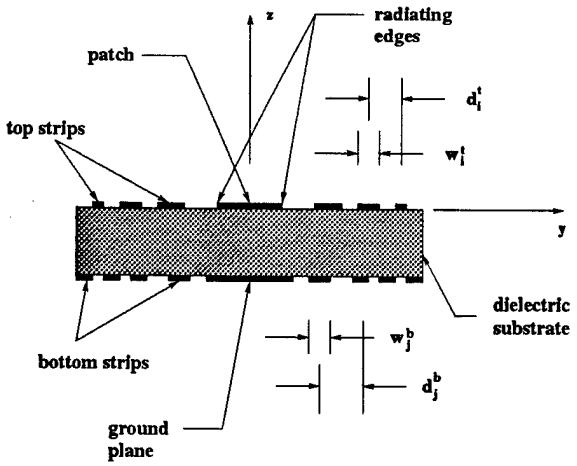

Figure 3.1: Microstrip antenna with parasitic strips (2-D)

3.2 2-D Modeling

A two-dimensional model is used to investigate the antenna behavior, see Figure 3.2. The radiating patch is replaced by two in-phase magnetic current sources. The far field antenna (E-plane) pattern is then obtained from those two magnetic current sources radiating in the presence of the metal strips. It is found that the calculated antenna patterns obtained from this two dimensional model have good agreement with the measured patterns as discussed in Chapter 4. Unfortunately, the model fails to predict the correct frequency range of the transition region (between surface wave and leaky wave). This is becasue the transition region depends both on the length and width of the metal strips. However, the two dimensional model assumes the strip length is infinite in the z-direction. Although the two dimensional model fails to predict the exact frequency range of the transition region, it does predict the general behavior of the antenna. Hence, it is a very useful and effective tool for studying the radiation mechanism of the microstrip antenna examined here.

3.3 Radiation Mechanism

The field behavior of the antenna can be separated into three distinct regions as frequency changes. At low frequency range, the strips do not have significant effects on the antenna radiation. Similar to the radiation mechanism of the single patch

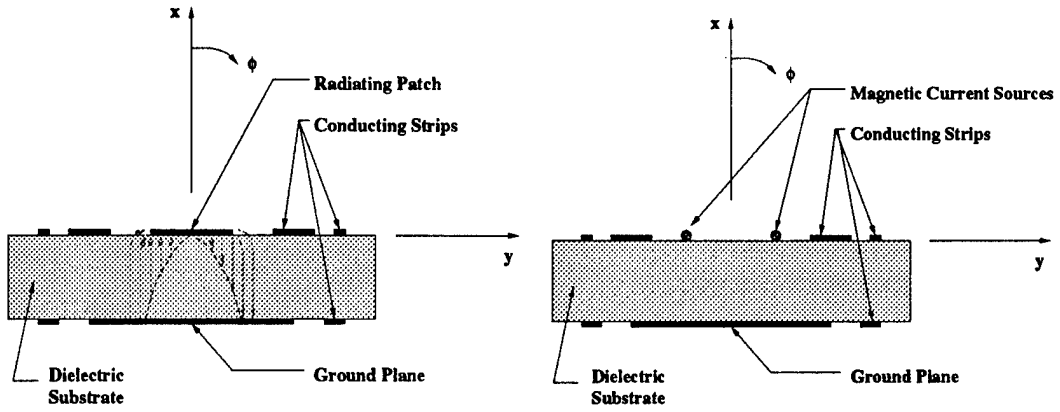

(a) Field (b) Model

Figure 3.2: 2-D model (E-Plane) of the patch antenna with parasitic strips

microstrip antenna, the antenna pattern is mainly combinations of the direct source field, the diffracted surface wave field, and the diffracted space wave field. The metal strips and the dielectric substrate act like a surface wave guiding structure.

At high frequency range, the metal strips and the dielectric region supports the forward propagating leaky wave. As the wave progresses along the region from the radiating edge of the patch to the termination of the dielectric, a small amount of energy leaks out of every opening (between strips), so that only a negligible field is left at the truncation. Thus, the total field of the antenna is the combination of the direct source field, the leaky wave field, and the edge diffracted field as shown in Figure 3.3.

The frequency range between the low and high frequencies is the transition region between surface wave and forward leaky wave. As discussed in above, the structure supports surface waves initially. When the frequency is increased sufficiently, these surface waves becomes leaky waves and propagate in the backward (back-fire) direction. As the frequency is increased further, a forward propagating leaky wave arises. At this time, the energies are leaking out in both the forward and backward direction, and hence, the edge diffraction is very small. However, the backward leaky wave increases the diffraction in its direction. Finally, when the frequency is increased to the high frequency region, the forward leaky wave becomes dominant and less energy is

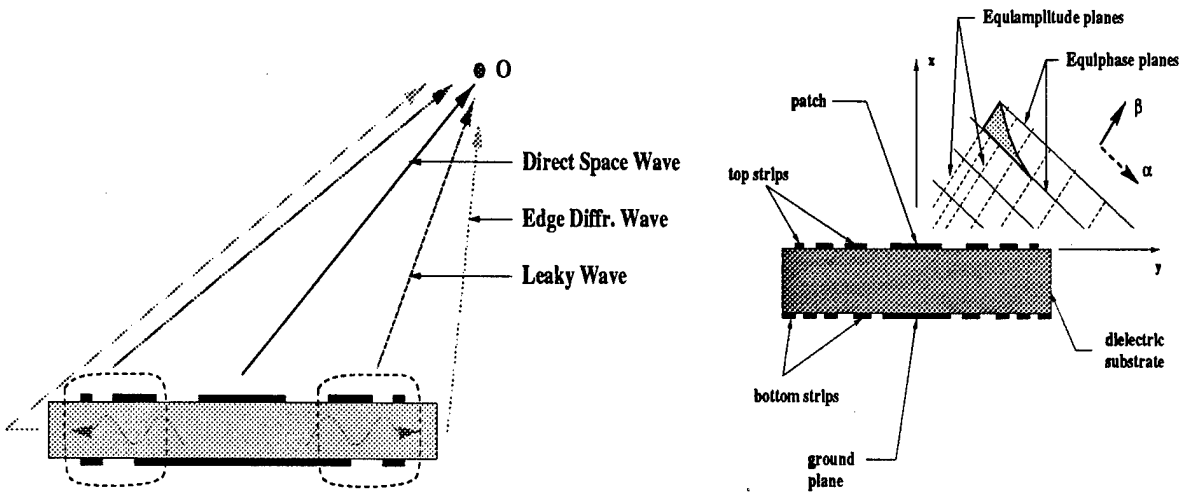

(a) Radiation mechanism

(b) Leaky wave

Figure 3.3: Various field components of microstrip antenna with parasitic strips

leaking in the backward direction. Note that the low to high frequency ranges depend on the antenna pattern bandwidth. Low frequency range means the lower frequencies relative to the pattern bandwidth, and *vice versa*.

3.4 Single Strip Effects

In order to study how the strip parameters affect the field behavior of the antenna, an analysis scheme is presented in Figure 3.4. First, it is necessary to know whether the strip affects the diffracted field. Second, it is important to understand how the strip affects the total diffracted field.

In Figure 3.4(a), the total diffracted field is obtained by subtracting the source field, which is the field of the patch radiating in the presence of an infinite grounded substrate, from the total field of the antenna. The scheme shown in Figure 3.4(b) isolates the effect of the strip on the field behavior of the antenna. This is done by subtracting the field of the finite substrate microstrip antenna from the field of the same antenna without the strip.

Even thought the configuration, shown in Figure 3.1 has strips both on top and on the bottom of the substrate, it is found that the first pair of strips closest to the

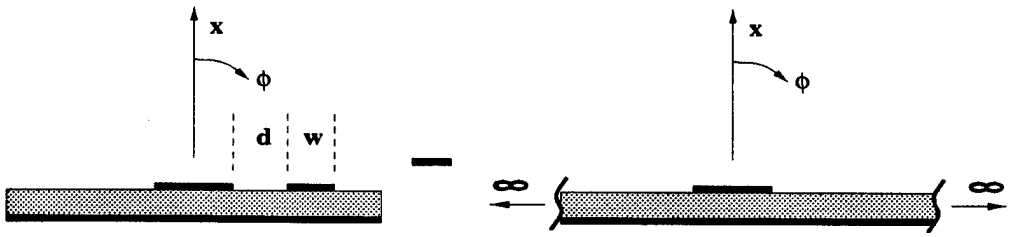

(a) Total diffracted field

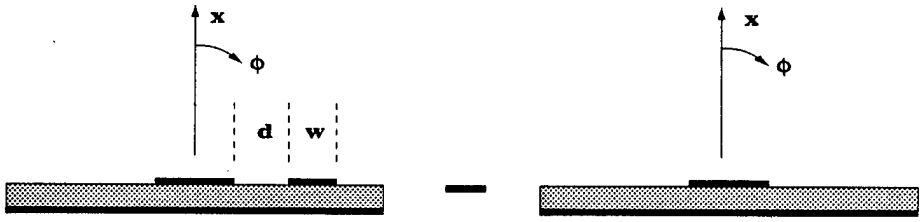

(b) Strip effects

Figure 3.4: Strip analysis schemes

radiating patch have the dominant effects on the antenna radiation. The effects from other strips are of secondary nature. Thus, studying the effects of a single strip or a pair of strips on the patch antenna can give a fairly general idea on the behavior of the antenna with many strips. In the following sections, the effects of various strip parameters on the antenna performance are investigated, namely, strip width, strip length and strip distance from patch.

3.4.1 Parameter Study - Strip Width

The width of the strip is the most critical parameter in determining its behavior and its effect on the patch antenna. Following the two analysis schemes depicted in Figure 3.4, Figure 3.5 is generated by varying the strip width from $0.75\lambda_d$ to $0.90\lambda_d$ at a fixed distance ($0.4\lambda_d$) from the radiating edge of the patch. The parameter λ_d is the wavelength in the dielectric at the design frequency. The design frequency is 5.23 GHz and the relative dielectric constant ϵ_r is 3.27 for all the different cases presented in this report.

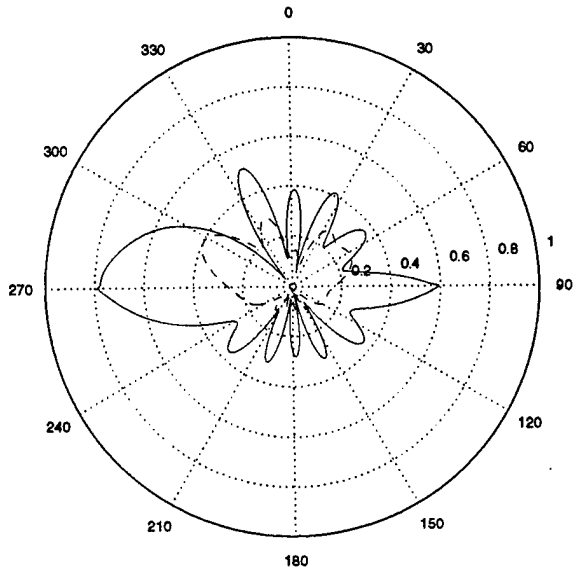

(a) d=0.4λ_d, w=0.75λ_d

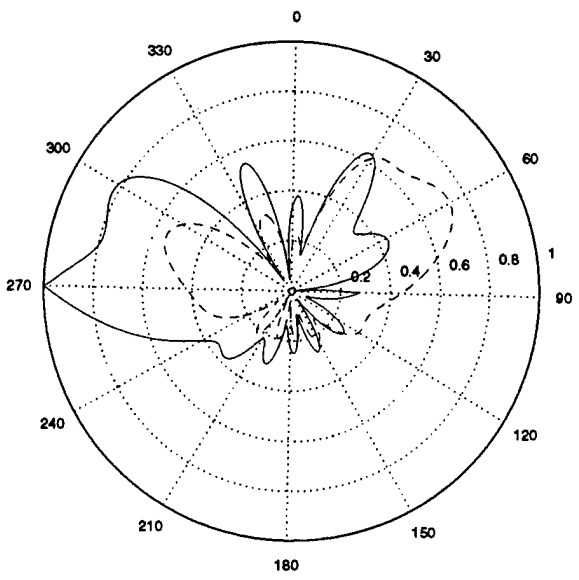

(b) d=0.4λ_d, w=0.80λ_d

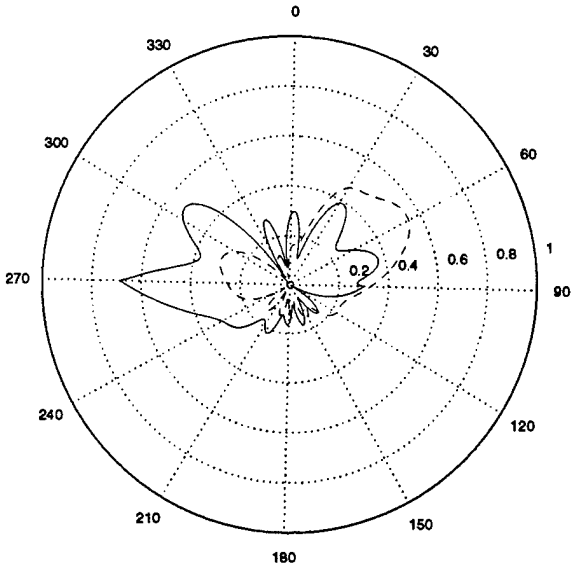

(c) d=0.4λ_d, w=0.85λ_d

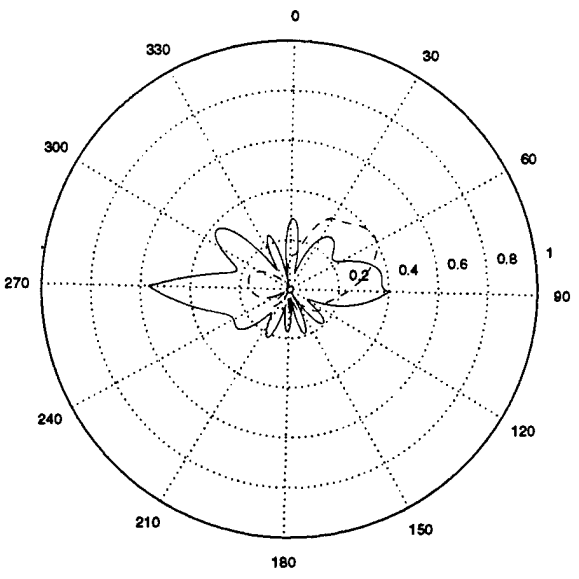

(d) d=0.4λ_d, w=0.90λ_d

Figure 3.5: Parametric study of strip width effects (single strip case): solid line - total diffracted field, dash line - strip effects

When the strip is electrically thin ($\leq 0.5\lambda_d$), the strip has little effect on the surface wave of the antenna. The diffracted fields are mainly from the surface wave diffraction. As the strip width increases, a backward leaky wave beam arises due to the presence of the strip as shown in Figure 3.5(a). In addition, the total diffracted field is increased in the 270° region (comparing to the diffracted field without any strip as shown in Figure 2.8) due to this backward propagation leaky wave.

When the strip width is increased further, a strong forward leaky wave beam arises and co-exists with the backward leaky wave beam as in Figure 3.5(b). Note that the total diffracted field is very small in the 90° region, but it is very strong in the opposite direction. This is because a large amount of energy has leaked out to free space, and hence, the edge diffraction due to the truncation of the dielectric slab (in the forward end) is small. However, other than the diffracted field in the 90° direction, the total diffracted field in the first quadrant ($0° \leq \phi < 90°$) increases. Again, the backward leaky wave field causes a strong diffracted field in the 270° region.

As the strip width increases from $0.8\lambda_d$ to $0.85\lambda_d$ (Figure 3.5(c)), the total diffracted field decreases. This is because the strength of both the forward and backward leaky wave fields has decreased. Nonetheless, the forward leaky wave field is still relatively strong even though the backward leaky beam reduces by a significant amount. Further increase of the strip width causes the two leaky wave fields to decrease even more as observed in Figure 3.5(d). The reduction of the leaky wave beam in the forward direction increases the diffracted field in the 90° direction. Overall, the total diffracted field is less than the diffracted field without the strip (Figure 2.8) in the 90° direction after the excitation of the forward leaky wave field.

3.4.2 Parameter Study - Strip Distance

Unlike the strip width which controls the excitation of the leaky wave modes, the distance of the strip from the radiating patch controls the leaky wave propagation direction. Again following the two strip analysis schemes introduced in Figure 3.4, Figure 3.6 is generated by varying the distance of the strip from the radiating edge from $0.5\lambda_d$ to $0.8\lambda_d$ and with a fixed strip width ($0.85\lambda_d$).

Observing Figure 3.6(a) through 3.6(d), the forward leaky wave beam moves toward broadside as the separation between the patch and the strip increases. However, the strength of the leaky wave beam does not change significantly, only reduces in a small amount. Also note that, the total diffracted field (in the 270° region) first decreases when the separation distance is increased from $0.5\lambda_d$ to $0.6\lambda_d$. Then when the distance increases further, the diffracted field increases.

In the next section, the two parameters are again examined. However, a pair of metal strips is added (one on each side of the patch). After investigating the effects of one strip, the behavior of the antenna due to the pair of strips is easier to understand.

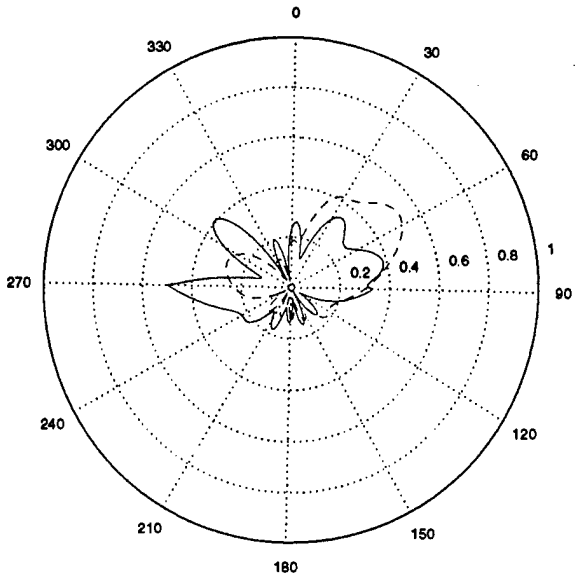

(a) d=0.5λ_d, w=0.85λ_d

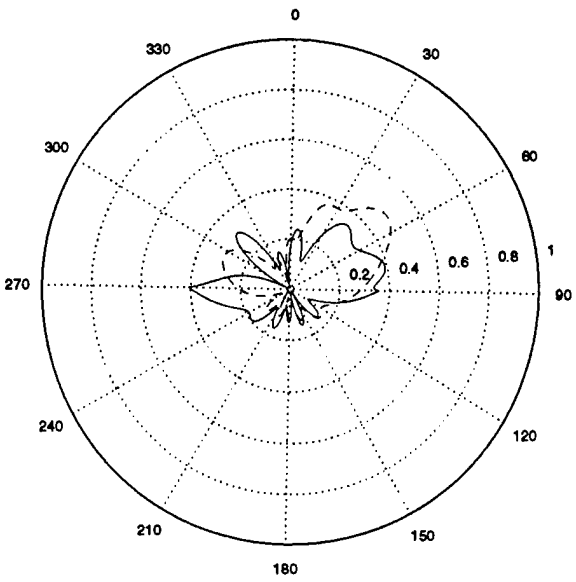

(b) d=0.6λ_d, w=0.85λ_d

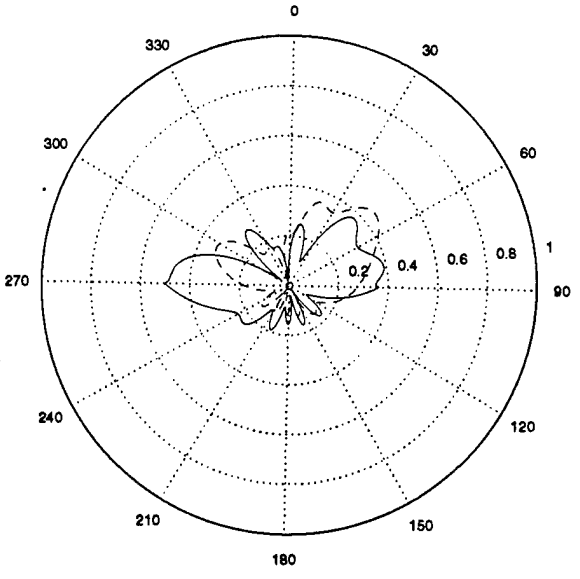

(c) d=0.7λ_d, w=0.85λ_d

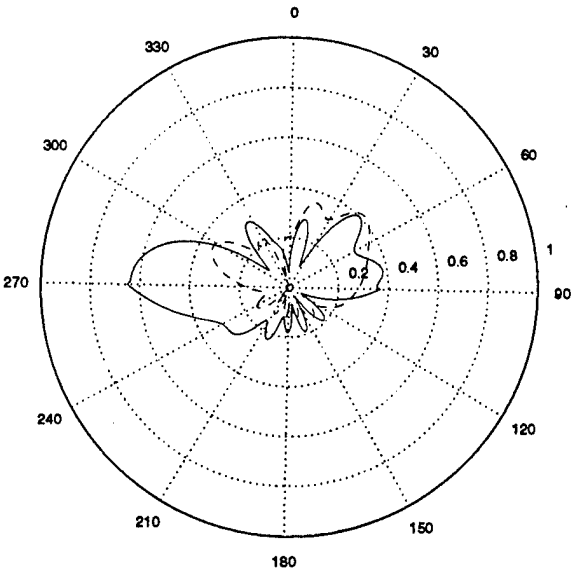

(d) d=0.8λ_d, w=0.85λ_d

Figure 3.6: Parametric study of strip distance effects (single strip case): solid line - total diffracted field, dash line - strip effects

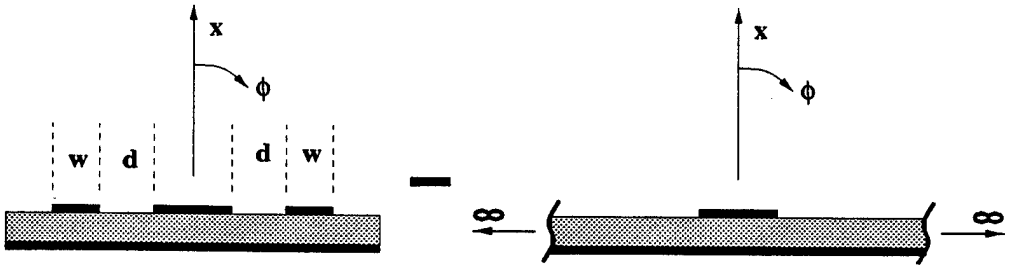

(a) Total diffracted field

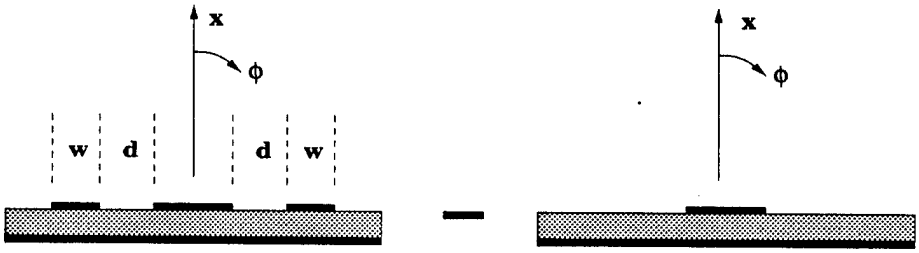

(b) Strip effects

Figure 3.7: Pair strip analysis scheme

3.5 Strip Pair Effects

As in the previous section, the analysis schemes to be used in this section are shown in Figure 3.7. In this case, the effect of a pair of strips, one on each side of the patch, is examined. As expected, the diffracted field due to the presence of the two strips is different from the diffracted field in the one strip case. Moreover, antenna patterns for different cases are also plotted.

3.5.1 Parameter Study - Pair Strip Width

In Section 3.4.1, a parametric study of the width of a single metal strip near the patch antenna was carried out. However, to obtain a symmetric pattern, a pair of strips is needed. In addition, the field behavior due to the two strips results in a different diffracted field.

As before, when the strips are electrically thin, the diffracted field does not change significantly. The main contribution to the diffracted field is still the surface wave diffracted field. As the width increases (single strip case), a backward leaky wave field arises and increases the total diffracted field in the 270° region. The increase of the diffracted field strength is also observed for the two strip case as shown in Figure 3.8(a) when $w = 0.75\lambda_d$. Also, three strong diffracted beams are observed due to the interaction of the fields. These three diffracted beams significantly distort the main-beam of the antenna as shown in Figure 3.9. Note that in this case the side lobe level is higher due to the addition of the strips.

Two very strong leaky wave beams are excited as the width of the strips increases from $0.75\lambda_d$ to $0.8\lambda_d$ as depicted in Figure 3.8(b). From Figure 3.10, it is clearly shown that the main-beam of the antenna pattern is distorted due to these two strong beams. One the other hand, the diffracted fields in the 90° and 270° regions are smaller than the case where w equals $0.75\lambda_d$.

When the strip width is increased further, the total diffracted field becomes small (Figure 3.8(c) and (d)). The two diffracted beams (along the 30° and 330° directions) add in phase (constructive interference) to the main-beam of the antenna pattern. The resultant antenna pattern has a fairly "flat-top" main-beam and low side lobes level as shown in Figure 3.11 and Figure 3.12.

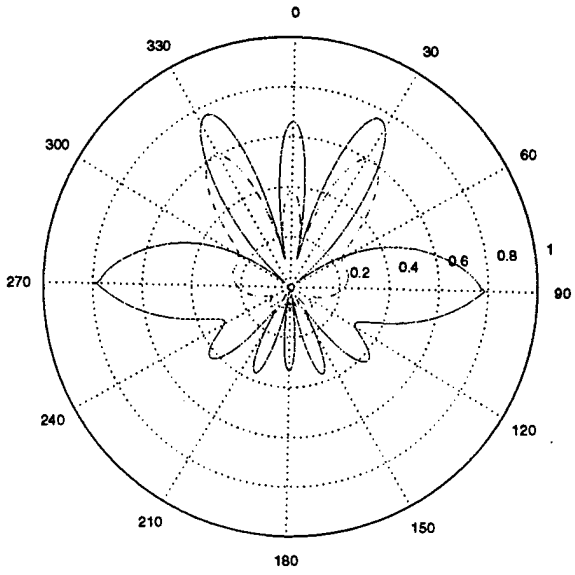

(a) d=0.4λ_d, w=0.75λ_d

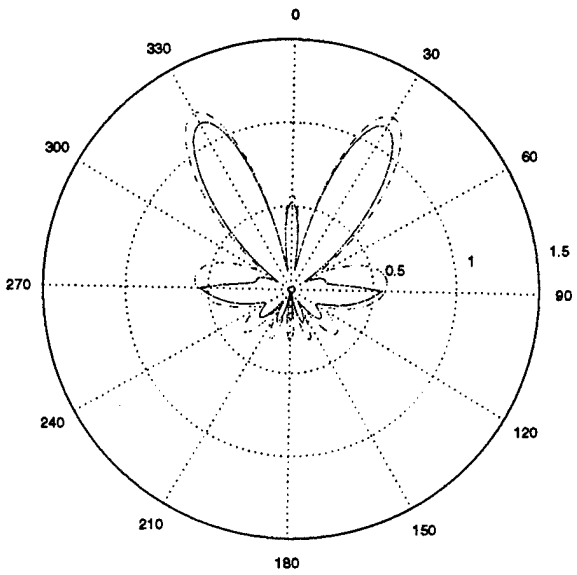

(b) d=0.4λ_d, w=0.80λ_d

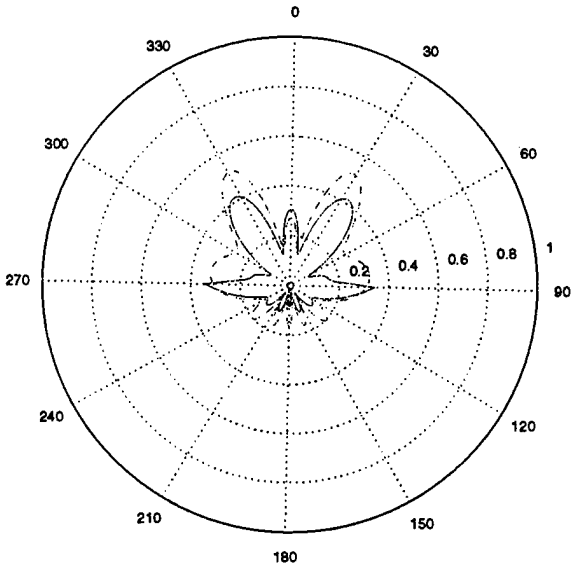

(c) d=0.4λ_d, w=0.85λ_d

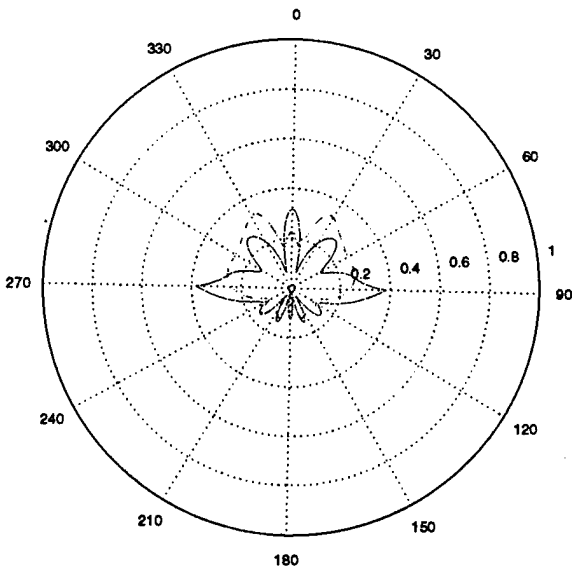

(d) d=0.4λ_d, w=0.90λ_d

Figure 3.8: Parametric study of strip width effects (two strip case): solid line - total diffracted field, dash line - strip effects

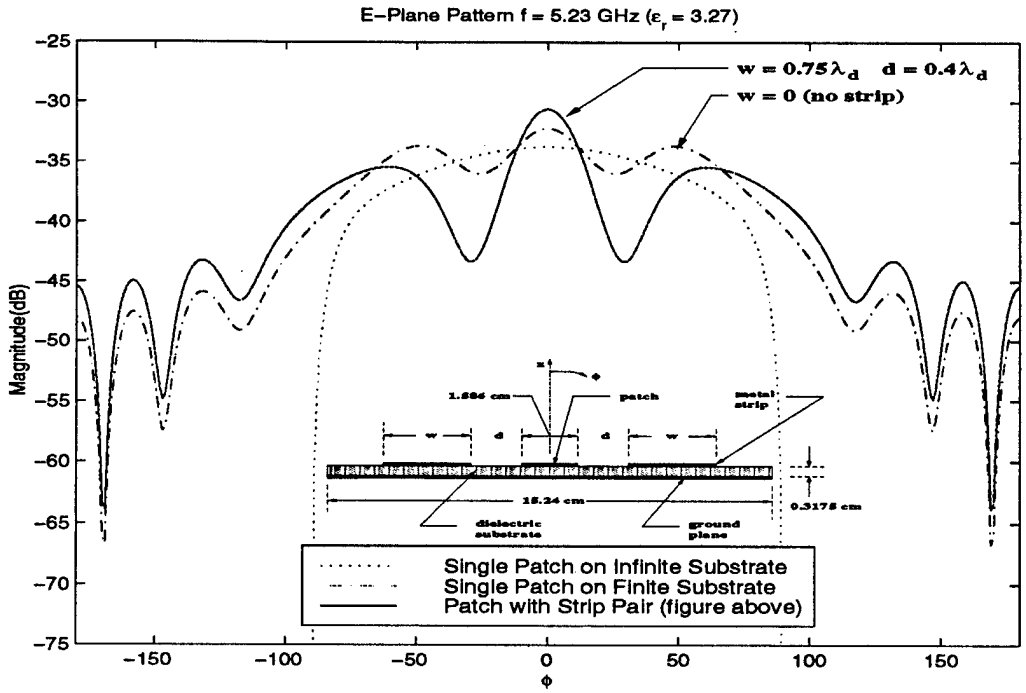

Figure 3.9: Two-strip antenna E-Plane pattern: d=0.4λ_d, w=0.75λ_d

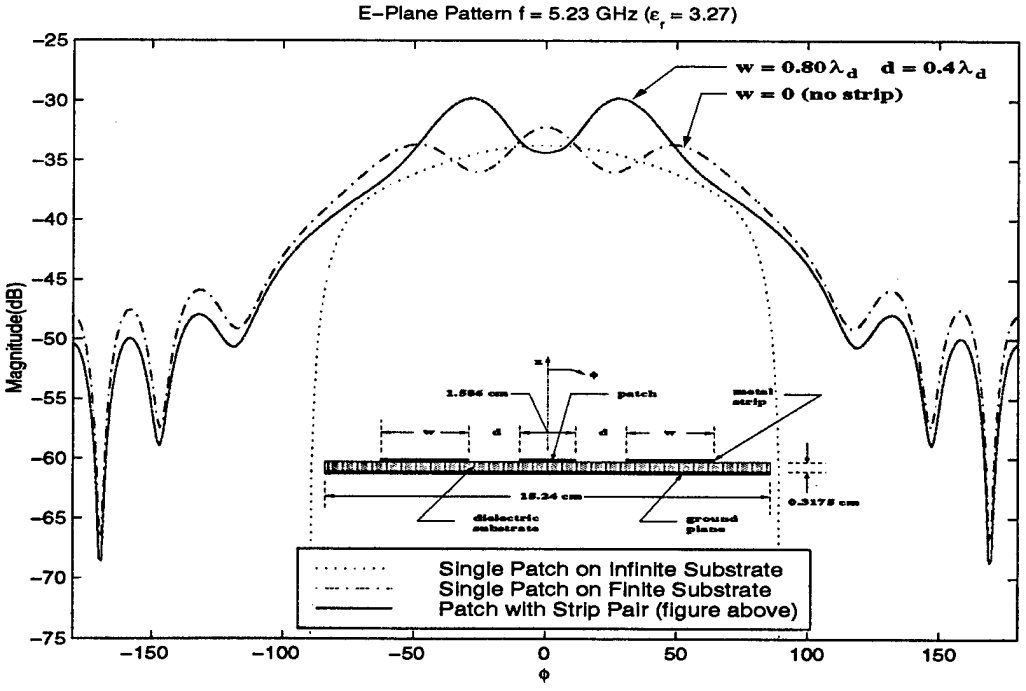

Figure 3.10: Two-strip antenna E-Plane pattern: d=0.4λ_d, w=0.8λ_d

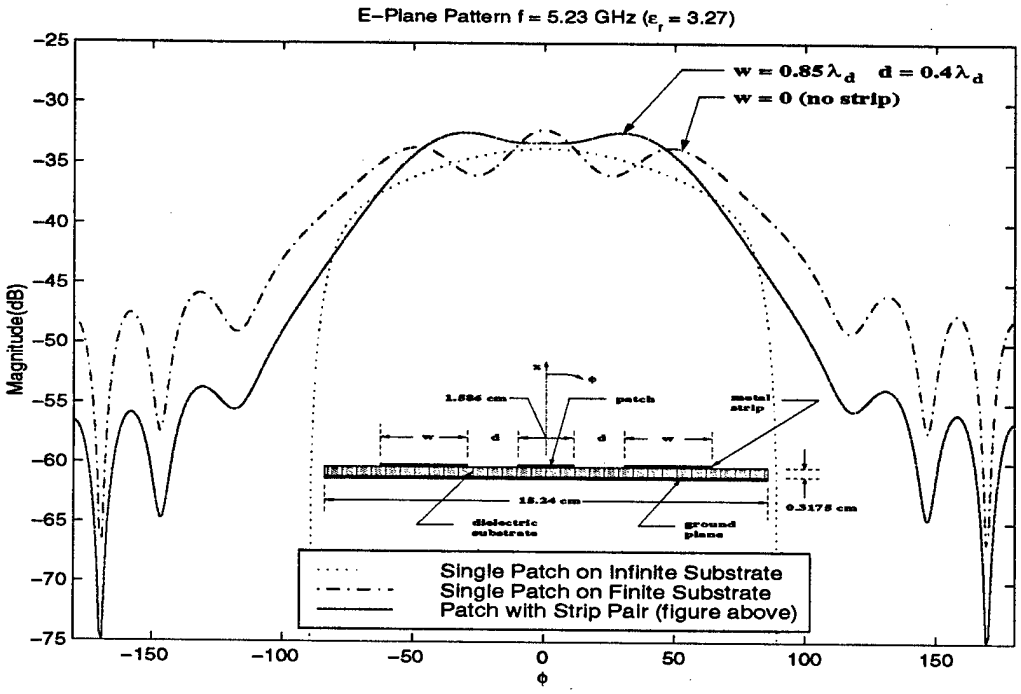

Figure 3.11: Two-strip antenna E-Plane pattern: d=$0.4\lambda_d$, w=$0.85\lambda_d$

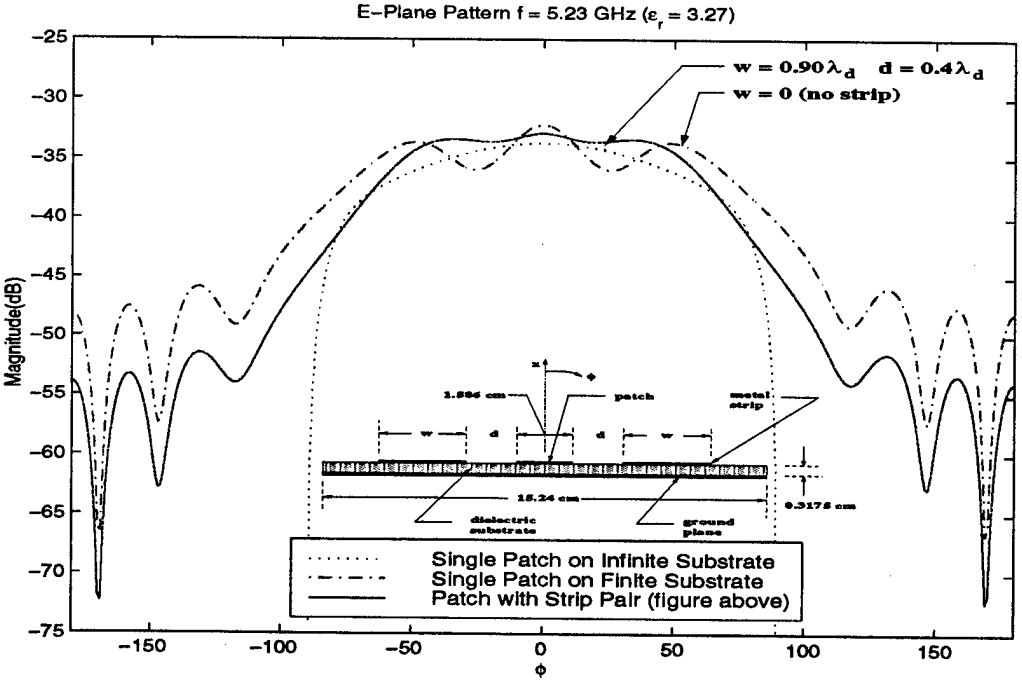

Figure 3.12: Two-strip antenna E-Plane pattern: d=$0.4\lambda_d$, w=$0.9\lambda_d$

3.5.2 Parameter Study - Pair Strip Distance

In this section, the effect of the distance of the pair strips on the field behavior of the antenna is studied. The result is different from the single strip case.

In the single strip case, this parameter controls the leaky wave beam direction without significant change in the field strength. For the two strip case as shown in Figure 3.13, the general "shape" (direction of diffracted field and null locations) of the total diffracted field does not change significantly, but the strength of the diffracted field increases as the strips are moved further away from the patch.

The antenna patterns for the four different cases shown in Figure 3.13 are plotted in Figures 3.14 through 3.17, respectively. Although the total diffracted field increases as the distance increases, the side lobes of the pattern remain small while the beamwidth of the main-beam increases. Note that for the case when d is equal to $0.8\lambda_d$, the beamwidth is larger than the other cases and there is a more obvious "dip" in the main-beam.

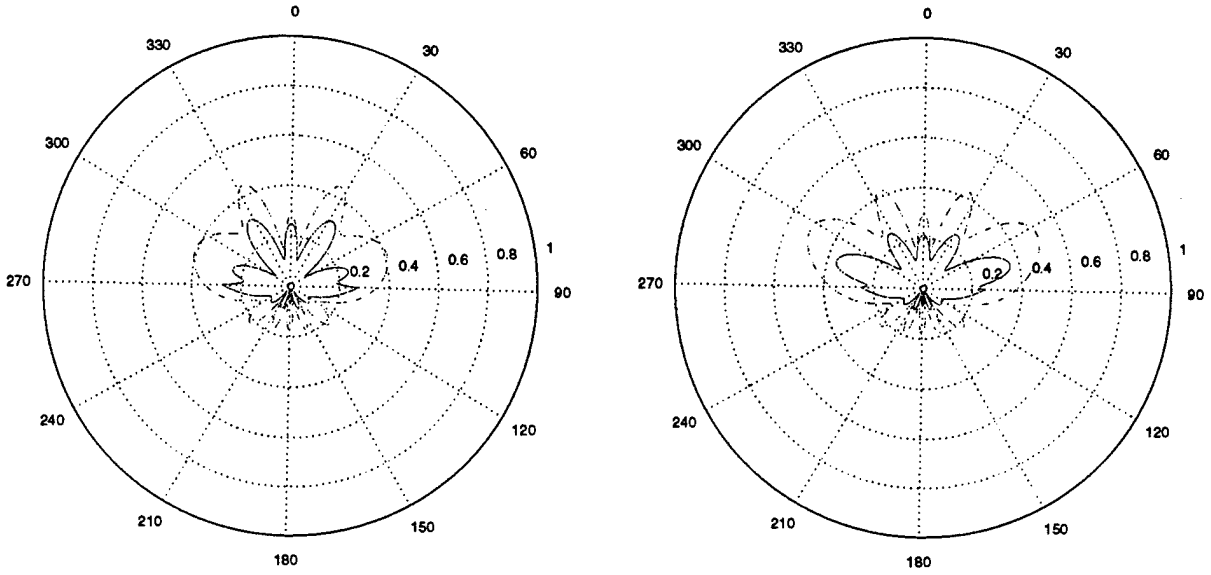

(a) d=0.5λ_d, w=0.85λ_d

(b) d=0.6λ_d, w=0.85λ_d

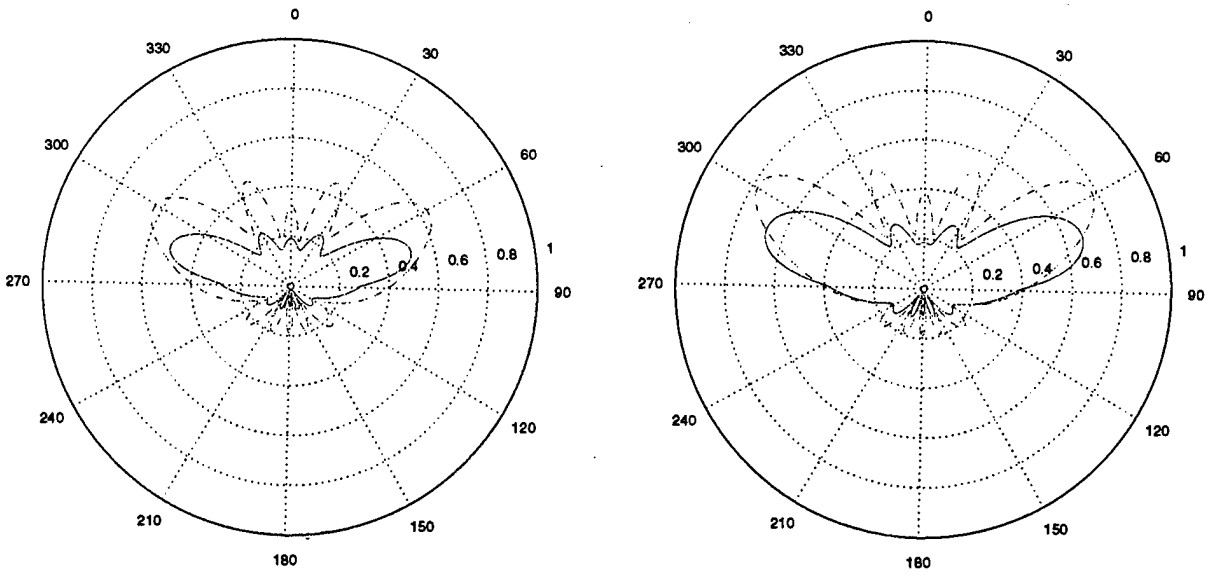

(c) d=0.7λ_d, w=0.85λ_d

(d) d=0.8λ_d, w=0.85λ_d

Figure 3.13: Parametric study of strip distance effects (two strip case): solid line - total diffracted field, dash line - strip effects

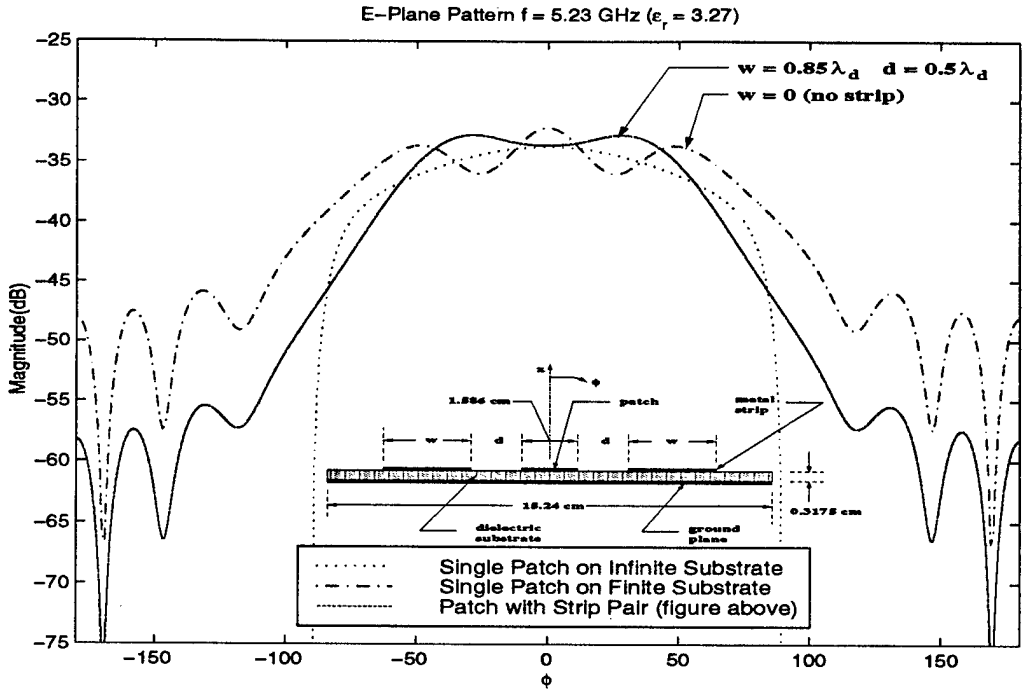

Figure 3.14: Two-strip antenna E-Plane pattern: d=0.5λ_d, w=0.85λ_d

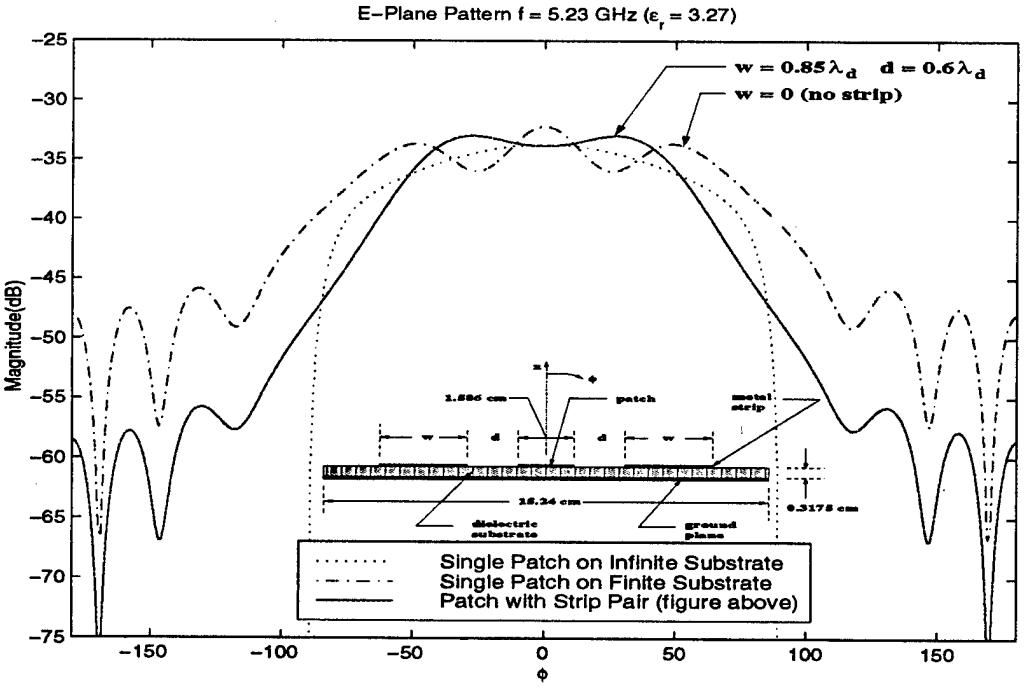

Figure 3.15: Two-strip antenna E-Plane pattern: d=0.6λ_d, w=0.85λ_d

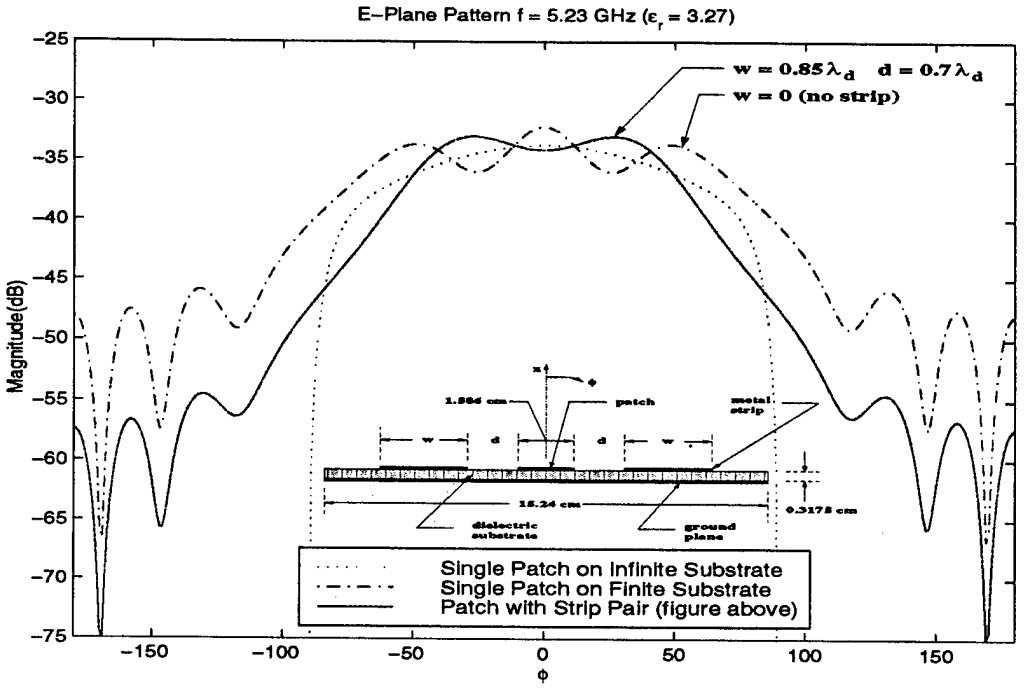

Figure 3.16: Two-strip antenna E-Plane pattern: d=0.7λ_d, w=0.85λ_d

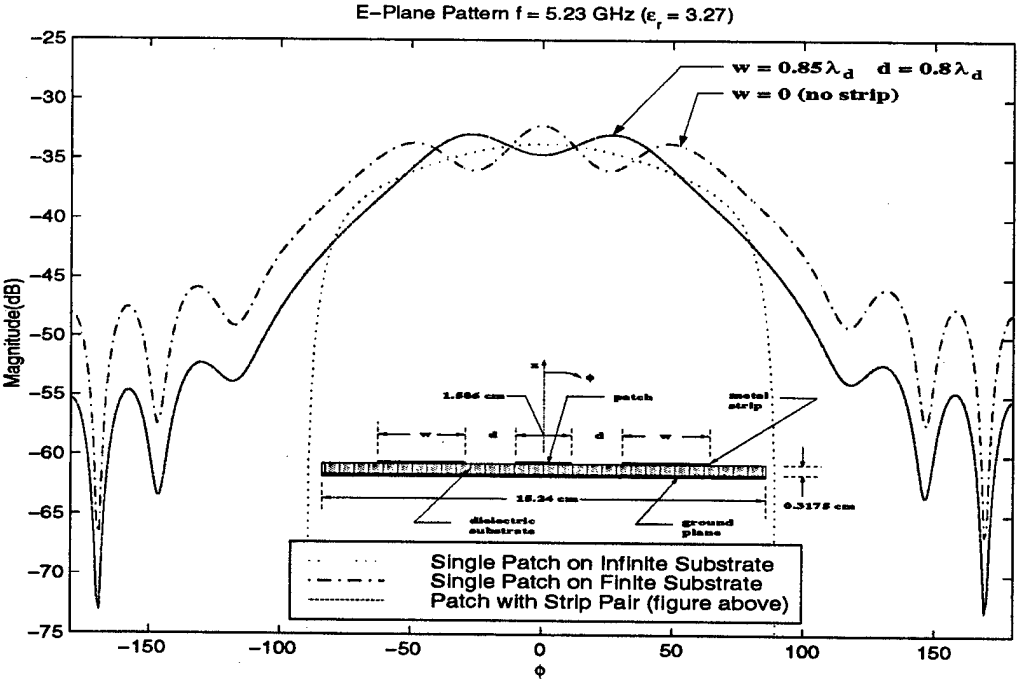

Figure 3.17: Two-strip antenna E-Plane pattern: d=0.8λ_d, w=0.85λ_d

Chapter 4

Design and construction of patch antenna with parasitic strips

4.1 Introduction

In Chapter 3, a scheme was presented to control the surface wave behavior of microstrip antennas. Since there is not a simple relationship between the strip parameters and the field behavior of the antenna, it is necessary to employ an optimization algorithm to obtain an optimal design. Thus, an adaptive genetic algorithm (GA) has been developed for this study. The details of this method are discussed in Appendix A. The implementation of the fitness (objective) function as well as experimental results based on the optimal design are presented in this chapter.

4.2 Objective Function

There are many different ways to set up a fitness function depending on the problem. Since the fitness function is the only way for a GA to communicate with the actual physical problem, all the constraints on the problem should be implemented as part of the fitness evaluation. This means that a good understanding of the physical problem is necessary and essential to set up the object function. In addition, a well developed fitness function can help direct the GA in the searching process.

An objective or cost function F is chosen to be

$$F(w^g, n^t, n^b, w_i^t, d_i^t, w_j^b, d_j^b) = \alpha_s F_s + \alpha_m F_m \tag{4.1}$$

in order to meet the two requirements (minimizing diffracted field and maintaining a "flat-top" main-beam pattern). The parameters of the fitness function are the ground plane width (w^g), the number of conducting strips needed on top and bottom (n^t and n^b), the width of and distance between each top (bottom) strip i (j) ($w_{i(j)}^{t(b)}$ and $d_{i(j)}^{t(b)}$) as shown in Figure 3.1. The first term, F_s, in equation (4.1) is to minimized the diffracted field and is given by

$$F_s = \sum_{\phi=-\pi}^{\pi} \alpha_1(\phi) P_d^2(\phi) \tag{4.2}$$

where $P_d(\phi)$ is the diffracted field and $\alpha_1(\phi)$ is a penalty coefficient at each angle ϕ. The second term, F_m, in (4.1) is to maintain the plateau-like main-beam pattern in the broadside direction and is given by

$$F_m = \sum_{\phi_m=-\pi/4}^{\pi/4} \alpha_2(\phi_m)(P(\phi_m) - P_{avg})^2 \tag{4.3}$$

where $P(\phi_m)$ is the total radiated field at each angle ϕ_m, P_{avg} is the average value of the total radiated field in the main-beam region, and $\alpha_2(\phi_m)$ is also a penalty coefficient at each angle ϕ_m. Finally, the coefficients, α_s and α_m in (4.1), are the weighting parameters for F_s and F_m. The penalty coefficients are used to control the side-lobe levels at different angles. In addition, if one is interested in changing the beamwidth of the antenna, this can be done by including this factor into the cost function. Physically, this means the beamwidth of the antenna can be changed by controlling the leaky wave beams.

4.3 Optimization Result

The optimized result is shown in Figure 4.1. The resultant design has four pairs of metal strips on the top of the substrate and a pair of strips on the bottom. As mentioned previously in Chapter 3, the largest leakage of energy is from the first pair of strips. In fact, the optimized width of the first pair of strips is approximately equal to $0.8425\lambda_d$ (at $f = 5.23$ GHz), and the distance from the radiating edge of the patch is approximately equal to $0.6521\lambda_d$. Recalling the results from Figures 3.9

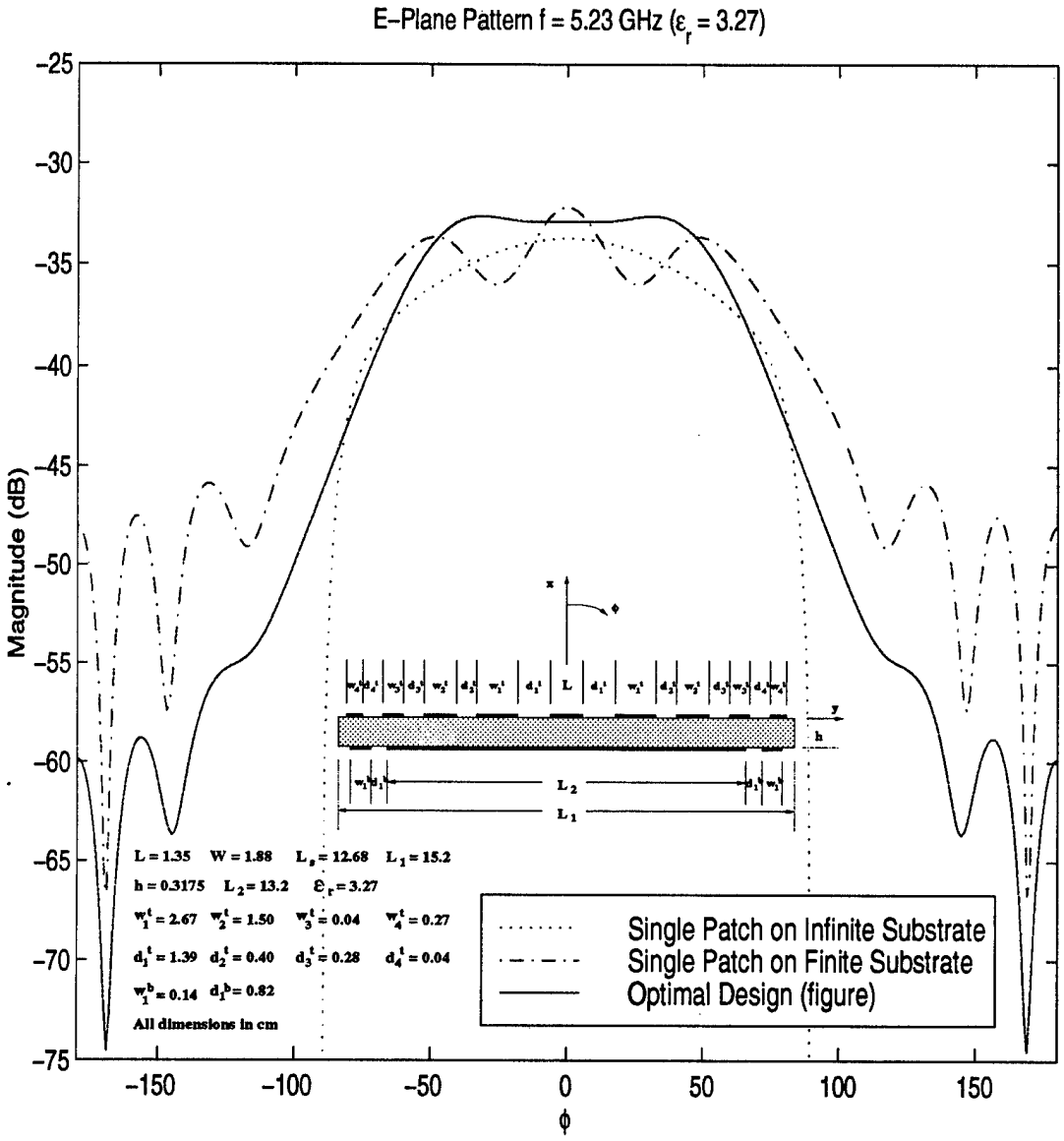

Figure 4.1: Calculated result of optimized design based on the 2-D model

through 3.12 and Figures 3.14 through 3.17, the optimized dimensions of the first pair of strips agree with dimensions of the pair strips analyzed in Chapter 3. The function of the other strip pairs is to help obtain the "flat-top" main-beam, to further lower the side-lobes and increase the pattern frequency bandwidth. Note that the idea of also creating leakage in the bottom of the substrate is to give another degree of freedom when applying this scheme to electrically thin substrate antennas. Since the surface waves are weak in thin substrate antennas, applying only the top strips to the antenna does not improve the antenna performance significantly. Hence, allowing leakage in the bottom of the substrate helps the performance of thin substrate antennas. Unfortunately, this scheme does not work well with very thin substrate antennas. On the other hand, the surface wave in these antennas is often very weak, and thus, there is no need to control it.

Figure 4.2 shows the E-plane pattern of the optimal design at different frequencies. The antenna pattern does not vary significantly through the frequency band. Therefore, the antenna has a fairly large pattern bandwidth.

4.4 Experimental Results

The optimal design was fabricated and tested. The measured antenna patterns are plotted along with the calculated results in Figures 4.3 through 4.6. The experimental results show good agreement with the calculated ones. However, the transition region occurs in a different frequency range from the calculated data. The transition region is the region (frequency domain) where the surface waves are modified and become leaky waves. Before discussing the details of this frequency shift, the general antenna behavior across the frequency range is first described. Similar to the behavior described in Chapter 3, Figures 4.3 and 4.4 show that the strips do not have much effect at the low frequency range below transition region. The side-lobe level of the antenna remains the same as the level of a single patch antenna. Besides, the main-beam is also distorted by the strong diffracted field. However, the side-lobe level reduces significantly as the frequency increases to the high frequency region (above

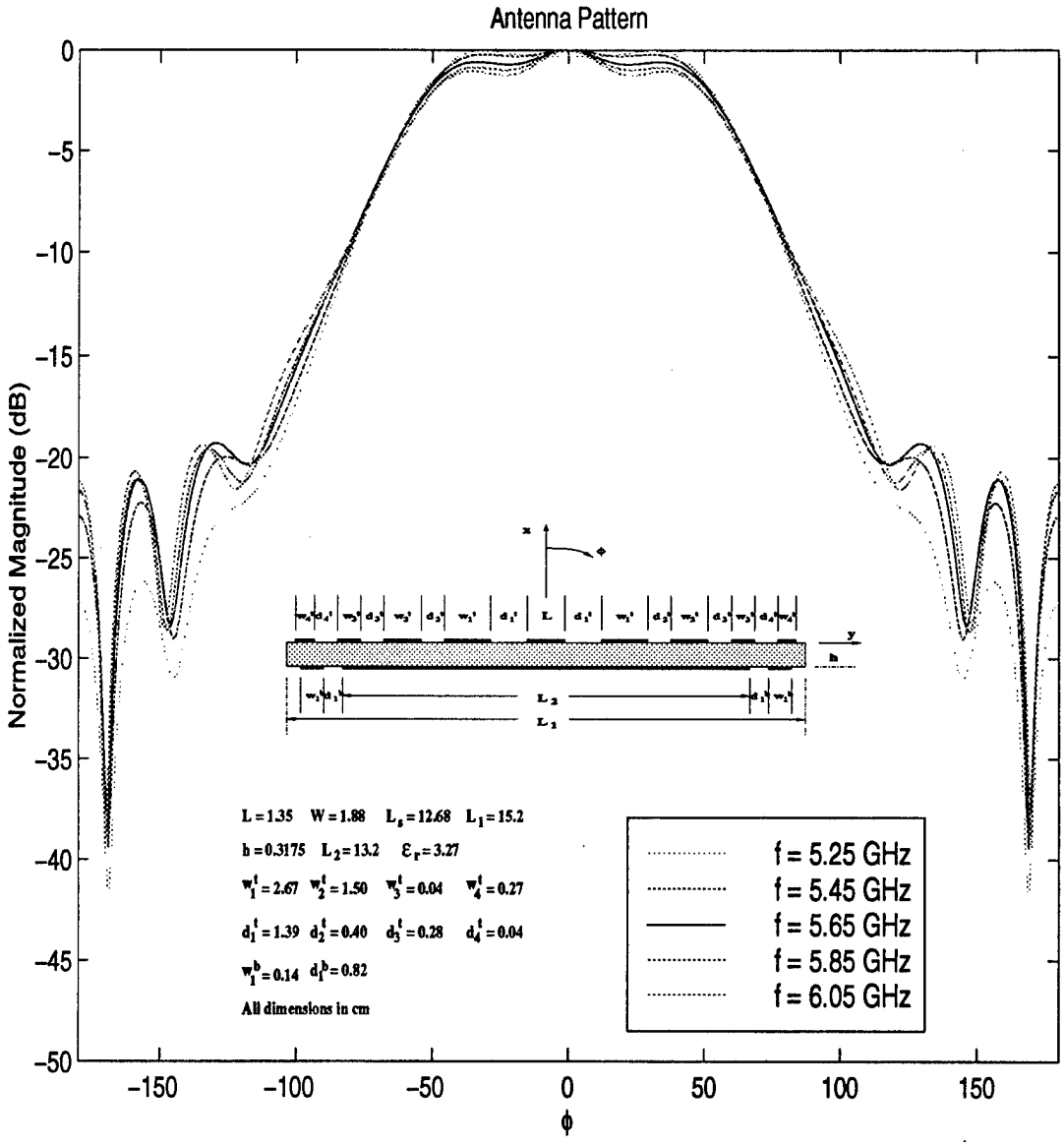

Figure 4.2: Calculated E-Plane pattern of optimized design at different frequencies

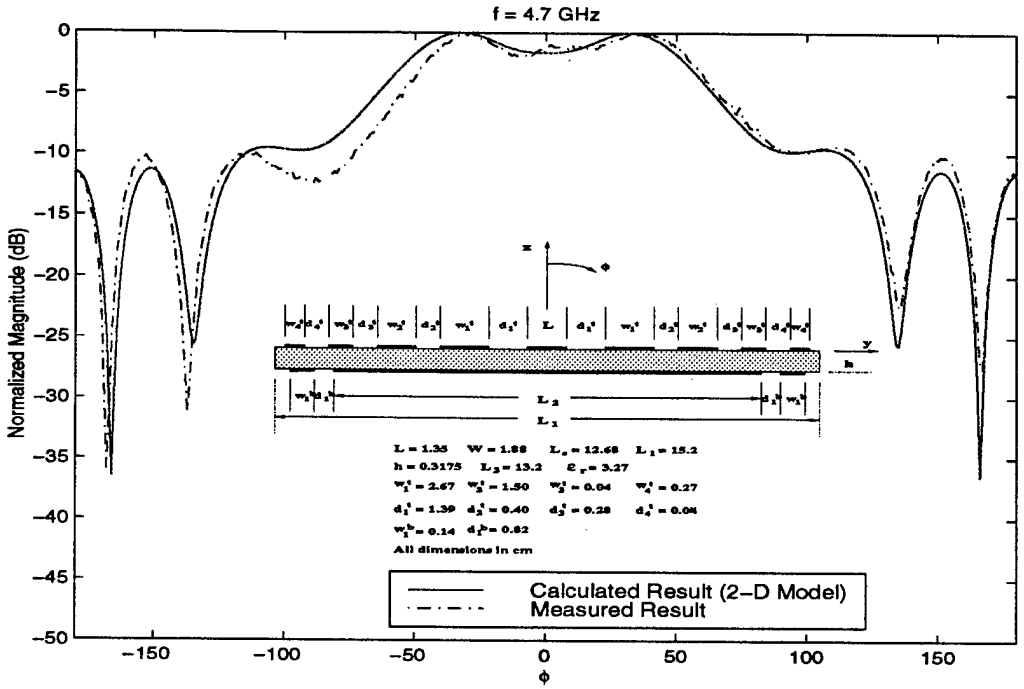

Figure 4.3: Calculated and measured result at f = 4.7 GHz

transition region) as shown in Figure 4.5. In addition, a "flat-top" main-beam is also observed due to weaker diffracted fields.

The comparison of the measured antenna patterns between the single patch antenna and the optimal design antenna is shown in Figure 4.7 for the E-plane and Figure 4.8 for the H-plane, respectively. As expected, the H-plane pattern of the single patch and the patch-strip designs are almost the same. This is because the edge diffracted fields on the H-plane are weak for the single patch and adding the strips does not have much of an effect. On the other hand, it is clear that there is significant improvement of the E-plane pattern in terms of side-lobe levels and the main-beam pattern due to the presence of the metal strips. Note that the main-beam pattern becomes more directive and hence improves the antenna directivity. Moreover, since this scheme is applied to a thick substrate antenna, the resultant antenna has a larger bandwidth than many thin substrate antennas.

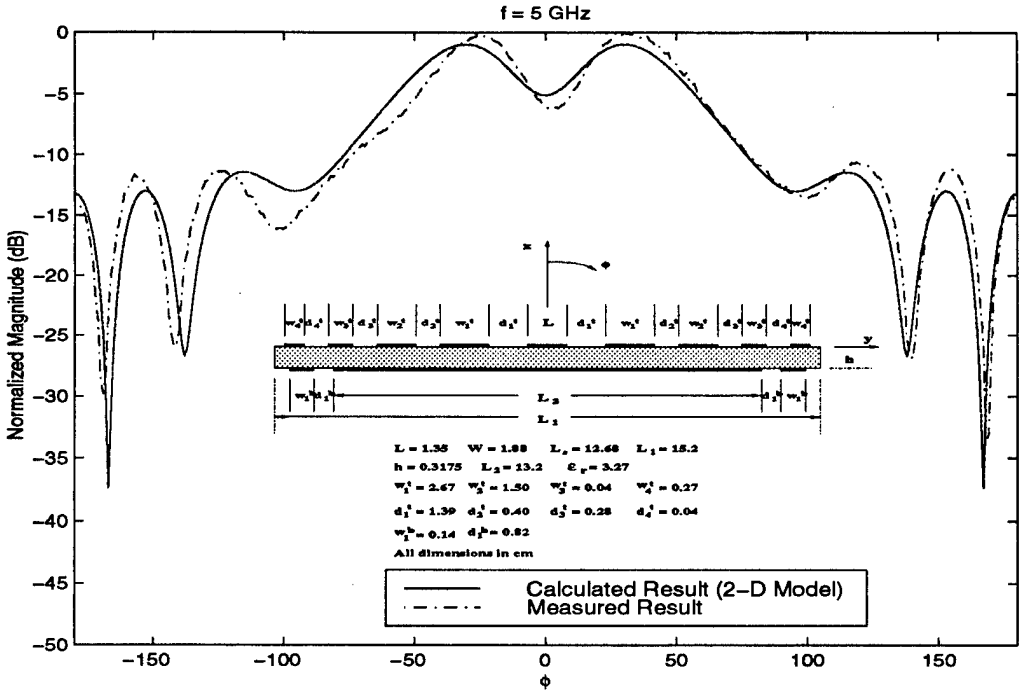

Figure 4.4: Calculated and measured result at f = 5.0 GHz

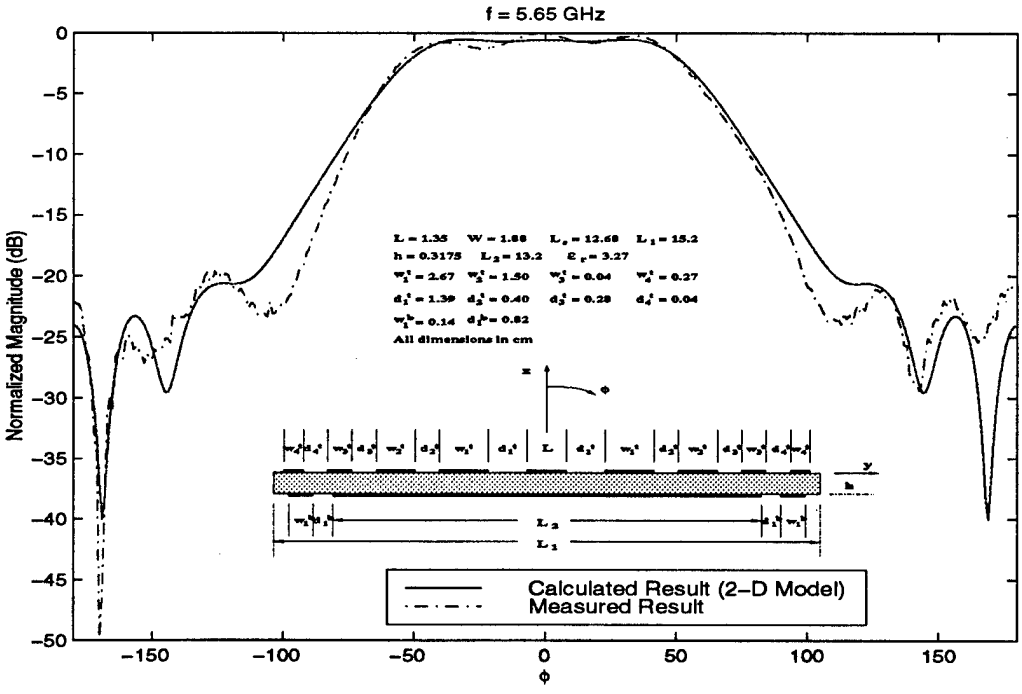

Figure 4.5: Calculated and measured result at f = 5.65 GHz

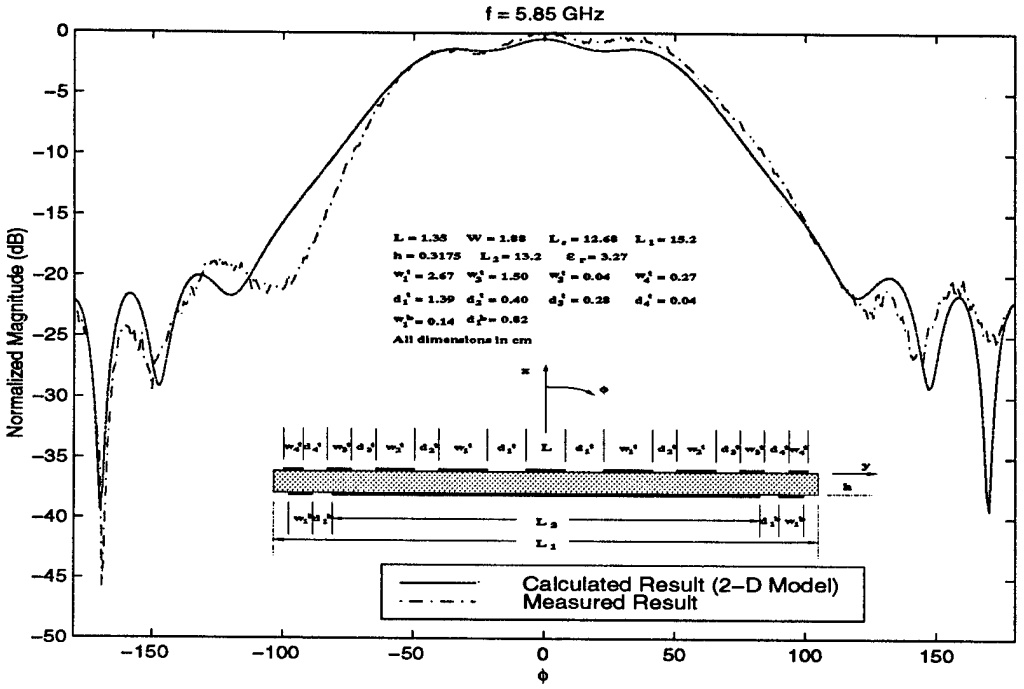

Figure 4.6: Calculated and measured result at f = 5.85 GHz

4.5 Transition Region

The transition region is the frequency region where surface waves change to become leaky waves. It was observed that this region shifts to a higher frequency region for the experimental data. The inconsistency between measured and calculated results in this region is due to the inability of the 2-D model to account for the effect of the strip length. In the two-dimensional model, the strips are assumed to be infinite in the z-direction, and the radiating patch is modeled by two magnetic current line sources (also infinite in z direction). However, this is not true in the actual case since the antenna has finite size. Therefore, there is a need to investigate the effect of this parameter. This is done experimentally.

To simplify the problem, different strip lengths for a pair of strips of fixed width size are first investigated. Figures 4.9 to 4.11 show the measured antenna patterns of a patch antenna with a pair of metal strips (fixed strip widths $0.9\lambda_d$ and different strip lengths). If L_s equals to $2\lambda_d$, the transition region occurs in the frequency range between 4.9 GHz and 5.2 GHz. At lower frequencies, the antenna pattern is very

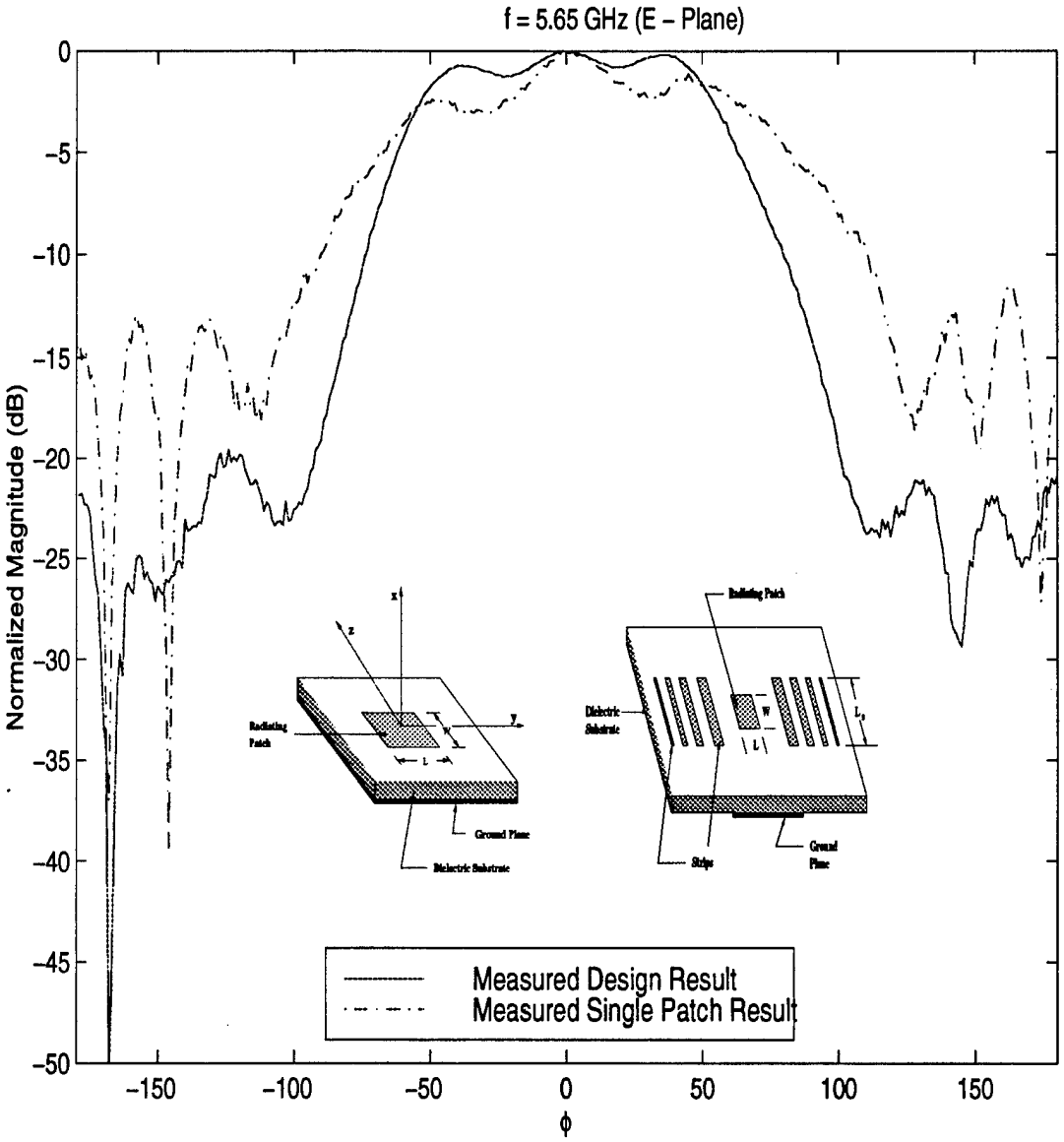

Figure 4.7: Comparison between single patch and optimal design (E-Plane)

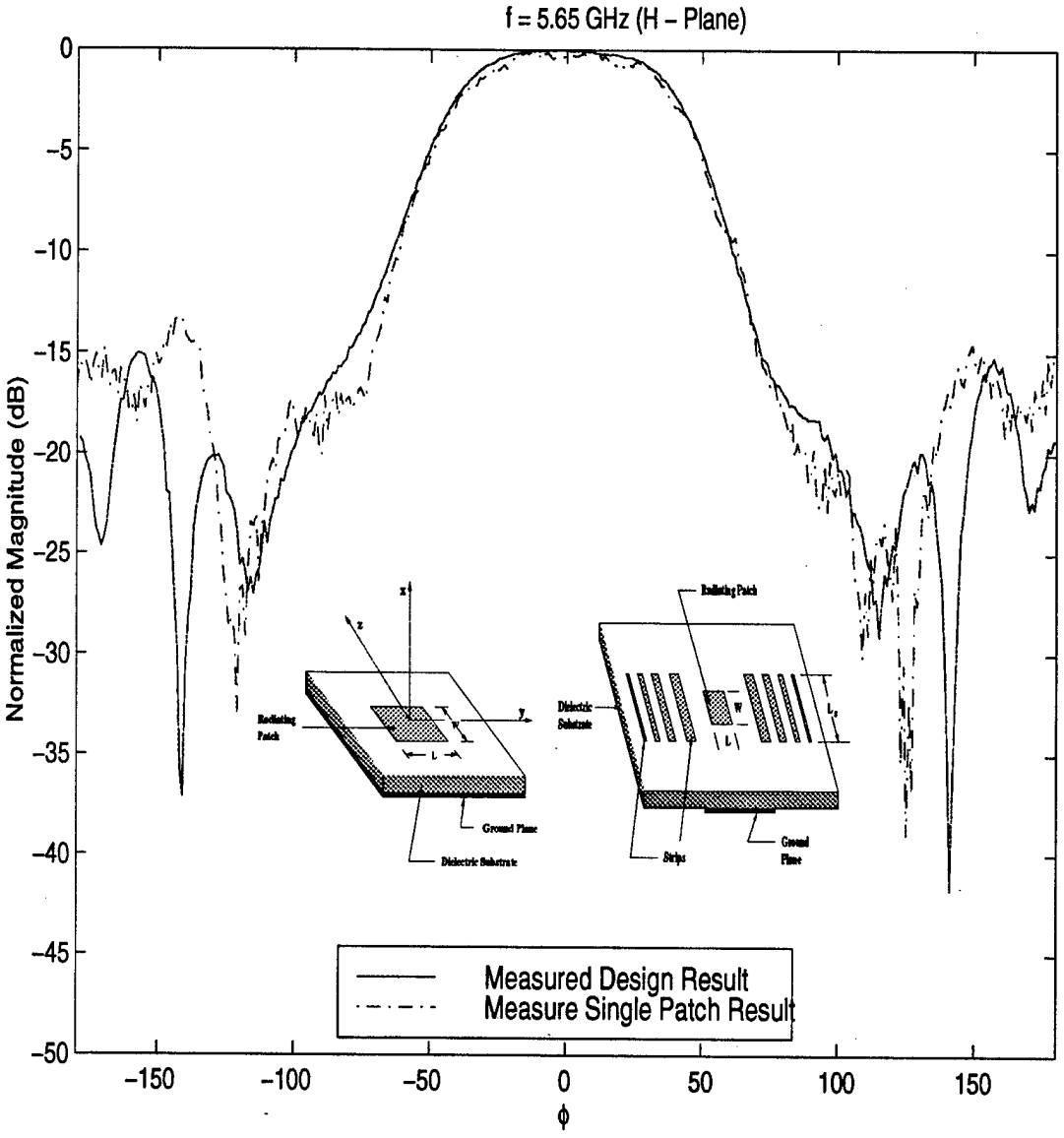

Figure 4.8: Comparison between single patch and optimal design (H-Plane)

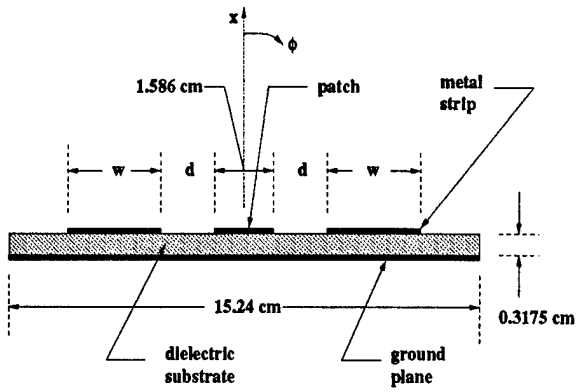

(a) d = 1.269 cm, w = 2.855 cm

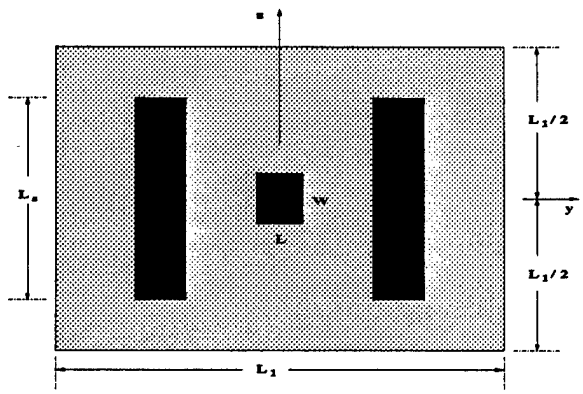

(b) L_s = 6.344 cm

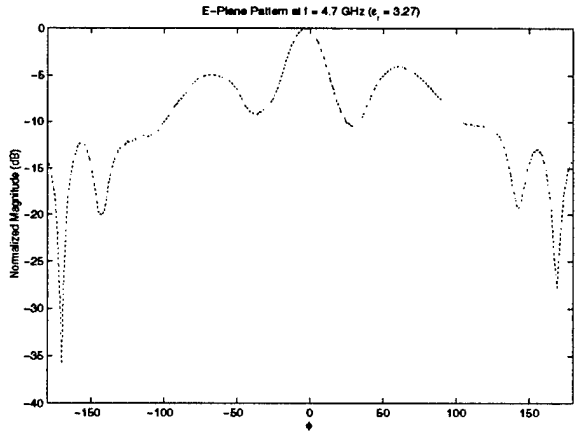

(c) E-Plane pattern at f = 4.7 GHz

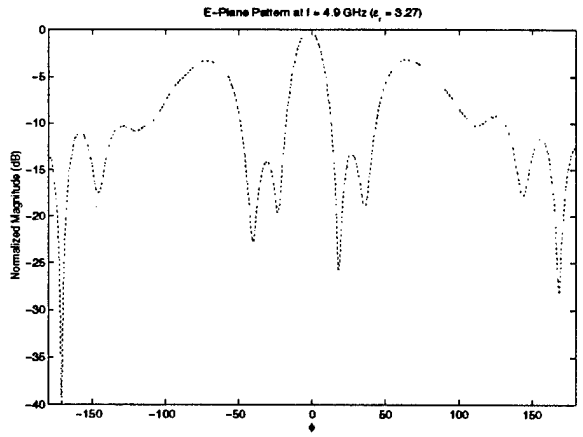

(d) E-Plane pattern at f = 4.9 GHz

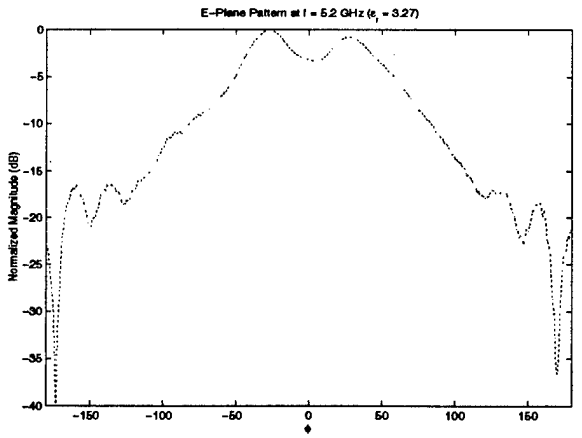

(e) E-Plane pattern at f = 5.2 GHz

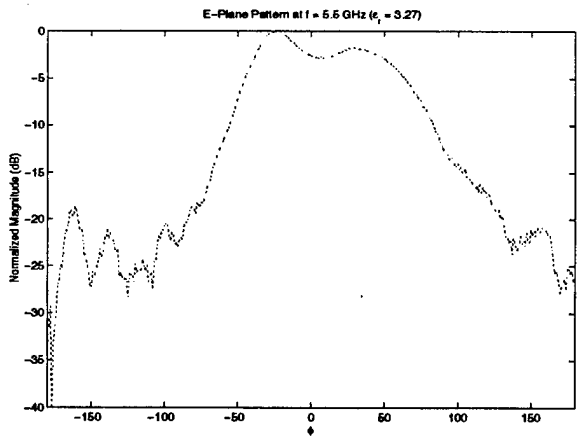

(f) E-Plane pattern at f = 5.5 GHz

Figure 4.9: Parametric study of strip length effects (two strip case: L_s = 6.344 cm)

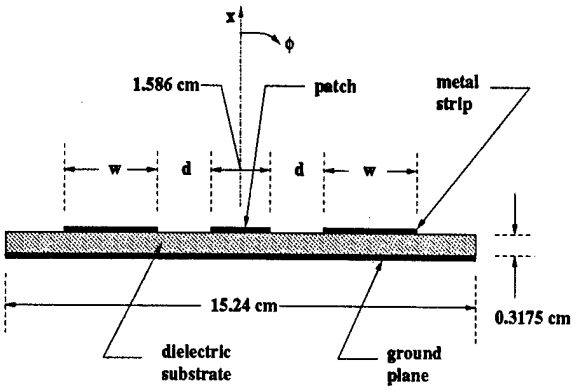

(a) d = 1.269 cm, w = 2.855 cm

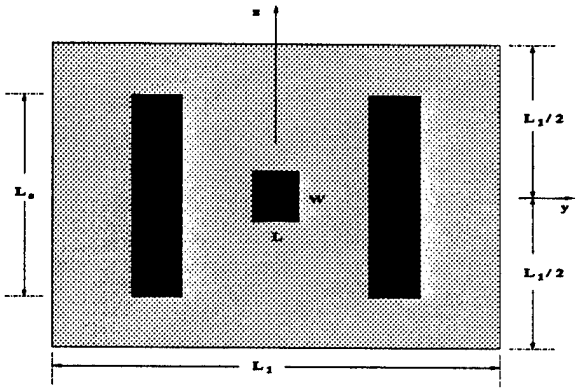

(b) L_s = 3.172 cm

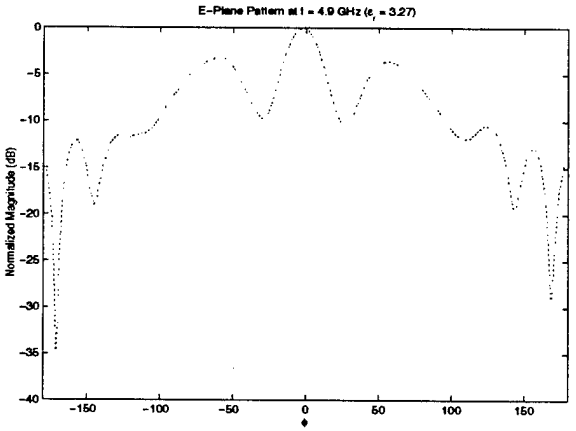

(c) E-Plane pattern at f = 4.9 GHz

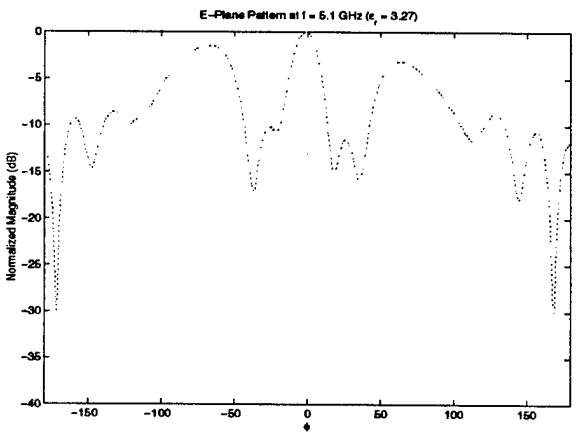

(d) E-Plane pattern at f = 5.1 GHz

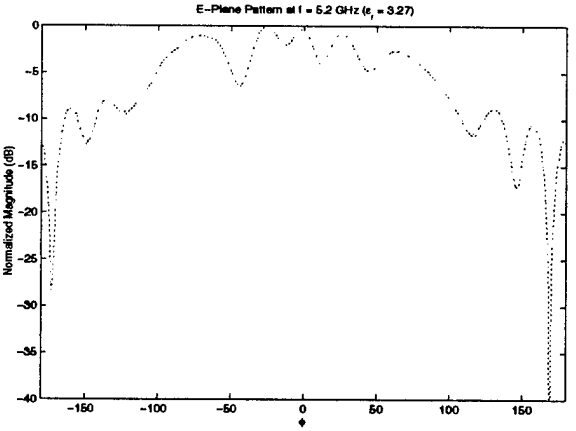

(e) E-Plane pattern at f = 5.2 GHz

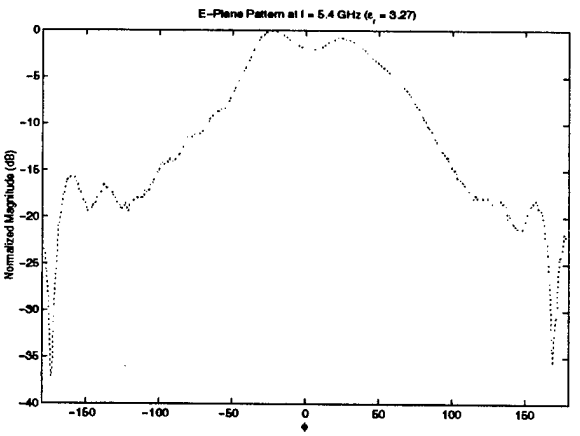

(f) E-Plane pattern at f = 5.4 GHz

Figure 4.10: Parametric study of strip length effects (two strip case: L_s = 3.172 cm)

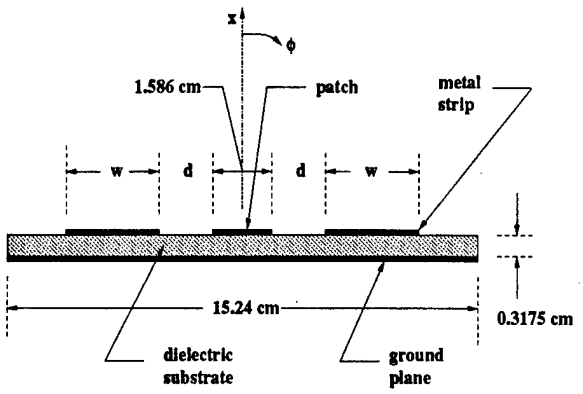

(a) d = 1.269 cm, w = 2.855 cm

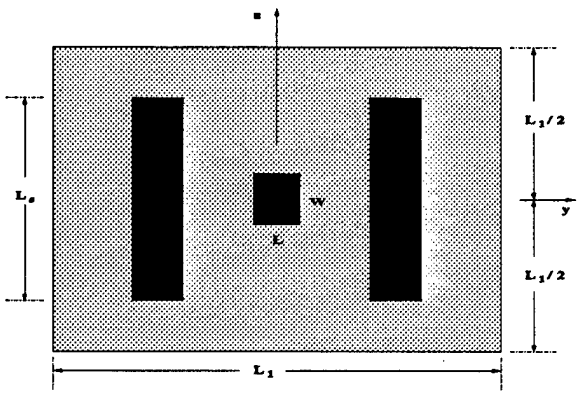

(b) L_s = 1.586 cm

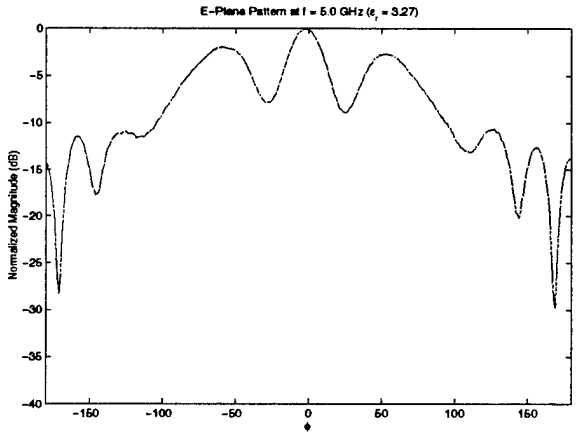

(c) E-Plane pattern at f = 5.0 GHz

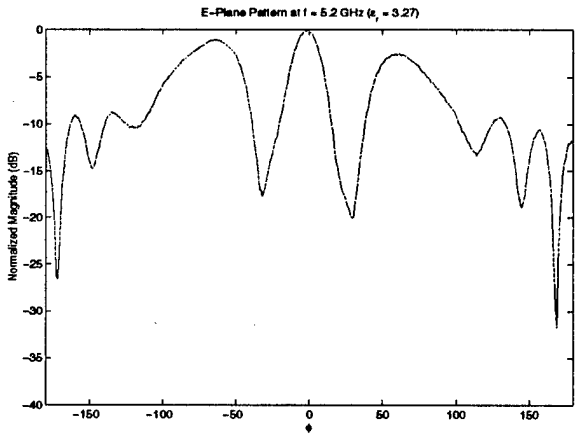

(d) E-Plane pattern at f = 5.2 GHz

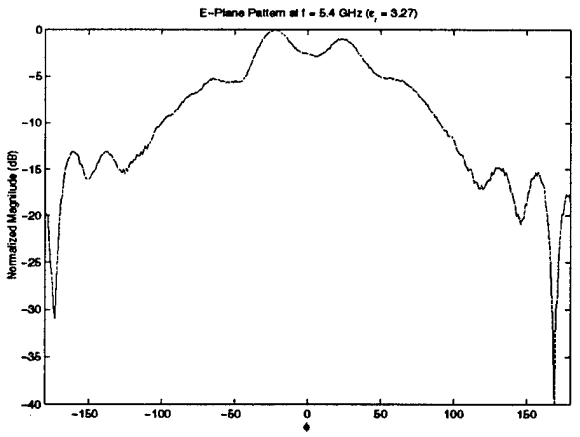

(e) E-Plane pattern at f = 5.4 GHz

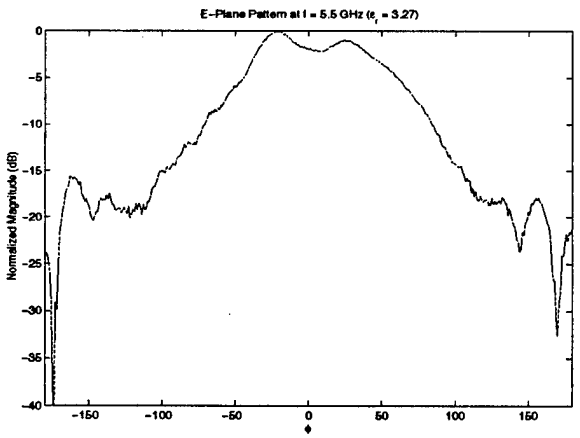

(f) E-Plane pattern at f = 5.5 GHz

Figure 4.11: Parametric study of strip length effects (two strip case: L_s = 1.586 cm)

similar to the pattern of a single patch antenna as shown in Figure 4.9(c). This means that the strips do not have an important effect on the surface wave field. The main-beam pattern of the antenna is distorted by the two strong leaky wave beams (recall from Chapter 3) as the frequency increases (Figure 4.9(d)). When the frequency increases to 5.2 GHz as in Figure 4.9(e), the side-lobe levels decrease and a more directive main-beam results. The pattern does not change significantly with further increased in frequency as in Figure 4.9(f).

A similar phenomena occurs for other strip lengths. However, the frequency range where the changes occur is shifted. If L_s equals to $1\lambda_d$, the transition region shifts to a higher frequency range (5.1 GHz to 5.4 GHz). Further decreasing the strip length to $0.5\lambda_d$ causes the transition region to shift to a frequency range of 5.2 GHz to 5.5 GHz. Note that the antenna patterns are almost the same at 5.5 GHz for all the three strip lengths. In conclusion, the effect of the strip length is to change the transition frequency range. The shorter the strip length the higher the frequency shift, and *vice versa.*

From the above observation, it is clear that the optimal design should also take into account the frequency shift of the transition region due to the strip length effects. Figure 4.12 to Figure 4.14 show the measured antenna pattern of the final design with different strip lengths. The resultant patterns do indeed show the transition region shifting to a higher frequency range as the strip length decreases.

In conclusion, the measured results show good agreement with the calculated results except for the frequency range of the transition region. This is due to the inability of the two-dimensional model to account for the effect of the strip length. Lastly, the S_{11} and input impedance Z_{in} of the optimal design are shown in Figure 4.15 and Figure 4.16, respectively. Note that there is a "dip" in the S_{11} measured result around the 5.45 GHz frequency region. This is the transition frequency region for the strips where they have a strong negative impact on the input impedance. To shift this region below the operating frequency (5.23 GHz) of the patch, the strips should be redesigned to compensate the strip length effect when using a 2-D model.

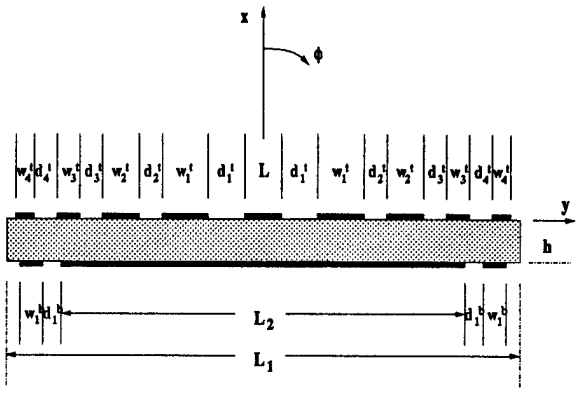

(a) Optimal design

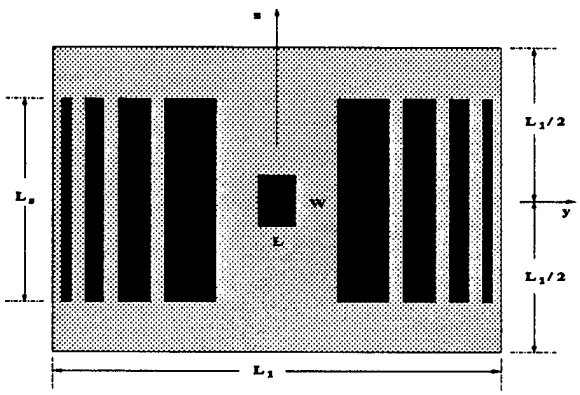

(b) $L_s = 12.688$ cm

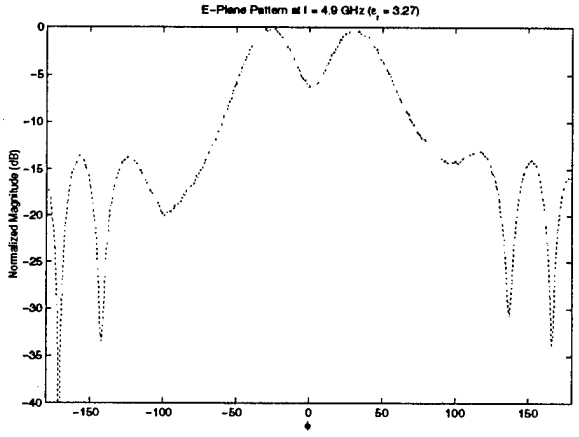

(c) E-Plane pattern at f = 4.9 GHz

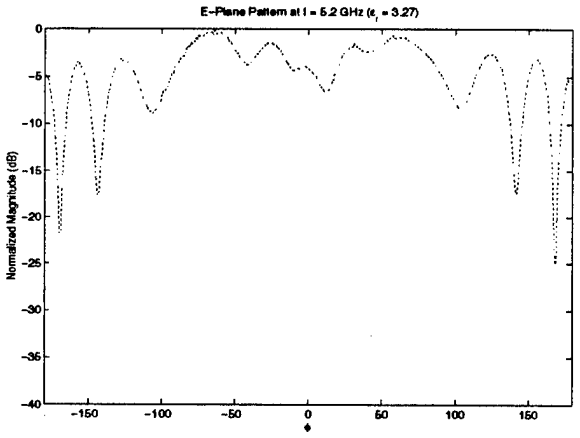

(d) E-Plane pattern at f = 5.2 GHz

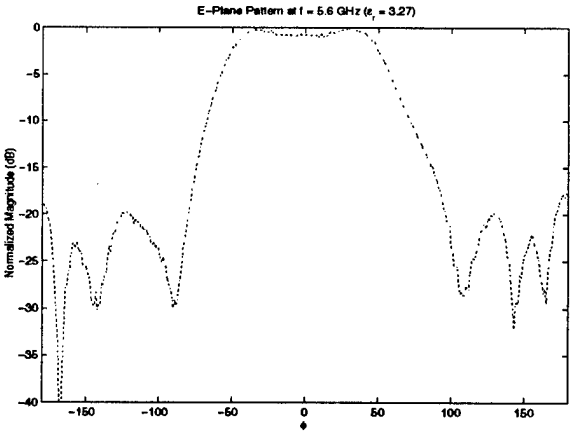

(e) E-Plane pattern at f = 5.6 GHz

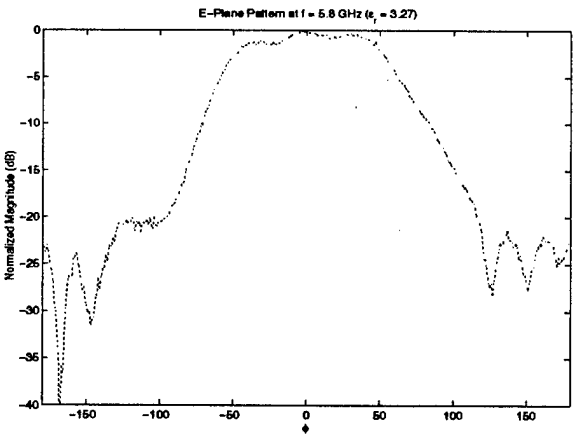

(f) E-Plane pattern at f = 5.8 GHz

Figure 4.12: Parametric study of strip length effects (optimal design: $L_s = 12.688$cm)

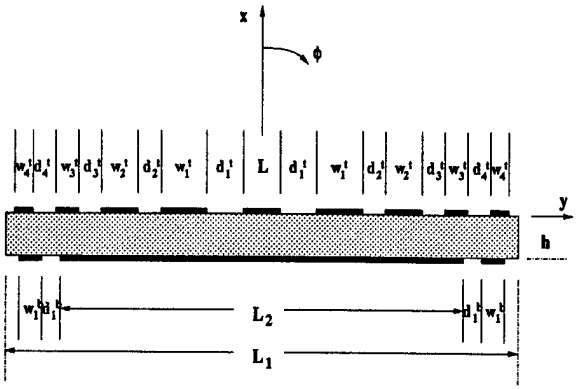

(a) Optimal design

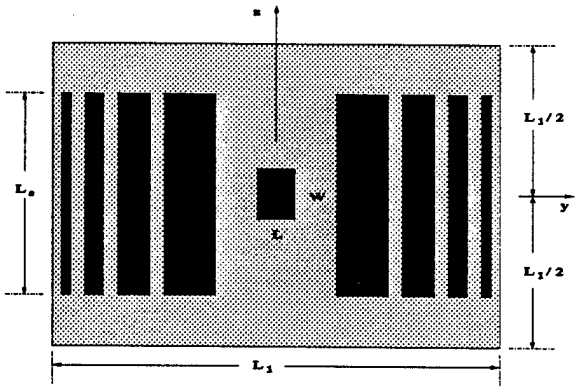

(b) $L_s = 11.102$ cm

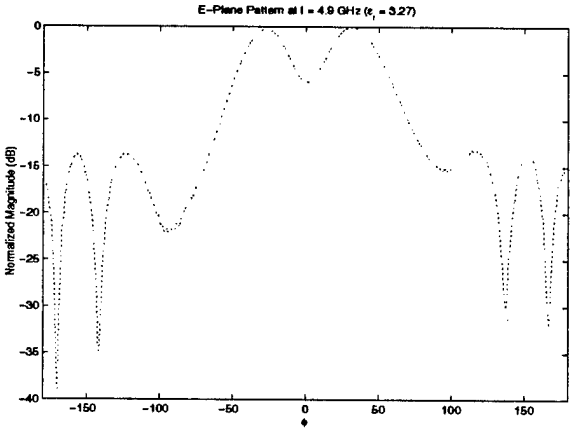

(c) E-Plane pattern at f = 4.9 GHz

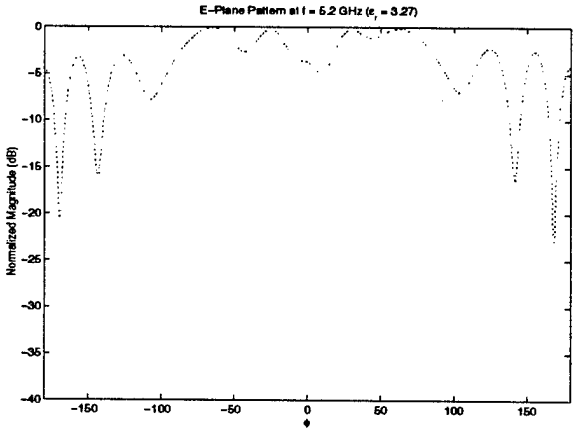

(d) E-Plane pattern at f = 5.2 GHz

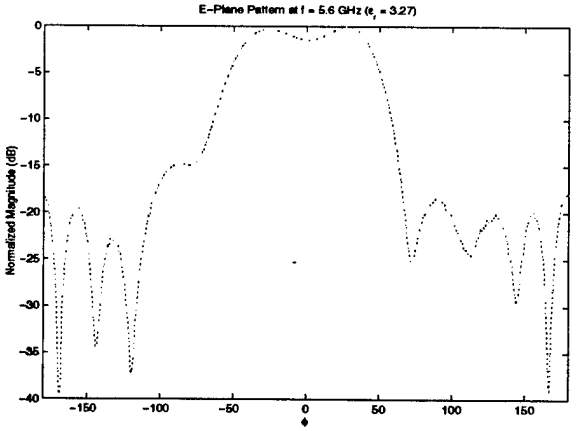

(e) E-Plane pattern at f = 5.6 GHz

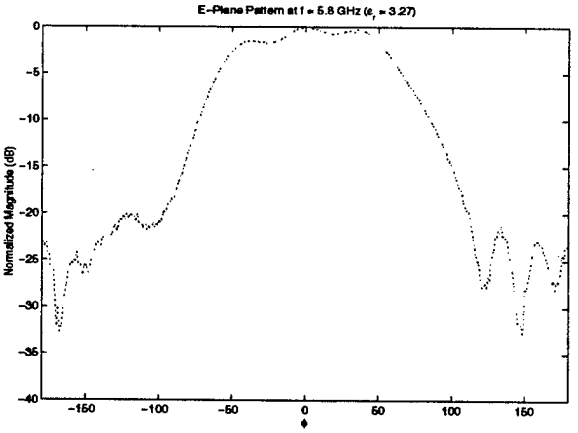

(f) E-Plane pattern at f = 5.8 GHz

Figure 4.13: Parametric study of strip length effects (optimal design: $L_s = 11.102$cm)

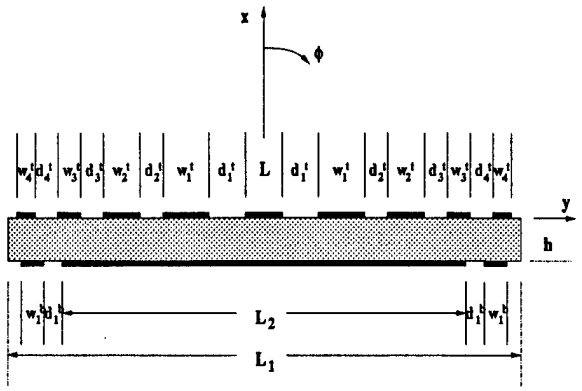

(a) Optimal design

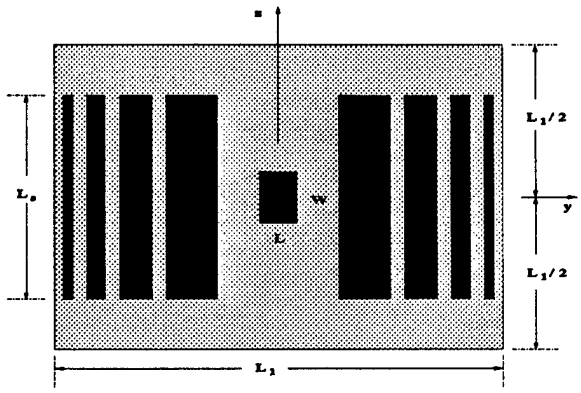

(b) $L_s = 9.516$ cm

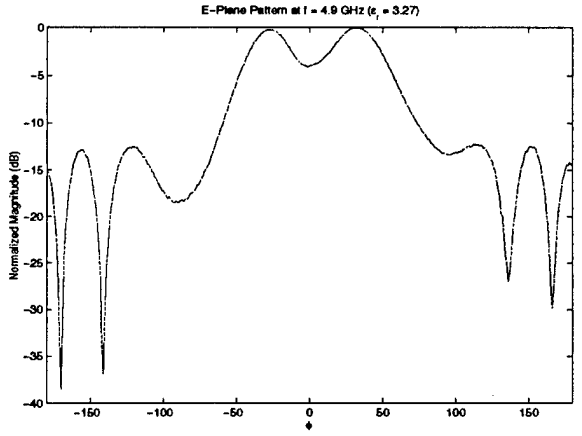

(c) E-Plane pattern at f = 4.9 GHz

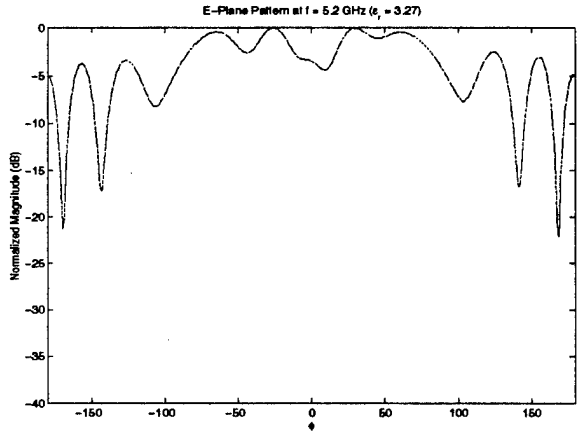

(d) E-Plane pattern at f = 5.2 GHz

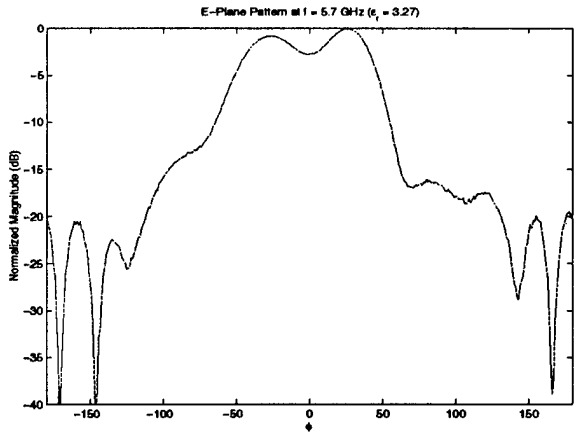

(e) E-Plane pattern at f = 5.7 GHz

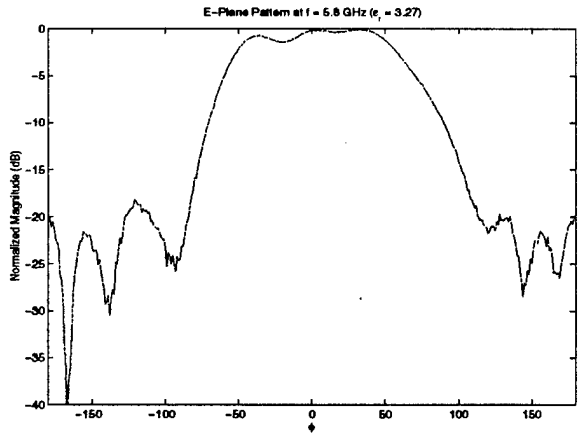

(f) E-Plane pattern at f = 5.8 GHz

Figure 4.14: Parametric study of strip length effects (optimal design: $L_s = 9.516$cm)

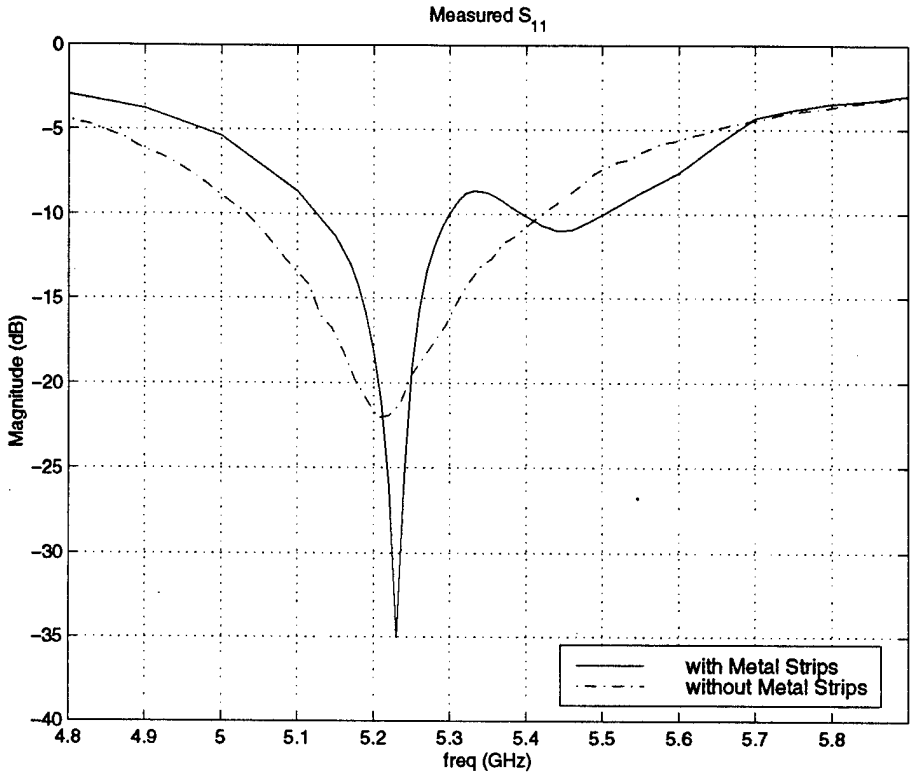

Figure 4.15: Measured values for S_{11}

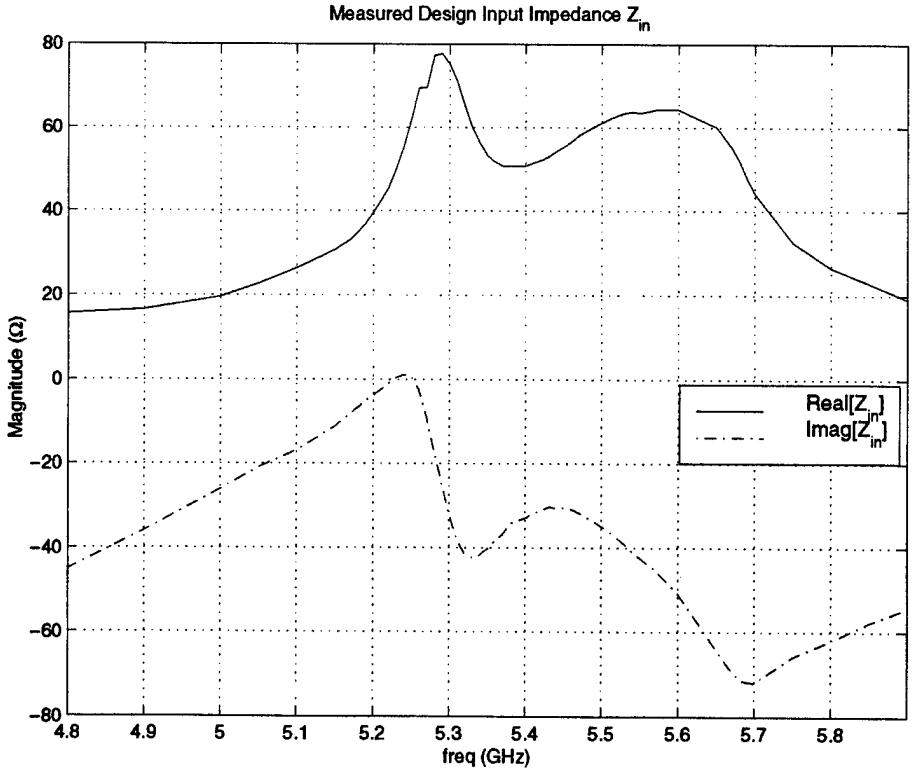

Figure 4.16: Measured value Z_{in}

Chapter 5

Preliminary Study of an Adaptive Printed Antenna Element

5.1 Introduction

In the previous chapters, the ability to control surface waves propagating in a dielectric substrate using conducting strips was established. In summary, one can control the surface wave behavior by placing conducting strips on the surface of the dielectric substrate. As expected, it was observed that the behavior of the dielectric surface, in conjunction with the metallic strips, is frequency dependent. Therefore, it is important to optimize the width and length of the strips to obtain the desired radiation pattern.

This chapter presents a preliminary study of an "adaptive" antenna element for GPS applications. A novel scheme for adaptively controlling the surface waves is introduced and is depicted in Figure 5.1. As shown in the figure, an array of diode-loaded metal strips is mounted on the same substrate as the microstrip patch. When the diodes are off, the metal strips have very small impact on the radiation pattern. However, when the diodes (all of the diodes or only some of the diodes) are on, the pattern changes. In other words, the resultant antenna has the ability to change/modify its radiation pattern depending on the operating state (on/off) of the diodes. Note that this novel concept gives antenna engineers more degrees of freedom in designing adaptive arrays because the element radiation pattern itself can be electronically controlled by changing the on and off states of the various diodes.

5.2 3-D Modeling

In the previous chapters, a two-dimensional MM-based model was used to study the antenna behavior. However, the model does not accurately predict the correct frequency range of the transition region as mentioned in Chapter 4. In addition, a two-dimensional model cannot be used to analyze the current antenna configuration because the strips are of finite length. Thus, a three-dimensional model is required to provide a more rigorous and accurate analysis.

A three-dimensional finite difference time domain (FDTD) code developed at the ElectroScience Laboratory [6]- [7] was used to investigate the antenna behavior. Since the adaptive GPS microstrip antenna was not built in this phase of study, it is important to first access the validity of the analysis tool (FDTD-based code). Figures 5.2 and 5.3 show the comparison of the E-plane and H-plane antenna patterns, respectively, between the calculated and measured results at 5.3 GHz for the optimal design described in Chapter 4. It is clear that the calculated and measured results are in good agreement. In addition, the FDTD program does predict the correct frequency range of the transition region. Figures 5.4 and 5.5 show the same comparison at a higher frequency. As expected, the 3-D FDTD code is more accurate than the 2-D Method of Moments, however, it is not as efficient.

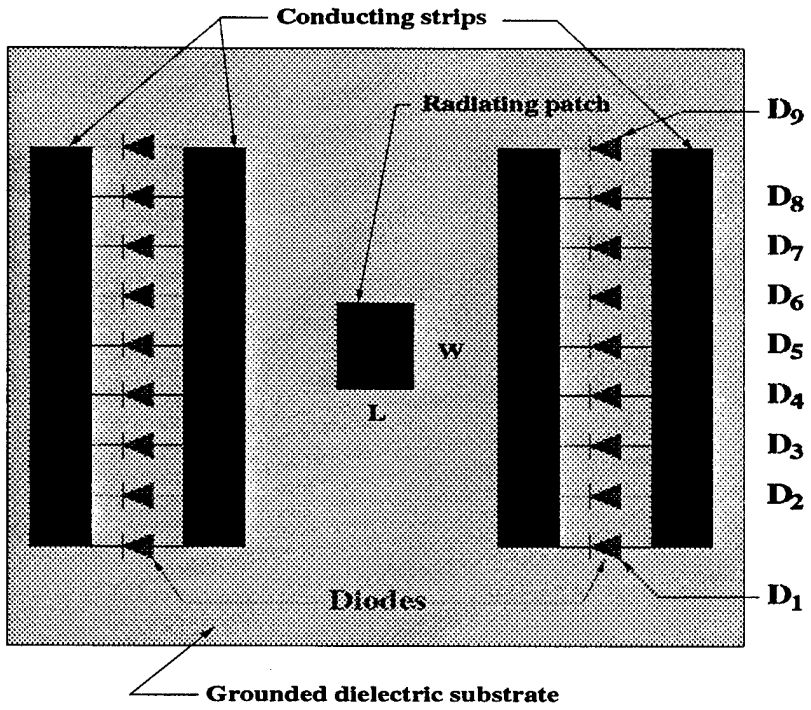

Figure 5.1: Microstrip antenna with diode-loaded parasitic strips on a grounded dielectric substrate

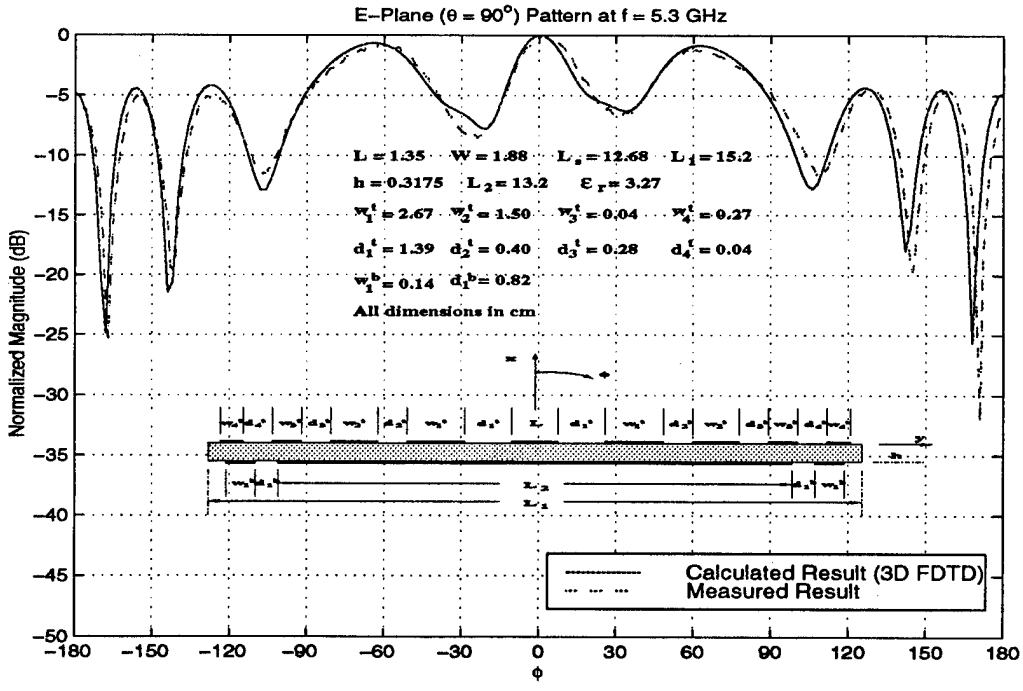

Figure 5.2: Calculated and measured E-plane pattern of the optimal design at f = 5.3 GHz

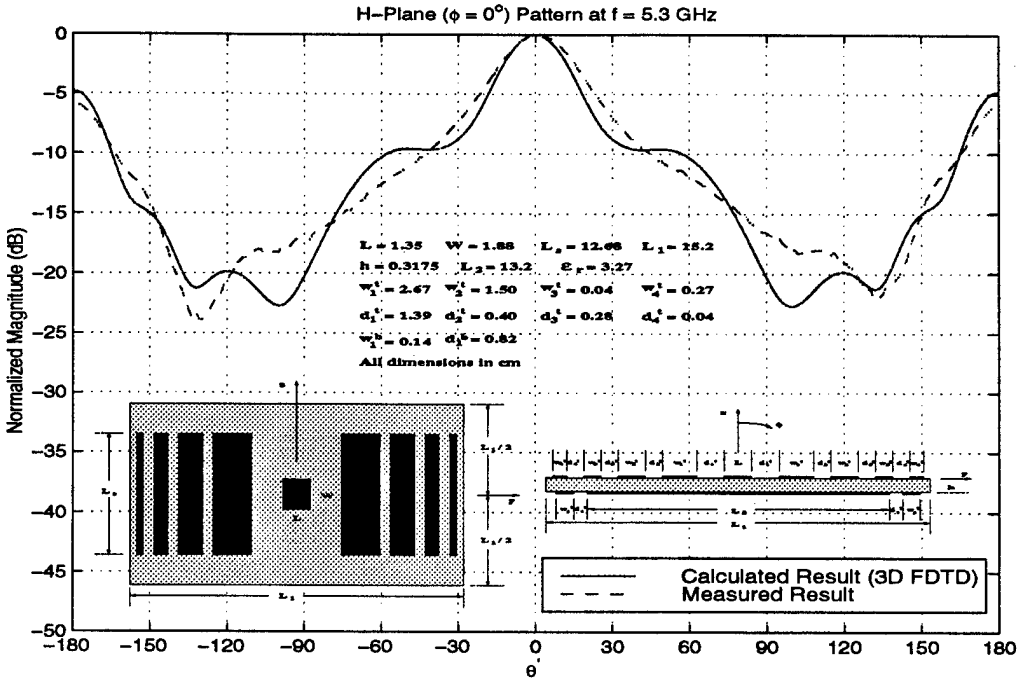

Figure 5.3: Calculated and measured H-plane pattern of the optimal design at f = 5.3 GHz

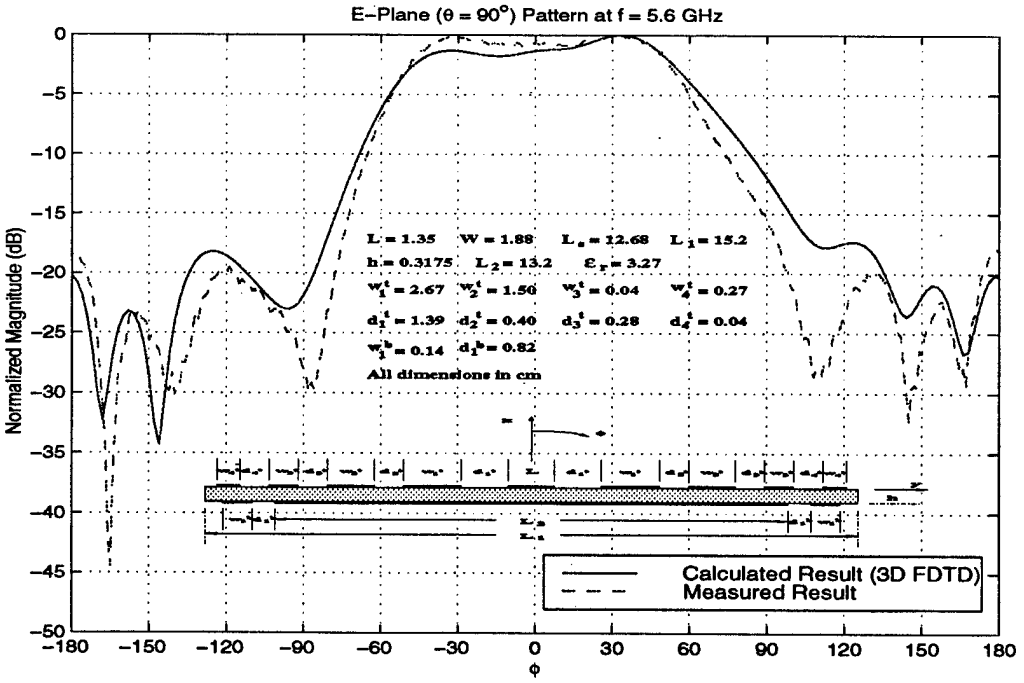

Figure 5.4: Calculated and measured E-plane pattern of the optimal design at f = 5.6 GHz

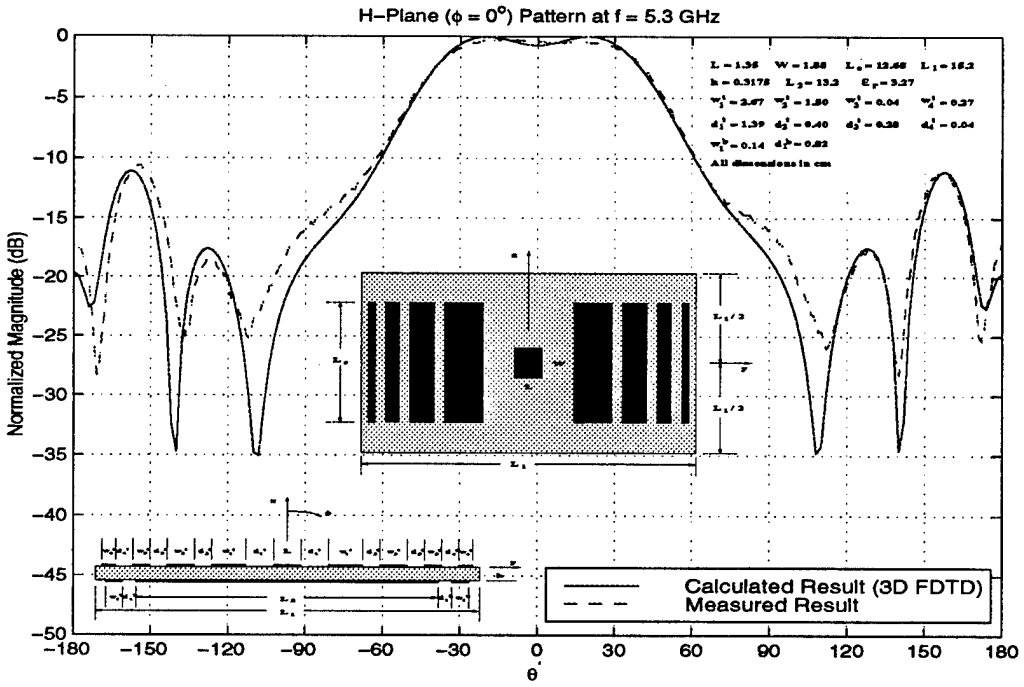

Figure 5.5: Calculated and measured H-plane pattern of the optimal design at f = 5.6 GHz

5.3 Radiation Mechanism

The radiation mechanism of the antenna configuration shown in Figure 5.1 can be separated into two distinct operating states. The two states correspond to the "on" and "off" states of the diodes. When ALL of the diodes are **on**, the two metal strips are electrically connected and effectively become a larger strip. This "larger" strip has an effective width which is sufficiently large (electrically) to convert surface waves to leaky waves, and hence, to change the radiation pattern of the antenna. When ALL of the diodes are **off**, the two strips do not have any significant effect on the radiation pattern. This is because the width of each strip is not large (electrically) enough to cause the wave conversions. Besides the two distinct states, the antenna can also operate when only a portion of the diodes are on and the others are off. In this case, the antenna performance depends on the number of diodes that are on as well as their location. In other words, the surface wave to leaky wave conversion efficiency is dependent on the number of diodes in the "on" state as well as their location.

It is important to note that the conversion mechanism is frequency sensitive. This implies that the dimensions of the strips should be carefully chosen. Otherwise, the mode of operation described above will not take place. For example, when the operating frequency is higher than the design frequency, the widths of the two separated strips may be large enough to have an impact on the surface waves. On the other hand, the effective width of the resultant "larger" strip may not be large enough to convert surface waves to leaky waves when the operating frequency is lower than the design frequency.

5.4 Design Example

In this section, a design example is presented to illustrate the application of the adaptive scheme to a single microstrip element. The first step is to design a pair of parasitic metal strips such that the resultant radiation pattern (Figure 5.7) is different from the original (without strips) pattern (Figure 5.6). The design and analysis of

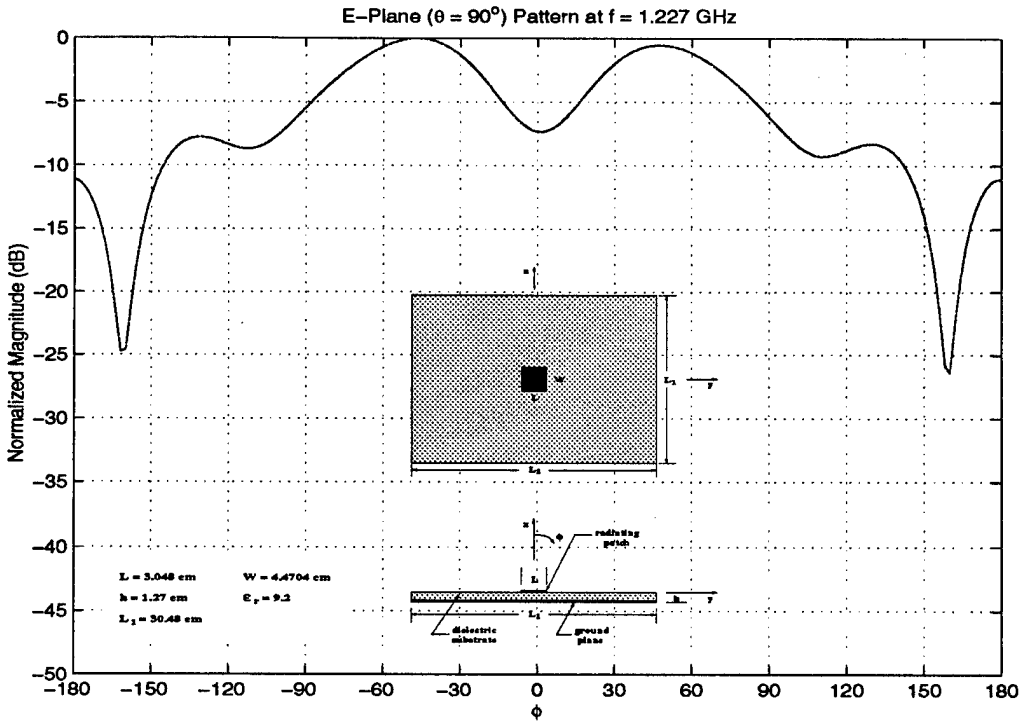

Figure 5.6: E-Plane pattern of a microstrip antenna at f = 1.227 GHz

the strip parameters are carried out in Chapter 3 and are not repeated here. The next step is to divide the metal strips into smaller pieces as shown in Figures 5.8 and 5.9. It is clear that this stage also represents the situation when all the diodes are off. Note that different patterns can be obtained by dividing the strips in different ways. It should be emphasized that no attempt was made is this study to optimize the design of this adaptive antenna.

The two patterns in Figures 5.8 and 5.9 are not the same because the surface wave to leaky wave conversion is different in both cases. The last step is to connect the strips back together with diodes as shown in Figure 5.10 and 5.11. These results clearly show that the beamwidth can be substantially modified with this adaptive scheme. Notice that the radiation pattern of the antenna in Figure 5.10 is similar to the pattern of the antenna in Figure 5.8. Also, the antenna pattern in Figure 5.11 is close to the pattern of the antenna configuration in Figure 5.7.

To conclude, a scheme for adaptively controlling surface waves in printed circuit antennas is presented in this chapter. Based on the calculated results shown here,

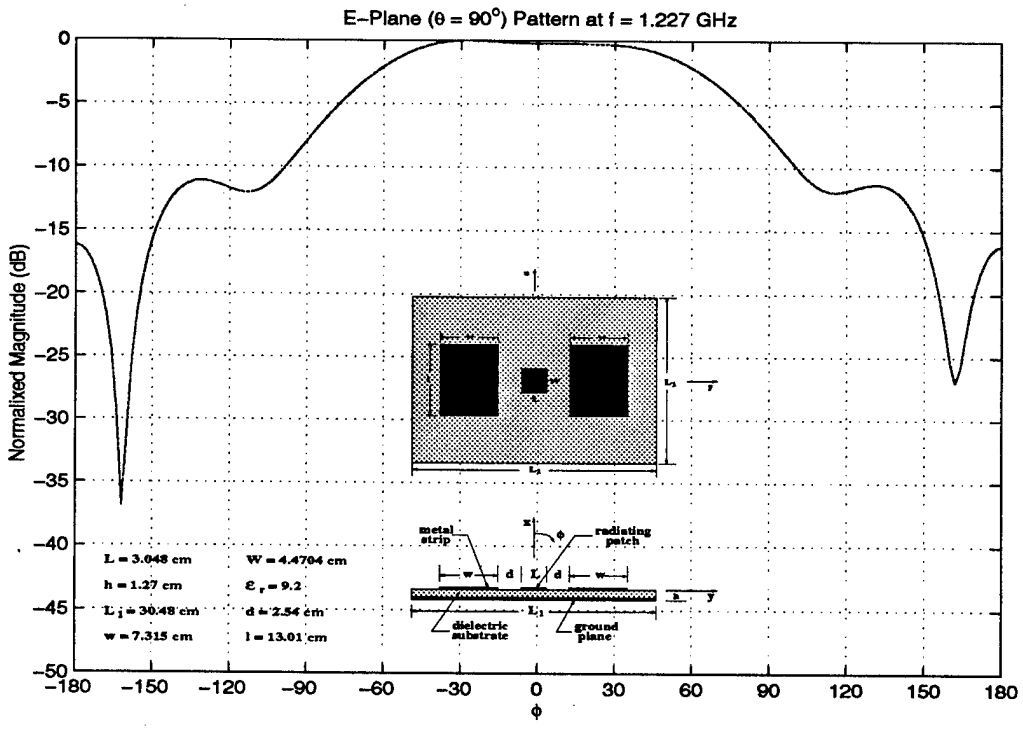

Figure 5.7: E-Plane pattern at f=1.227 GHz of a microstrip antenna with a pair of parasitic strips

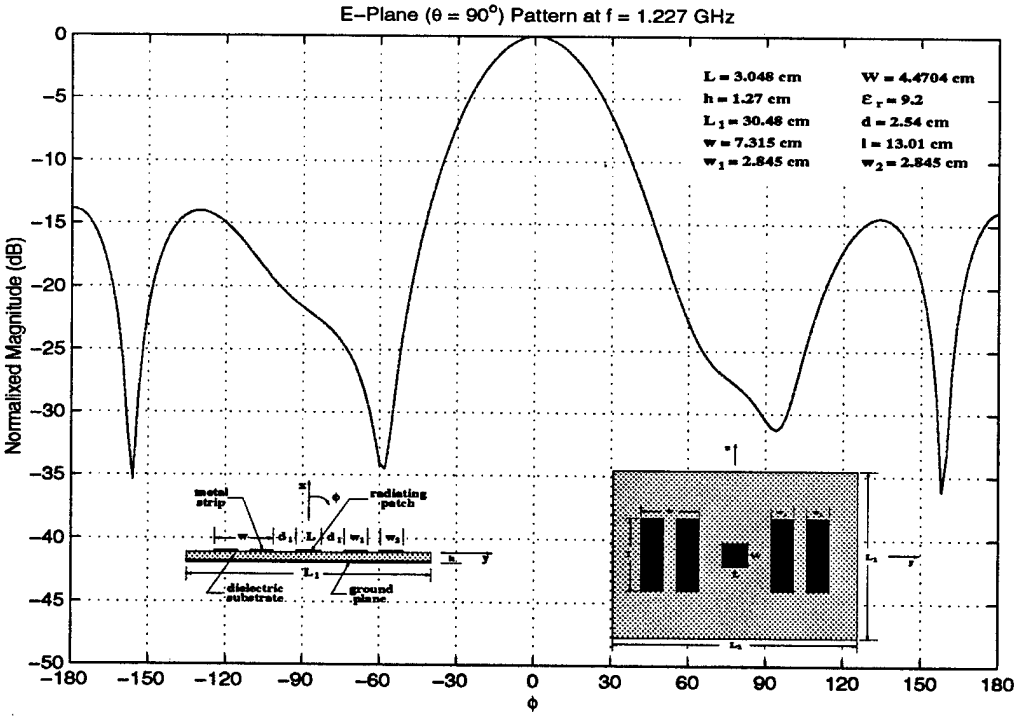

Figure 5.8: E-Plane pattern of a microstrip antenna at f = 1.227 GHz with each parasitic strip divided into two smaller ones

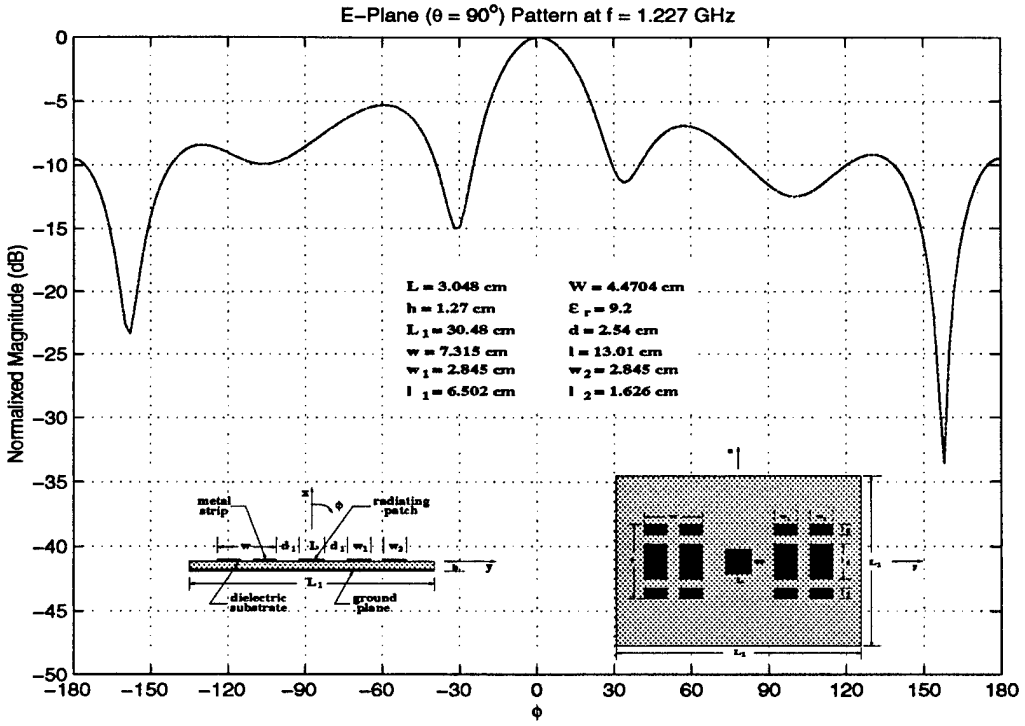

Figure 5.9: E-plane pattern of a microstrip antenna at f = 1.227 GHz with each parasitic strip divided into six smaller ones

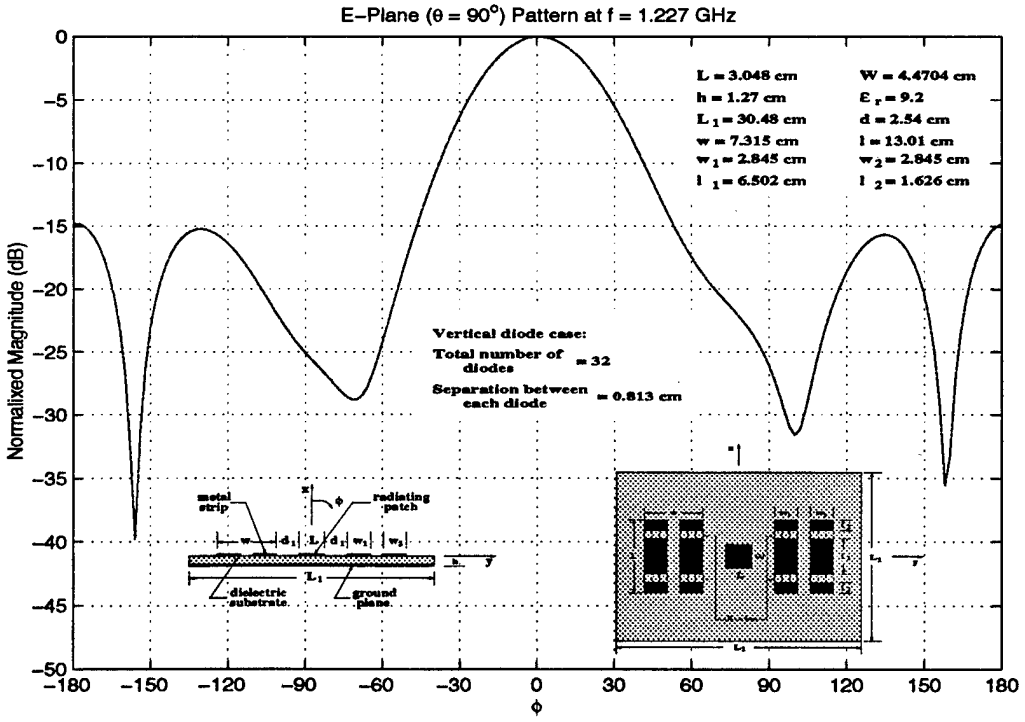

Figure 5.10: E-Plane pattern of a microstrip antenna at f = 1.227 GHz where only a portion of the diodes are on

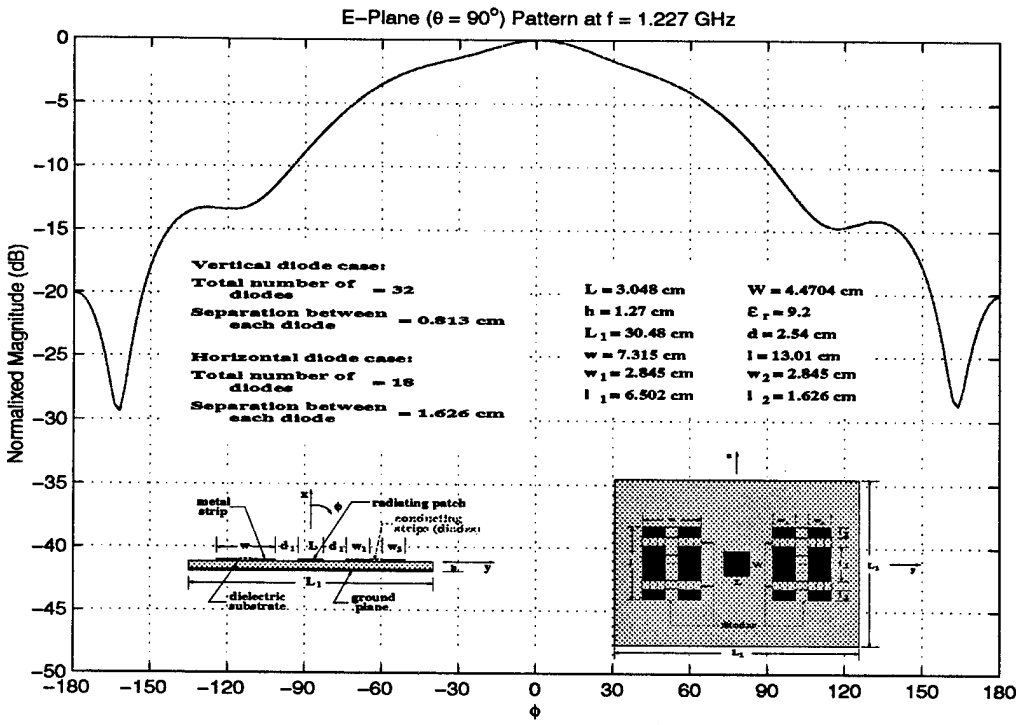

Figure 5.11: E-Plane pattern of a microstrip antenna at f = 1.227 GHz where all the diodes are on

it can be clearly seen that the radiation pattern can be modified by controlling the operation of the diodes. Unlike the antenna design in Chapter 4, the present design is not optimized. This is due to the fact that a three dimensional model is used to analyze the antenna behavior. It would be computationally expensive to optimize the antenna parameters using such a 3-D model. In addition, some critical parameters (the way the strips are divided, the number of diodes in the "on" stages, the separations between the "on" diodes, etc.) required additional investigation. However, the ability to control the surface waves, and hence, control the antenna pattern is well establish in this report.

Chapter 6

Conclusions

The development of a novel concept for the design of an "adaptive" printed antenna element for GPS applications is reported here. The concept is based on a scheme for controlling surface wave behavior on printed planar antennas. The key idea is to place metallic strips on the surface of the dielectric substrate. If properly designed, these parasitic strips convert surface waves (excited in the dielectric substrate) to leaky waves which can modify the field radiated by the patch antenna.

The details regarding the proper design of these parasitic strips were addressed in Chapters 2 and 3. To validate the scheme for controlling surfaces waves, measured results are presented in Chapter 4. With the exception of the transition region, the antenna performs as predicted by the calculated results based on a two-dimensional MM-based model.

To validate the scheme discussed in this report, an microstrip patch antenna was designed on a thick substrate. The dimensions of the parasitic metallic strips were obtained by means of an optimization routine. Due to the large number of constrained parameters that had to be optimized, an adaptive genetic algorithm (AGA) was implemented for this study. This algorithm is described in Appendix A. It is shown that the AGA performs better than ordinary GAs. To access the accuracy of the design, the optimized antenna was fabricated and tested. The measured results are presented in Chapter 4. The antenna performs as predicted by the calculated results based on a two-dimensional model with the exception of the transition region. It is found that the transition region is controlled by the length of the strips. The shorter

the length of the strips, the higher the frequency range and *vice versa.* The shift of the transition region can be taken into account by designing the strips (with 2-D models) for a transition region lower than the desired range.

The final chapter of this reports deals with the introduction of diode-loaded strips to design an adaptive antenna element. A 3-D FDTD-based code was used to calculate the fields radiated by this antenna element. Note that the diodes are modeled as thin wires when they are operating in the "on" state and are ignored when they are off. It is demonstrated that the radiation pattern can be modified by turning the diodes on and off. In this particular case, the beamwidth of the antenna is modified. No attempt to optimize the performance of this antenna was made. The goal was simply to demonstrate the concept.

Further research is needed to fully understand and predict the behavior of this adaptive antenna element. In particular, it is important to understand the current behavior on the parasitic strips when they are divided into smaller pieces. This will help us decide how to divide the strips and where to place the diodes to achieve a desired radiation pattern.

Appendix A

Genetic Algorithms

A.1 Introduction

Classical or calculus-based, enumerative, and random are three typical search techniques that are used most often in many optimization problems [19, 20].

Classical or calculus-based: These methods find the best solution based on a deterministic approach which requires the use of gradient or higher-order derivatives and a "good" initial guess.

Enumerative: To find the optimal solution, all possible solutions are tested in these methods.

Random: These random search methods, which are enumerative in nature, randomly select points on the search space to get the optimum.

The first category is often referred to as the local optimization technique and the second and third are global search methods. Most local search algorithms quickly converge to a solution. However, they suffer the disadvantage of getting stuck in local optima due to their strong dependence on the starting point (initial guess) of the process. In many cases, they are applicable only to *well-behaved* problems, such as differentiable problems. On the other hand, most enumerative and random optimization techniques are independent of the initial conditions, and do not require derivatives. However, they require excessive computation when optimizing many parameters, so that they tend to be slow.

Due to the failure of these conventional techniques, many researchers are looking for alternate approaches that can handle complex problems efficiently. Among those, evolutionary algorithms (EAs) have shown great improvement over the traditional methods [21, 22]. Genetic algorithms (GAs), evolution strategies (ESs), and evolutionary programming (EP), which were developed independently from each other, are the three main representatives of EAs. A detail discussion of these three algorithms can be found in reference [22].

Genetic algorithms (GAs) are robust, stochastic optimization techniques based on the Darwinian concept of natural selection. The *Darwinian theory of evolution* describes the adaptive change of species through generations by the principle of natural selection [22]. In other words, species, who are best adapted to their environmental conditions, are more likely to be selected for survival and further evolution. Ever since Holland [23] first generalized the concept of GA, there have been many research papers and dissertations establishing the applicability of GAs in function optimization, control systems, economic systems, neural networks, and various engineering applications. A flow chart of most genetic algorithms is shown in Figure A.1. There are four major differences between GAs and the conventional search algorithms [19].

1. GAs work with a coding of the parameter set, not the parameters themselves. Note that some people use parameter values directly in GAs, however, this will not fully use the advantage of GA [23].

2. GAs search from a population of samples, not a single point.

3. GAs use a payoff (objective/cost function) information. This is why GAs are not limited by restrictive assumptions (such as continuity and differentiable) about the search space. Objective functions in GA will be discussed in detail in a later section.

4. GAs use stochastic transition rules, not deterministic rules.

One of the most widely used genetic algorithm is the simple genetic algorithm (SGA) presented by Goldberg [19]. The main components of the SGA are the roulette

wheel selection operator, one-point crossover operator, simple mutation operator, and the fitness function, which will be discussed separately in successive sections. In this chapter, a brief discussion of some important genetic operators and issues regarding GAs are discussed. In addition, an adaptive genetic algorithm (AGA) is introduced. Unlike traditional GAs, the AGA is concerned on finding the optimal solution using minimal computation effort.

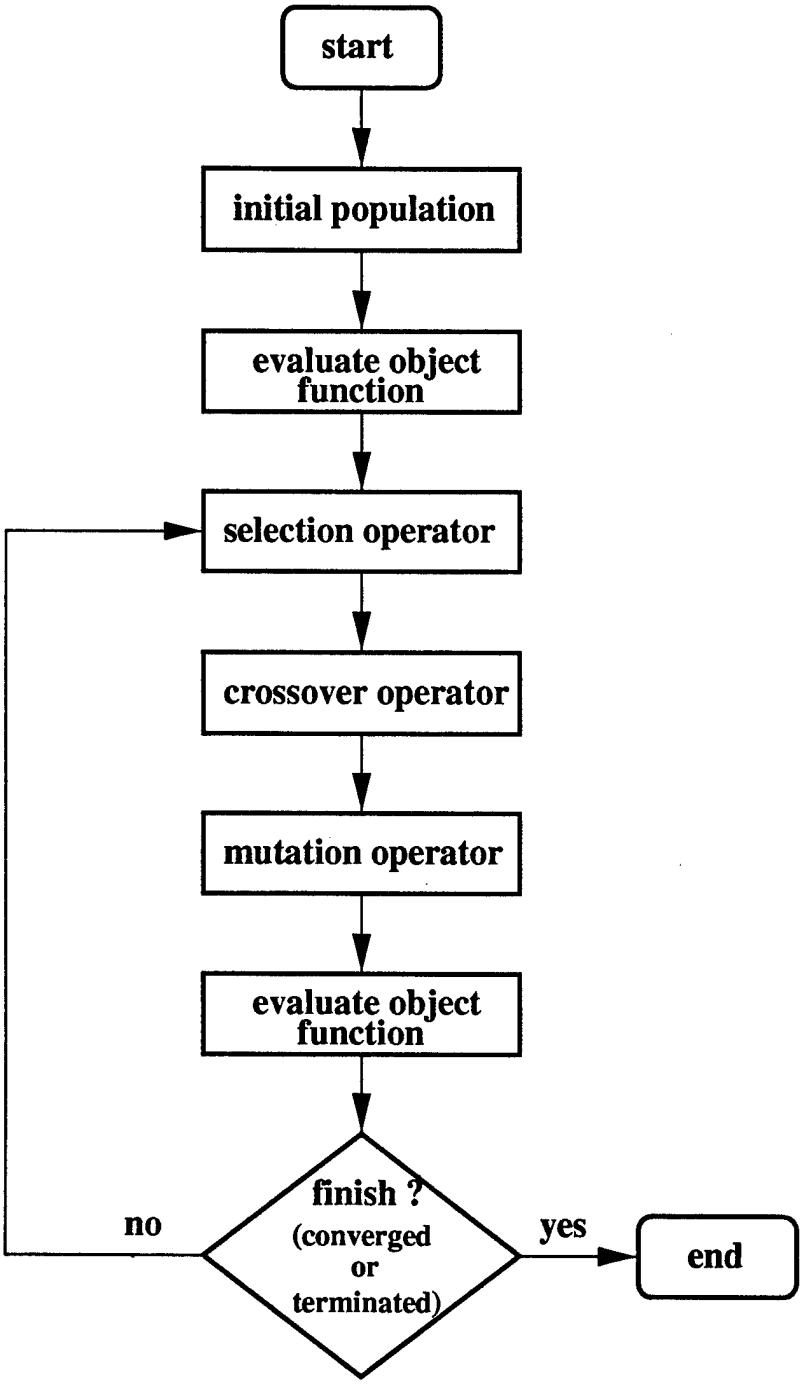

Figure A.1: Flowchart of general genetic algorithm

A.2 Initial Population

The initial population is generated randomly in many GA applications. In this section, the relation between an individual member of the population and the constrained parameters is discussed. Figure A.2 shows how a parameter x_i is coded into an individual. A parameter x_i with maximum value x_{max} and minimum value x_{min} is first coded into binary strings. Then, an individual is a collection of all the coded parameters, and the population is a collection of many individuals.

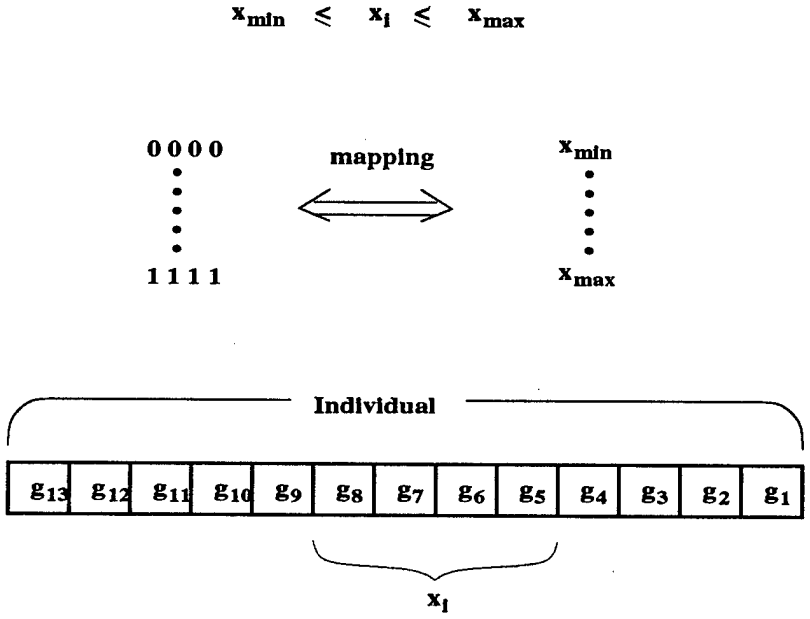

Figure A.2: Set up of an individual

In the example shown in Figure A.2, the parameter x_i is mapped into a 4 bit string. The string length (number of bits) determines the number of possible solutions of x_i between x_{max} and x_{min}. After obtaining its binary representation, x_i is placed into the gene location 5 to 8. There is no particular reason for placing the bit string of x_i in g_5 to g_8. In fact, one can choose to place the bits of x_i into different gene locations (no particular ordering) of the individual. In the example, the individual has a total number of 13 bits which is a collection of bits from the bit strings of x_i and other parameters.

During the evaluation of the fitness value (object/cost function), the individual is decoded back to the original values of the parameters. The fitness value of the individual is then calculated based on that particular set of parameters.

A.3 Selection Operators

The selection operator ensures that better fit individuals have better chances of being selected to reproduce. The better fit individuals in GA are individuals who have higher fitness values. In other words, individuals with a higher fitness value have a higher probability of reproducing one or more offspring in the next generation. The *selection pressure* is defined as the degree to which the better individuals are favored [24]. That means the higher the selection pressure, better fit individuals are selected and vice versa. Therefore, the population fitness improves over succeeding generations. In addition, GAs with higher selection pressures result in faster convergence rates. However, too low or too high selection pressures are both not appropriate. The convergence rate is slow for low selection pressure, and thus, the GA needs a longer time to obtain the optimum. On the other hand, there is an increased chance for GA to converge to an incorrect solution when the pressure is too high.

Two widely used groups of selection schemes are *proportionate selection* and *ordinal-based (rank-based) selection*. In proportionate selection, individuals are selected based on their fitness values relative to the fitness values of others. In ordinal-based selection schemes, individuals are selected based on their rank in the population. Miller [24] has compared the two, and shows that rank-based selection schemes have relatively higher selection pressures.

The algorithms of one proportionate selection scheme (roulette wheel) and two rank-based selection scheme (ranking and binary tournament) are discussed.

A.3.1 Roulette Wheel Selection

One of the most frequently used proportionate selection strategies is the roulette-wheel selection. The probability of the individuals in the current generation being selected into the mating pool is given as follows.

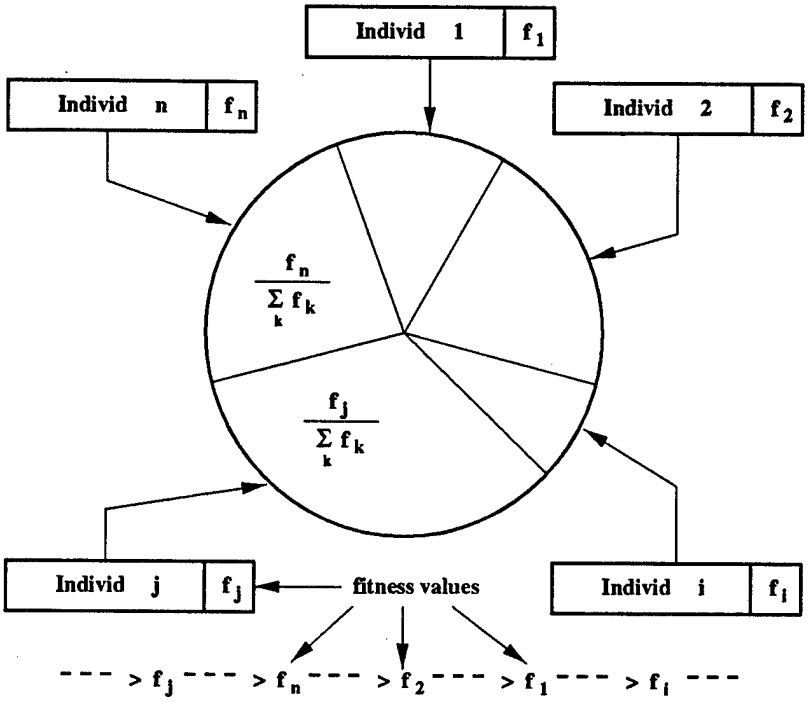

Figure A.3: Proportionate selection operator (roulette wheel)

$$p_{select}(i) = \frac{f_{individ}(i)}{\sum_{k}^{Npop} f_{individ}(k)} \tag{A.1}$$

where $Npop$ is the total number of individuals in the population and $f_{individ}(i)$ is the fitness value for the i th individual.

That means the probability of a particular individual being selected into the mating pool is proportional to its own merit with respect to the entire population. In other words, individuals are assigned a slot on a wheel according to their relative fitness value as shown in Figure A.3. Then, individuals are selected into the mating pool at the end of each wheel spinning until the mating pool is full. In this way, individuals with higher fitness values have a higher number of offspring in the succeeding generation. There is also a small chance for the fittest individual in the population of not being selected. Also, when the population size is small, this selection scheme does not work too well due to insufficient test samples.

A.3.2 Ranking Selection

In the ranking selection operator, individuals are ranked based on their fitness values (from the highest to the lowest). Then individuals with fitness values which are lower than a threshold fitness value are removed from the population. The remaining individuals are then entered into the mating pool. Therefore, individuals with high fitness values are guaranteed to be selected. Nonetheless, some useful information contained in inferior individuals may be loss due to the removal of these individuals.

A.3.3 Tournament Selection

As shown in Figure A.4, a group of individuals (usually two, which is also called binary tournament selection) is picked at random from the population with replacement (replacement means that after this particular selection process, the two individuals are placed back into the population, so that they have chance to be selected again). Then the individual with the highest fitness value in this group is selected into the mating pool. This process is repeated until the mating pool is full.

A.4 Crossover Operators

The idea behind crossing over between genes of two individuals is that some useful information (segments) of the two individuals (parents) should be combined to produce a new individual (child) that contains more useful information than both parents. By repeating the process of crossover between individuals in the population through generations, a "steady-state" (good overall) solution is obtained [23].

A.4.1 One-point Crossover

The most simple crossover strategy is the one-point crossover. Two individuals, parents, are randomly paired from the mating pool. Depending on the probability of crossover, p_c, if a crossing over is going to take place, then a crossing site is randomly chosen and crossing over takes place between the two parents to create two children as shown in Figure A.5. Therefore, each resulting child contains information from

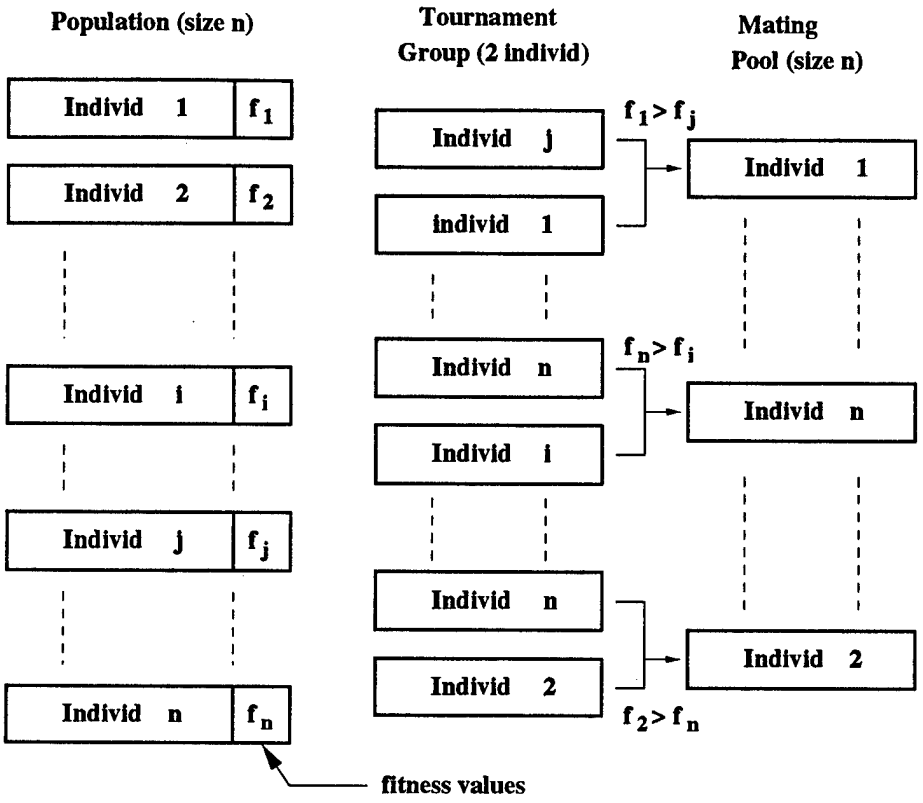

Figure A.4: Tournament selection operator

both parents. If a crossing over is not going to take place, then the two children simply become copies of the two parents.

A.4.2 Two-point Crossover

Similar to the one-point crossover operator, two parents are randomly paired from the mating pool. Instead of one crossing site, two crossing sites are randomly chosen in the two point crossover scheme (Figure A.6). The information contained in the two end points of the string is disrupted for the one-point crossover case. However, useful information contained in the two end points of the individuals passes onto the children in the two-point crossover case.

A.4.3 Uniform Crossover

After randomly pairing two parents from the mating pool, uniform crossover operator randomly exchange information at each gene location between the two parents as

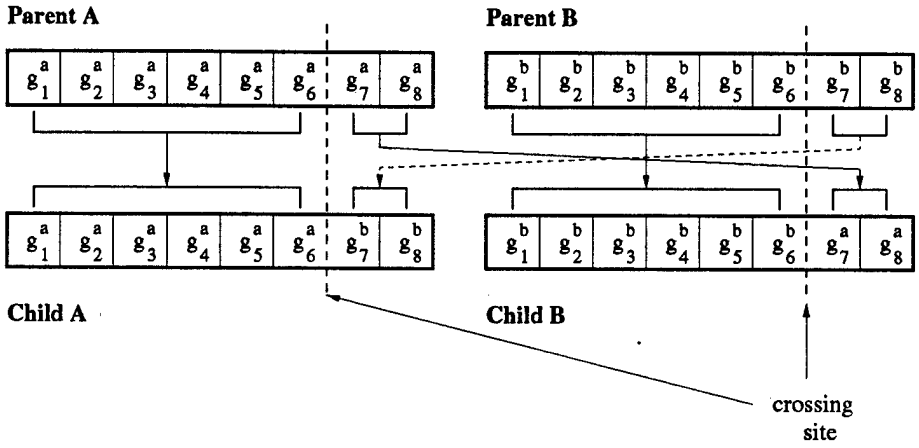

Figure A.5: One point crossover operator

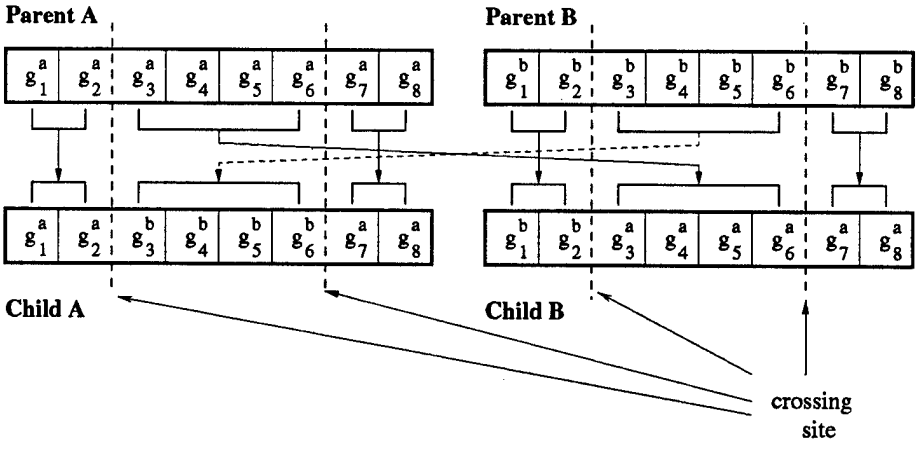

Figure A.6: Two point crossover operator

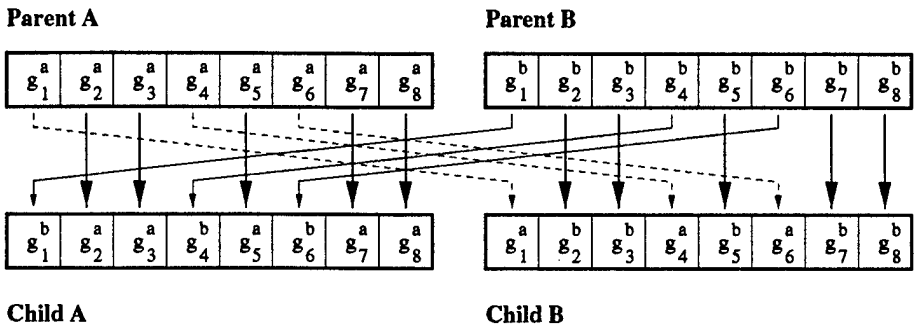

Figure A.7: Uniform crossover operator

shown in Figure A.7. It is clear that this operator has the disadvantage of disrupting the good strings. However, uniform crossover is very useful for searching alternative solutions when the optimized result begins to converge.

A.5 Mutation

The mutation operator introduces additional diversity into the population. It can be thought of as an insurance policy against premature convergence and loss of potentially useful genetic material. The operator randomly picks a gene location and changes its value. When binary code is being used, this means that it changes a 1 to a 0 and *vice versa.*

A.6 Fitness

There are many ways to assign fitness values to the individuals depending on different problems. Some of the more common methods are discussed below [20].

1. *Raw fitness (R_f)* This is the fitness value that is obtained from the problem itself without any modification. In other words, raw fitness is the same as the value obtained directly from the cost function or object function without any modification. If R_f is the error in the solution, then it is to be minimized, otherwise it is to be maximized.

2. *Standardized fitness (S_f)* The fitness function is designed such that it is always minimized. For example, if R_f is the error then $S_f = R_f$, else $S_f = R_{max} - R_f$, where R_{max} is the maximum value of the raw fitness.

3. *Adjusted fitness (A_f)* This fitness value always lies between 0 and 1. It is a non-linear increasing function and it is to be maximized. $A_f = \frac{1}{1+S_f}$

4. *Normalized fitness (N_f)* This fitness value also lies between 0 and 1 and it is to be maximized. $N_f = \frac{A_f}{\sum A_f}$

A.6.1 Fitness Scaling

During the start of a GA run, there may be a few extraordinary individuals in the population. These individuals would then occupy a significant proportion of the finite population in the next generation because of the selection operator. This is called *premature convergence* and is undesirable. On the other hand, in the later generations, the average fitness value of the population may be very close to the fitness value of the best individual. This is undesired too, because the chance of the best individual being selected to reproduce is low.

In order to solve these problems, a fitness scaling operator should be applied. This operator regulates the number of offspring that an individual reproduces for the next generation.

Goldberg [19] suggests the use of a linear fitness scaling operator. This particular operator requires a linear relationship between the raw fitness, f, and a scaled fitness, f', such as $f' = af + b$. The coefficients a and b are determined, so that the average scaled fitness, f'_{avg}, and the average raw fitness, f_{avg}, are equal. By doing this kind of simple fitness scaling, the chance of an early domination of extraordinary individuals is reduced. In addition, it provides a healthy competition environment among near equal individuals in the later generations.

A.7 Failure of Many Genetic Algorithms

There are three main reasons for the failure of many genetic algorithms [19, 20]. First, GAs find solutions by combining high fitness and short length subsets of genes (schema). However, there are some problems where the optimal solution does not contain the high fitness and low-order (short length) schema, but with high-order schema. In such cases, GAs move away from the global optimum and get stuck in local optimum. This kind of problems is called *deceptive* problem.

Second, high selective pressure prevents some individuals (containing useful features) to reproduce and contribute to the next generation. Hence, useful information may be loss which prevents GAs from finding the optimal solutions.

Third, early disruption of the high fitness schema may be caused by the use of improper crossover operators. Thus, GAs move again away from the global optimum. In order to minimize the above problems, the adaptive genetic algorithm is introduced in the next section.

A.8 Adaptive Genetic Algorithm

In most genetic algorithms, selection and crossover operators are preselected by the designers and do not change in the optimization process. For example, the simple genetic algorithm (SGA) uses roulette wheel selection and one point crossover operators. Since different operators have advantages/disadvantages over the others, some GAs may work better than the others depending on the cost function. Thus, it may be a good idea to change the operators during the optimization process such that the resultant algorithm is more powerful. Based on this idea, an adaptive genetic algorithm (AGA) is presented in here. A flowchart of AGA is shown in Figure A.8.

In AGA, the selection and crossover operators introduced previously are changed during the optimization process based on the convergence properties of the process. In other words, since no two selection schemes can be used at the same time, a particular scheme is chosen based on the convergence properties of the population of the previous generation. Since ranking selection has the highest selective pressure among the three operators, it can be used to help the GA quickly converge to a solution. When the GA begins to converge, the selection operator switches to the binary tournament scheme. This scheme has a lower selective pressure so that lower fit individuals (with some useful information) have a better chance to pass useful information to the next generation to help the GA obtain the optimum solution. The roulette wheel selection acts as an intermediate step between the other two schemes.

Following the same idea, a crossover operator is selected based on the convergence properties of the population. The one point crossover is used to help the GA converge faster since it is less disruptive to the population. The uniform crossover operator slows down the convergence and helps the GA to find a better solution. Like the roulette wheel selection, the two point crossover scheme acts as an intermediate step between the one point and uniform crossover operators.

The mutation operator in the proposed AGA is also different from the traditional mutation operators. In most GAs, the mutation rate is fixed throughout the run. In AGA, the mutation rate changes according to the convergence of the GA. The

mutation rate is kept low to help GA converge. When GA starts to converge, the mutation rate is increased and thus decreases the convergence rate to keep searching for better solutions (if any).

Based on the above ideas, the AGA is applied to two different fitness functions. In the next section, it is shown that the performance of AGA is indeed better than GAs that only use a particular pair of selection and crossover operators.

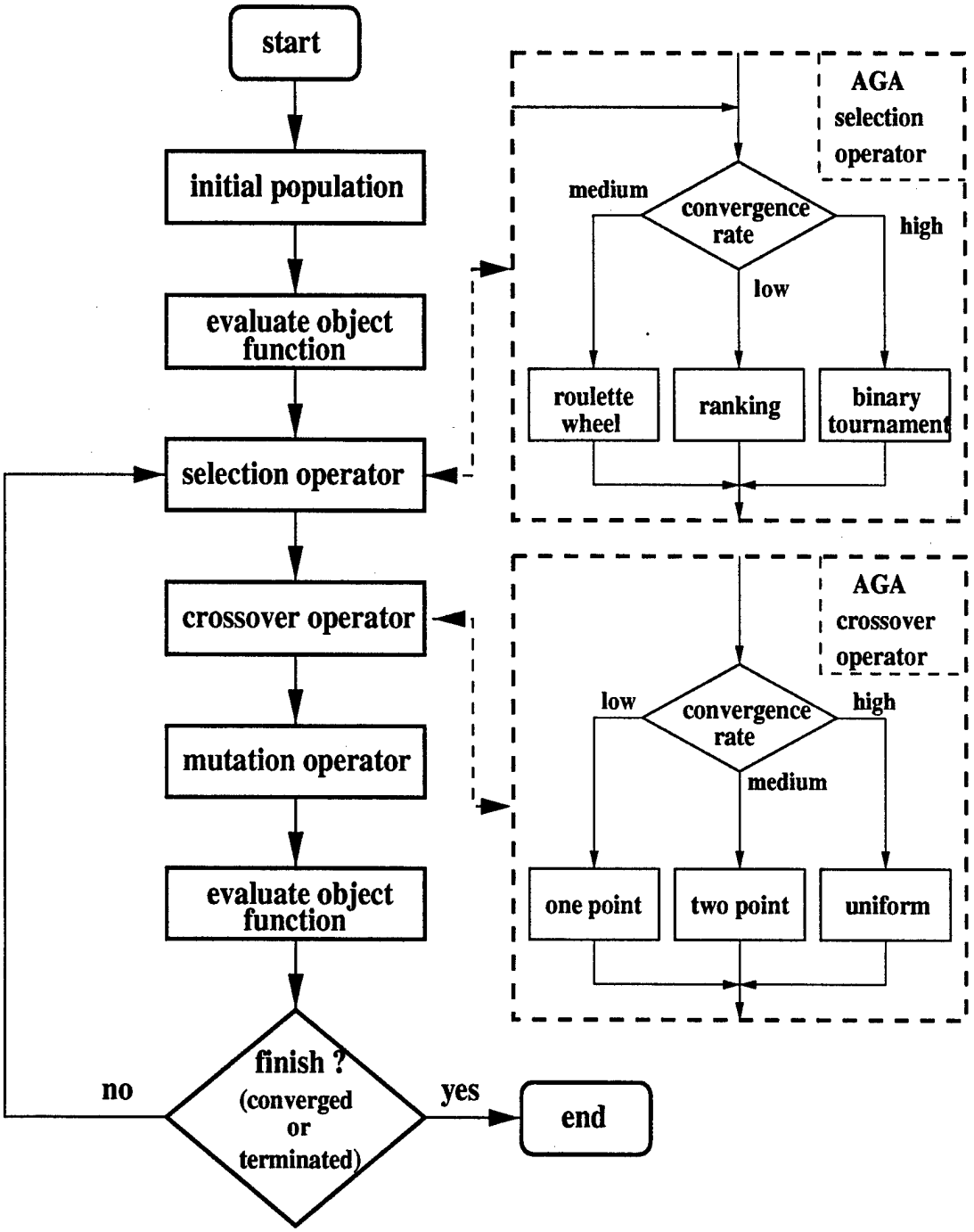

Figure A.8: Flowchart of adaptive genetic algorithm

A.9 Optimization Examples

In this section, two optimization examples using AGA are presented.

A.9.1 Ackley's Function

Ackley's function is a test function obtained by modulating an exponential function with a cosine wave of moderate amplitude [22]. The function is given by

$$f(\vec{x}) = -c_1 \exp\left(-c_2\sqrt{\frac{1}{n}\sum_{i=1}^{n} x_i^2}\right) - \exp\left(\frac{1}{n}\sum_{i=1}^{n}\cos(c_3 x_i)\right) + c_1 + e \qquad \text{(A.2)}$$

where $\vec{x} = [x_1, x_2, \ldots, x_n]$ are n variables and c_1 and e are arbitrary constants. A three dimensional plot of the function with **two** parameters is shown in Figure A.9(a). A strictly hill-climbing local optimization algorithm would surely get trapped in a local optimum. However, a search algorithm which can scan a slightly larger neighborhood would be able to cross the local optimum to reach the global optima. Hence, it is a reasonable test case. Figures A.9(b) to (d) show the optimization results (finding the global minimum with fitness value of 1) of AGA and other GAs with different combinations of operators. Note that the optimizations are performed with **40** parameters of the function. In addition, the performance curves are the average results of **50** runs.

It is clear that AGA performs better than the other GAs except for GAs with ranking selection operators. The good performance of the GAs with ranking selection is because the ranking scheme concentrates many individuals in the neighborhood of the global optima, hence, offering a better chance to obtain the optimum result (global minimum). However, ranking based GAs can easily get stuck in local optimum as shown in the next example.

A.9.2 Two Peaks Sinc Function

In this example, the fitness function is constructed in such a way that it has two unequal peaks. The function is given by

$$f(x_1, x_2) = 0.9\left|\text{sinc}\left(\frac{x_1 + 10}{5.5\pi}\right)\text{sinc}\left(\frac{x_2 + 10}{5.5\pi}\right)\right| + \left|\text{sinc}\left(\frac{x_1 - 70}{2.5\pi}\right)\text{sinc}\left(\frac{x_2 - 70}{2.5\pi}\right)\right| \qquad \text{(A.3)}$$

where x_1 and x_2 are the two parameters. The plot of the function is shown in Figure A.10(a). It is clear that the function has a global optima (maximum) when $x_1 = x_2 = 70$ and has a local optima (local maximum) at $x_1 = x_2 = -10$. Also note that the local optima has a larger neighborhood (wider peak). Hence, many algorithms get stuck in this local optima.

The optimization results are shown in Figures A.10(b) to (c). Again, the results are based on the average of 50 runs. It is very clear that the AGA outperform all the other GAs. Note that unlike the previous example, the ranking-based GAs have the worst performance among the tested GAs.

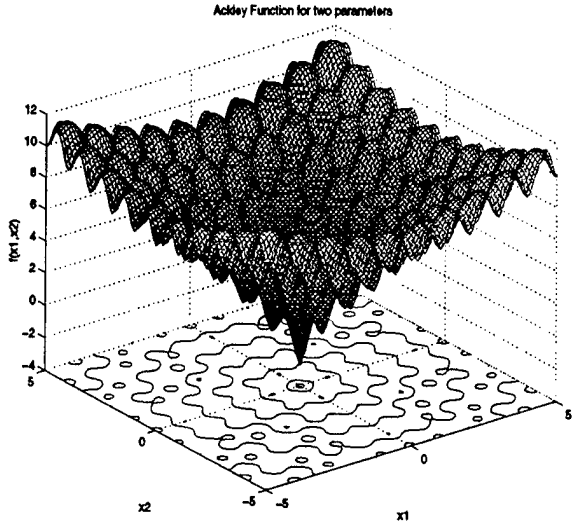

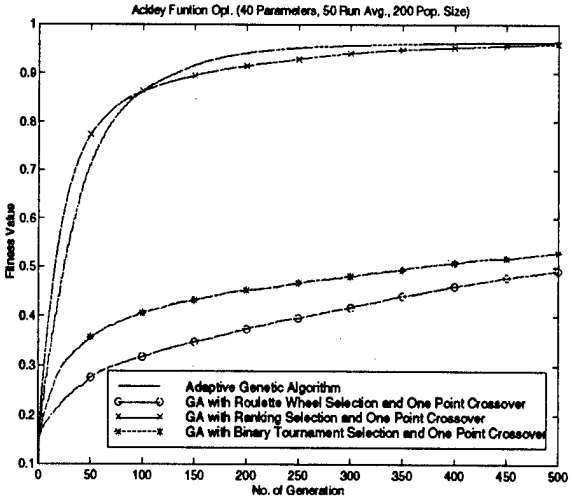

(a) Fitness function

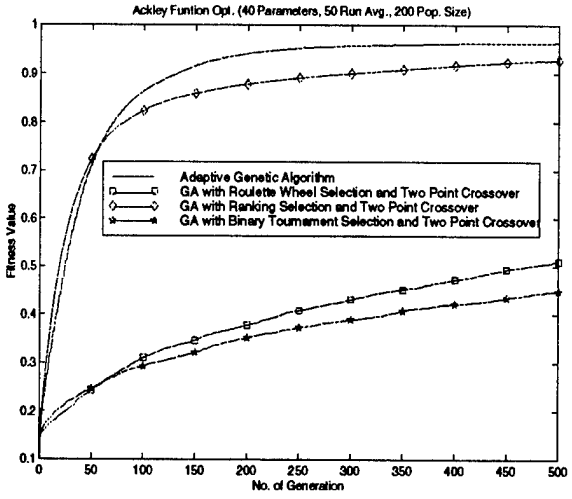

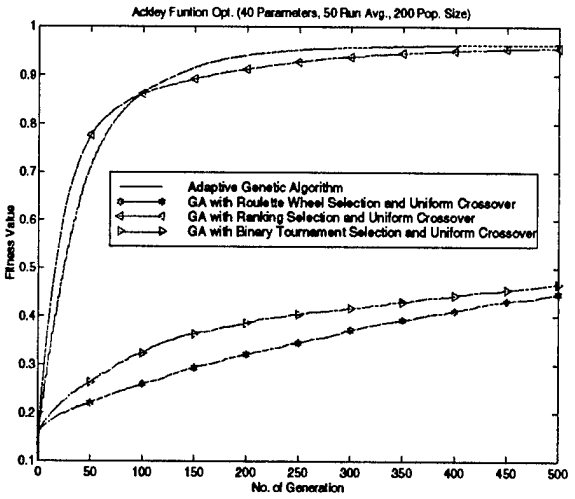

Figure A.9: Performance comparisons between genetic algorithms with different combinations of operators using ackley fitness function

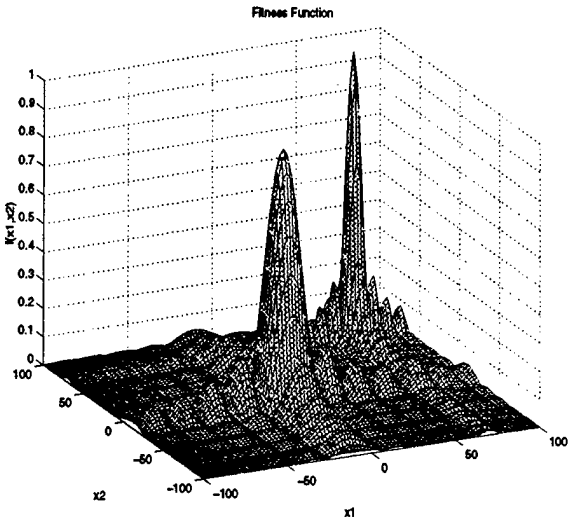

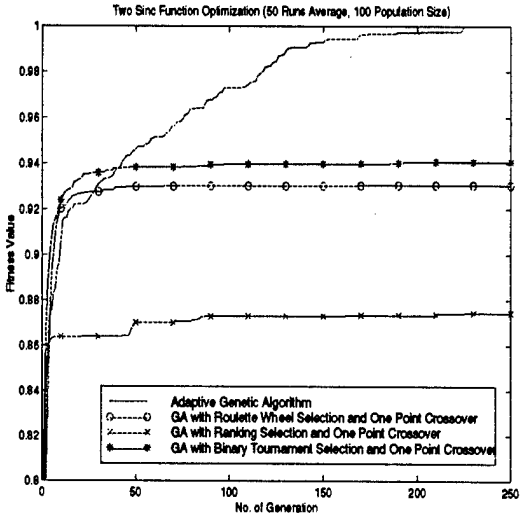

(a) Fitness function

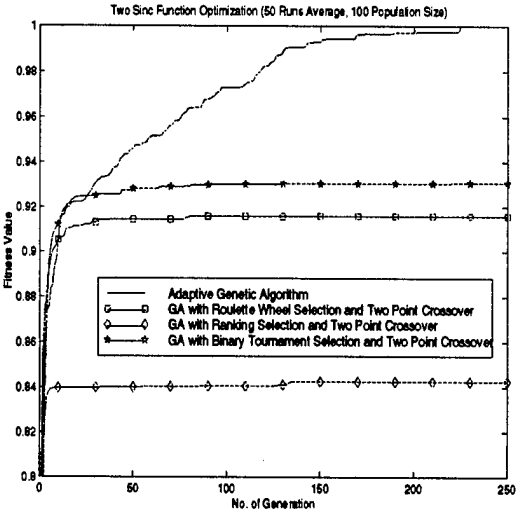

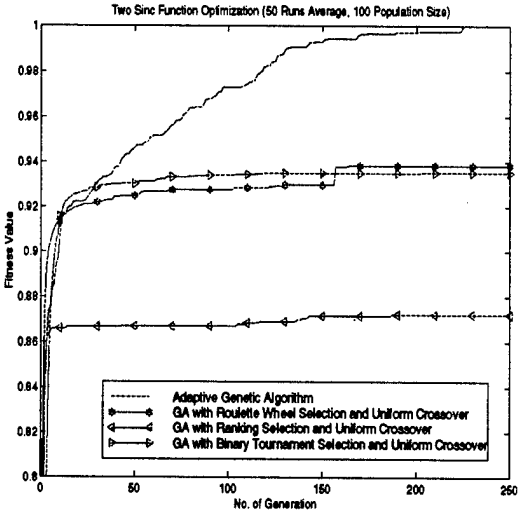

Figure A.10: Performance comparisons between genetic algorithms with different combinations of operators using two sinc fitness function

Bibliography

[1] P. B. Katehi and N. G. Alexopoulos, "On the effect of substrate thickness and permittivity on printed circuit dipole properties," *IEEE Trans. Antennas Propagat.*, vol. 31, pp. 34–39, Jan. 1983.

[2] N. G. Alexopoulos, P. B. Katehi, and D. B. Rutledge, "Substrate optimization for integrated circuit antennas," *IEEE Trans. Microwave Theory and Techniques*, vol. 31, pp. 550–557, July 1983.

[3] E. Chang, S. A. Long, and W. F. Richards, "An experimental investigation of electically thick rectangular microstrip antennas," *IEEE Trans. Antennas Propagat.*, vol. 34, pp. 767–772, June 1986.

[4] M. Kara, "Empirical formulas for the computation of the physical properties of rectangular microstrip antenna element with thick substrates," *Microwave Opt. Technol. Lett.*, vol. 14, pp. 115–121, February 1997.

[5] I. J. Bahl and P. Bhartia, *Microstrip Antennas.* Massachusetts: Artech House, 1980.

[6] V. Erturk, "Design and analysis of an active integrated transmitting antenna," M.S. Thesis, The Ohio State University, 1996.

[7] V. Erturk, R. Rojas, and P. Roblin, "Hybrid analysis/design method for active integrated antennas," *IEE Proceedings, Microwaves, Antennas & Propagation*, in print.

[8] J. R. James, P. S. Hall, and C. Wood, *Microstrip Antenna Theory and Design.* IEE, London: Peter Peregrinus, 1981.

[9] K. R. Carver and J. M. Mink, "Microstrip antenna technology," *IEEE Trans. Antennas Propagat.*, vol. 29, pp. 2–24, Jan. 1981.

[10] H. Legay and L. Shafai, "New stacked microstrip antenna with large bandwidth and high gain," *IEE Proc.-Microw. Antennas Propagat.*, vol. 141, pp. 199–204, June 1994.

[11] R. B. Waterhouse and N. V. Shuley, "Full characterisation of varactor-loaded, probe-fed, rectangular, microstrip patch antennas," *IEE Proc.-Microw. Antennas Propagat.*, vol. 141, pp. 367–373, Oct. 1994.

[12] D. M. Pozar and B. Kaufman, "Increasing the bandwidth of a microstrip antenna by proximity coupling," *Electronic Lett.*, vol. 23, pp. 368–369, April 1987.

[13] F. Schwering and A. A. Oliner, *Millimeter-Wave Antennas*, ch. 17. NY: Van Nostrand Company, 1988.

[14] W. F. Richards, *Microstrip Antennas*, ch. 10. NY: Van Nostrand Company, 1988.

[15] A. G. Derneryd, "Linearly polarized microstrip antenas," *IEEE Trans. Antennas Propagat.*, vol. 24, pp. 846–851, Nov. 1976.

[16] M. F. Otero, "Radiation and scattering from a complex material cylinder in the presence of an impedance wedge," Ph.D. Dissertation, The Ohio State University, 1995.

[17] M. Kragalott and E. H. Newman, "A user's manual for the general cylinder code (GCYL)," Tech. Rep. 722644-1, The Ohio State University ElectroScience Lab., June 1990.

[18] D. M. Pozar, "Considerations for millimeter wave printed antennas," *IEEE Trans. Antennas Propagat.*, vol. 31, pp. 740–747, Sept 1983.

[19] E. D. Goldberg, *Genetic Algorithms in Search, Optimization and Machine Learning.* MA: Addison-Wesley, 1989.

[20] S. Raman and L. M. Patnaik, "Optimization via evolutionary processes," *Advances in computers*, vol. 45, pp. 156–196, 1997.

[21] M. Gen and R. Cheng, *Genetic Algorithms and Engineering Design.* NY: Wiley, 1997.

[22] T. Bäck, *Evolutionary Algorithms in Theory and Practice.* NY: Oxford Univ., 1996.

[23] J. H. Holland, *Adaptation in Natural and Artificial Systems.* MI: Univ. Michigan, 1975.

[24] B. L. Miller and D. E. Goldberg, "Genetic algorithms, selection schemes, and the varying effects of noise," IlliGAL Report 95009, University of Illinois at Urbana-Champaign, November 1995.